

Parametrically enhanced two-loop contributions to $b \rightarrow s\gamma$ in a Two-Higgs-Doublet Model

Zur Erlangung des akademischen Grades eines

DOKTORS DER NATURWISSENSCHAFTEN

von der Fakultät für Physik
des Karlsruher Instituts für Technologie (KIT)

genehmigte

DISSERTATION

von

Dipl.-Phys. Peter Christoph Wiegand
aus Schrobenhausen

Tag der mündlichen Prüfung: 27.10.2017

Referent: Prof. Dr. Ulrich Nierste
Korreferent: Prof. Dr. Matthias Steinhauser

Contents

1. Introduction	1
1.1. The Standard Model of elementary particle physics	6
2. The Two-Higgs-Doublet model	9
2.1. The CP-conserving Two-Higgs-Doublet of type II	10
2.2. Renormalisation of the Two-Higgs-Doublet model	14
3. $\tan \beta$ enhanced corrections to $b \rightarrow s\gamma$ in the Two-Higgs-Doublet Model of type II	23
3.1. Introduction to effective field theory	24
3.1.1. A question of scales	24
3.1.2. Matching for $b \rightarrow s\gamma$	26
3.2. Status of the SM predictions and first checks of Medusa	30
3.3. $b \rightarrow s\gamma$ in the Two-Higgs-Doublet Model	33
3.3.1. Status	33
3.3.2. $m_\tau^2 \tan^2 \beta$ contributions to $b \rightarrow s\gamma$ in the Two-Higgs-Doublet Model	34
3.3.3. Treatment of γ_5	39
3.3.4. The $\tan^2 \beta$ enhanced quark contributions to $b \rightarrow s\gamma$ in the 2HDM	48
4. The Mathematica package Medusa for two loop calculations in flavour physics	52
4.1. Overview of the structures and used packages	54
4.2. The treatment of γ_5 in FeynArts	56
4.3. Asymptotic expansion in small momenta	59

4.4. The loop Integrals	66
4.4.1. One-loop integrals in D dimensions	66
4.4.2. The tensorial two-loop vacuum integral with three masses	68
4.4.3. Checks	71
4.5. Functions and structures of Medusa	72
5. Conclusion	79
A. Feynman diagrams of the y_b induced $\tan \beta$ enhanced terms in $b \rightarrow s\gamma$	81
B. Feynman diagrams of the Higgs-coupling induced $\tan \beta$ enhanced terms in $b \rightarrow s\gamma$	88

CHAPTER 1

Introduction

The Standard Model of elementary particle physics, encompassing our current knowledge of known particles and their interactions, is still very successful. After being completed with the discovery of the Higgs boson at the experiments at the Large Hadron Collider (LHC), the LHC continues to test and confirm Standard Model predictions in many processes, as has been done in previous experiments over the years. One notable deviation from this pattern are the flavour anomalies, occurring and persisting throughout different experiments in flavour-violating decays of B and K mesons.

Despite the great successes of the Standard Model and its many confirmations of its predictions at collider experiments, many conceptual puzzles and cosmological questions are still left unanswered. The most pressing shortcoming is the lack of an explanation of dark matter. Dark matter is required to understand many astrophysics experiments and essential in cosmological predictions. Furthermore there is no explanation why there is matter at all, since the amount of CP violation, the difference of the behavior of particles and anti-particles, is not large enough and the electro-weak phase transition is not strong enough.

There are also conceptual issues hinting at the incompleteness of our understanding of fundamental particle physics. Since the incompleteness discussed above requires an extension of the Standard Model at higher energy scales, in the form of new particles, it is still unclear how the mass of the Higgs particle is stabilised against the quantum

corrections due to the new particles. This is the so called hierarchy problem. Furthermore, there is no understanding of the large hierarchy among flavour-conserving and flavour-violating Yukawa couplings, which is referred to as the flavour puzzle. Note that these are not consistency problems of the Standard Model, which in itself is a self-consistent theory up to very high energies. Another conceptual hint is the quantisation of the electric charges. While in the Standard Model the values of the electric charges are fixed by experiment and theoretically constrained by the cancellation of the chiral anomalies, they might also be remnants of a larger symmetry unifying the Standard Model interactions to one.

Of the above mentioned problems, only the hierarchy problem is associated with a vague energy scale in the region of TeV. This means that we would expect to find deviations from our predictions when reaching this energy scale in collisions. Since this scale is within the reach of the LHC many people had high hopes that the large increase of centre of mass energy at the LHC would lead to the discovery of a new zoo of unknown particles. Nonetheless no unexpected fundamental particles could be found so far.

In general, there are two ways to detect new particles: Direct production, followed by the detection of a characteristic signature of their subsequent decay or indirect measurement of the effects through quantum corrections due to the new particles in precision observables. Since for the direct production the available energy in the collision is the most important factor, the biggest step in the discovery potential was made when the LHC increased the centre of mass energy by an order of magnitude in comparison with the Tevatron. For the second strategy the processes considered happen at low energy and the potential for discovery lies in pushing the precision in both experiment and theory to the point where small effects due to heavy unknown particles become apparent. In this aspect the near future will be an exciting time as the Belle II experiment for precision measurements will have its first physics run in 2018 and will continue taking data throughout the 2020s.

Already in the past indirect effects of particles appeared long before their existence was confirmed by direct production at a collider. The most famous example is the prediction of the third generation by Kobayashi and Maskawa [54] to explain CP-violation. Another example is the prediction of the charm quark by Glashow, Iliopoulos and Maiani[41] which plays an important role in explaining the smallness of flavour changing neutral currents, measured at the time. In both cases there were tensions in

experimental results which probed energy scales above the energy of the experiment. But the models proposed by [54] and [41] included additional heavier particles that could, through quantum corrections, solve the tensions. Thus it seems natural to assume that also in the future we will first see hints of new particles via their virtual contributions, through quantum corrections.

Important processes to look out for are rare decays and neutral meson mixing. We understand quantum field theory in terms of perturbation theory, expressing theory predictions as series of smaller and smaller quantum corrections. In rare decays and meson mixing, the leading contribution of the Standard Model is already at one loop level. This makes the decays rare compared to processes that are possible at tree level, hence implying the possibility that a new contribution is comparatively large, if it occurs at lower order. Nonetheless there is the caveat that this approach requires a lot of effort to precisely predict and measure these rare decays. As this strategy has proven to be successful in the past we choose this path and investigate rare decays in this thesis.

The required precision comes with the need of going to higher orders in perturbation series, which makes the calculation of theory predictions much more complex. The calculation of additional terms in the perturbation series is organised in the calculation of amplitude represented by Feynman diagrams. The number of the diagrams rises quickly with the expansion order, yet the steps of the calculation of each diagram are similar. With the bigger scope of the calculation comes therefore the need for automation. To this end we implemented a Mathematica package, encompassing all the steps necessary for the calculation, hence providing the possibility to perform similar calculations very quickly.

There is also the question of how to proceed conceptually. As we are faced with the fact that the Standard Model is both working very well and has obvious shortcomings that still need to be addressed, the strategy of our research can be motivated threefold:

1. trying to solve the grand problems themselves by extending the symmetry or particle content of the Standard Model in an ultra violet complete way,
2. improving the precision of the Standard Model prediction in the hope of detecting small deviations,
3. trying to understand the possible effects of additional particles at an experimentally accessible scale.

The distinction between the first and the last point is that with the first approach complete models are introduced trying to solve multiple of the above mentioned issues at once. Since the Standard Model problems, with the exception of the hierarchy problem, do not come with a clear scale to tell us how massive the particles associated with a solution might be, many complete models at high scales have little testable predictions. In most cases, the natural scales related to a larger symmetry encompassing all Standard Model gauge groups are by far larger than the reach of any experiment existing or conceivable in the near future. Furthermore a lot of the rich structure at the high scales gets lost when calculating potential effects on physical processes within reach of experiments. Testing minimal extensions however can tell us where to look for possibly detectable unknown particles. This is the strategy of point 3, which we follow in this thesis. The minimal extensions can be seen as building blocks that have to be embedded in the complete theory tackling more of the problems.

There is still one remark to be made, since there are two ways to approach this problem. The first is a model independent approach using effective field theories. This technique, in which all possible extended interactions of Standard Model particles are investigated, has the advantage that general, model independent statements can be made, but the drawback that it is hard to associate deviations from the Standard Model predictions to specific models. The second strategy is to use simple benchmark models, which constitute a specific minimal extension of the Standard Model. This allows for statements about certain aspects of the theory. For example the Higgs sector, implementing the spontaneous symmetry breaking, or the possibility of additional gauge interactions, which would come with a new gauge boson. This is the approach followed in this thesis.

Since the Higgs sector became experimentally accessible most recently and might still hold the possibility for surprises, we investigate the Two-Higgs-Doublet model as a benchmark model. In this model the particle content of the Standard Model is extended by adding one additional scalar doublet, while the gauge group is left untouched. This is a feature that can occur as a low energy limit of several ultra violet complete extensions of the Standard Model. For this reason, investigating the Two Higgs Doublet Model gives us the possibility to gain information about a range of different models.

We are specifically looking for $\tan\beta$ enhanced contributions to $b \rightarrow s\gamma$ in the Two Higgs Doublet Model of type II. They arise both through the Yukawa couplings of the b quark and the τ and through Higgs couplings. $b \rightarrow s\gamma$ is a well studied process.

The current Standard Model prediction [65] includes next-to-next-to-leading-order corrections from quantum-chromo-dynamics (QCD) [66]. More importantly in the Two-Higgs-Doublet Model the same precision is available [45]. Due to the above mentioned precision in the matching, the perturbative error due to the unknown higher order corrections is estimated to be $\pm 3\%$ [67]. There is another $\pm 3\%$ error due to the interpolation in m_c in the calculation of the interference of the operators $Q_{1,2}$ and Q_7 [29]. This makes the branching ratio $\bar{B} \rightarrow X_s \gamma$ to the source of the strongest bound on the charged Higgs mass $M_{H^\pm} > 570 - 800 \text{ GeV}$ [67] in the region of intermediate and large $\tan \beta$. On the experimental side there have been several measurements of the CP- and isospin-averaged $\bar{B} \rightarrow X_s \gamma$ branching ratio at CLEO [21], BaBar [61, 6, 60, 59] and Belle [2, 62, 1]. By averaging over all measurements the current experimental value [5]

$$\mathcal{B}_{s\gamma}^{\text{exp}} = (3.32 \pm 0.15) \times 10^{-4} \quad \text{for } E_0 = 1.6 \text{ GeV} \quad (1.1)$$

is obtained. E_0 is the cut on the photon energy.

The precise experimental value, the phenomenological importance and the low perturbative uncertainty make it worthwhile to investigate the $\tan \beta$ enhanced effects. A priori they are expected to be of the order of electro-weak corrections, i.e. percent level corrections. In the regions of large $\tan \beta$, i.e. $\tan \beta \in [50, 60]$, the Yukawa coupling of the b quark is $\mathcal{O}(1)$, which implies the possibility of larger corrections. There are also corrections proportional to $\tan \beta$ due to Higgs couplings. Since the couplings of the proposed additional physical Higgs bosons in the Two Higgs Doublet Model are experimentally hard to constrain, this type of contributions can also be of $\mathcal{O}(1)$.

Outline

We will start with presenting the Standard Model in Section 1.1 and the Two-Higgs-Doublet model in Section 2. In Section 2.2 we will remark on the renormalisation of the Two-Higgs-Doublet model.

We will investigate the $\tan \beta$ -enhanced correction to the rare decay $b \rightarrow s\gamma$ in Chapter 3. To this end we will first briefly introduce the effective theory used for this purpose in Section 3.1. Then the status of the Standard Model prediction and the experiment will be briefly reviewed in Section 3.2. In Section 3.3 we will first review the status of the theory predictions, then introduce the newly calculated contributions from leptonic subloops in Section 3.3.2. The contributions from quark subloops and the contribution

due to Higgs self-couplings will be presented in Section 3.3.4.

The calculations were performed in an automatised approach with the newly developed Mathematica package Medusa, which will be introduced in Chapter 4. Here we will first present the general structure and then proceed to review some of the technical aspects of the calculation. The final part of the chapter briefly reviews the implementation of the package. In Chapter 5 we will conclude.

1.1. The Standard Model of elementary particle physics

In this section we will review the parts of the Standard Model relevant to the discussion in Chapters 2 and 3. A complete introduction can be found in many textbooks for instance [14]. The focus will be on the Higgs sector, since the extension of the Higgs sector with a second doublet will be investigated in this thesis. The full Lagrangian can be split into distinct sectors governing certain the interaction and kinematics of the respective particles

$$\mathcal{L}_{\text{SM}} = \mathcal{L}_{\text{gauge}} + \mathcal{L}_{\text{f}} + \mathcal{L}_{\text{H}} + \mathcal{L}_{\text{Yuk}}. \quad (1.2)$$

In the gauge sector $\mathcal{L}_{\text{gauge}}$ the kinematics and the interactions of the gauge bosons are defined. The fermionic sector \mathcal{L}_{f} entails the kinematic terms of the fermions as well as their gauge interactions. The sectors that are most important for this thesis are firstly the Higgs sector \mathcal{L}_{H} , which is defined in Equation 1.3 below. It entails the self-coupling of the Higgs-boson and governs the spontaneous symmetry breaking [36, 47], which explains the masses of the weak gauge bosons. Secondly the Yukawa sector \mathcal{L}_{Yuk} , which is defined in Equation 1.8 below. The Yukawa sector describes the coupling of the fermions to the Higgs boson and is responsible for both the fermion masses as well as flavour violation.

Experimentally we observe that the gauge bosons mediating the weak interaction are massive. To explain this observation the Higgs mechanism [36, 47] has been introduced, which implements a spontaneous breaking of the electro-weak symmetry $SU(2) \times U(1)_Y$ to the $U(1)_{EW}$ of quantum-electrodynamics. It is defined in the Higgs sector of the Standard Model Lagrangian in Equation (1.2)

$$\mathcal{L}_{\text{H}} = (D_{\mu}\phi)^{\dagger}(D^{\mu}\phi) - V(\phi) \quad (1.3)$$

with

$$V(\phi) = \frac{\lambda}{4} (\phi^\dagger \phi)^2 - \mu^2 \phi^\dagger \phi. \quad (1.4)$$

The field ϕ is a $SU(2)$ doublet

$$\phi = \begin{pmatrix} \phi^+ \\ \phi_0 \end{pmatrix} \quad (1.5)$$

with Hypercharge $Y = 1$. The potential is chosen such that the neutral component of the doublet ϕ acquires a non zero vacuum expectation value

$$\langle \phi \rangle = \begin{pmatrix} 0 \\ \frac{v}{\sqrt{2}} \end{pmatrix} \quad (1.6)$$

with $v = 246\text{GeV}$. After spontaneous symmetry breaking one physical scalar field remains, the Higgs field h . The other scalar degrees of freedom, the Goldstone fields G^+ and G_0 , provide the longitudinal degrees of freedom of the weak gauge bosons, which acquire a mass from the kinetic term of the Higgs field. The doublet is parametrised by these fields as

$$\phi(x) = \begin{pmatrix} G^+(x) \\ \frac{v}{\sqrt{2}} + h(x) + iG_0(x) \end{pmatrix} \quad (1.7)$$

The fermion masses are due to the vacuum expectation value of the Higgs field as well. The coupling of the Higgs field to fermions is given by the Yukawa sector of the Lagrangian

$$\mathcal{L}_{\text{Yuk}}^{SM} = - \sum_{j,k=1}^3 \left[y_{jk}^d \bar{Q}_j \phi d_{Rk} + \tilde{y}_{jk}^u \bar{Q}_j \tilde{\phi} u_{Rk} + y_{jk}^e \bar{L}_j \phi e_{Rk} + h.c. \right] \quad (1.8)$$

where $\tilde{\phi} = i\sigma_2 \phi^*$ is the charge conjugated Higgs doublet.

The Yukawa coupling matrix elements have a priori arbitrary values. When diagonalising the coupling matrix by a biunitary transformation, flavour changing interactions are introduced in the coupling of the W boson.

In Chapter 3 we will investigate the flavour changing process $b \rightarrow s\gamma$. In the Standard Model this process is mediated by the W boson. The interactions of the W boson are defined in the electro-weak part [73, 80, 40] of the gauge Lagrangian $\mathcal{L}_{\text{gauge}} = \mathcal{L}_{\text{EW}} + \mathcal{L}_{\text{QCD}}$. We will only need the interactions of the W and present the Lagrangian

for the mass eigenstates W^\pm after spontaneous symmetry breaking

$$\mathcal{L}_W = \frac{g_2}{\sqrt{2}} \sum_{i,j=1}^3 \left[V_{ij} \bar{u}_i^L \gamma^\mu d_j^L W_\mu^+ + V_{ij}^* \bar{d}_i^L \gamma^\mu u_j^L W_\mu^- \right]. \quad (1.9)$$

where the CKM matrix [54] is

$$V_{\text{CKM}} = \begin{pmatrix} V_{ud} & V_{us} & V_{ub} \\ V_{cd} & V_{cs} & V_{cb} \\ V_{td} & V_{ts} & V_{tb} \end{pmatrix}. \quad (1.10)$$

To express the hierarchy of the CKM matrix elements it is convenient to use the Wolfenstein parametrisation [82]. The CKM matrix is then given by

$$V_{\text{CKM}} = \begin{pmatrix} 1 - \frac{\lambda^2}{2} & \lambda & A\lambda^3(\rho - i\eta) \\ -\lambda & 1 - \frac{\lambda^2}{2} & A\lambda^2 \\ A\lambda^3(1 - \rho - i\eta) & -A\lambda^2 & 1 \end{pmatrix} + \mathcal{O}(\lambda^4). \quad (1.11)$$

The Wolfenstein parameter $\lambda = 0.22506 \pm 0.00050$ [72] is seen as an expansion parameter. In Section 3.3.4 we will expand in this parameter to second order to reduce the number of diagrams. Effectively this removes the first generation from the calculation, as the CKM matrix element connecting the b quark with the first generation is suppressed by λ^3 . It also simplifies the renormalisation of the CKM matrix discussed in Section 2.2.

CHAPTER 2

The Two-Higgs-Doublet model

The Two-Higgs-Doublet model (2HDM) is one of the simplest extensions of the SM. The model we will present here has to be seen as a stepping stone in a bottom up approach, since it neither solves any of the aforementioned conceptual problems of the SM nor answers the questions, concerning for example dark matter and matter antimatter asymmetry. The model is mainly of interest due to it being an extension to the Higgs sector, which, regarding experimental confirmation, is the most recently probed element of the SM. Thus it might be possible to measure deviations of the Standard Model prediction in the experimental programme of LHC, which emphasises determining the nature of the Higgs-sector, by measuring Higgs couplings and properties. From this point of view the 2HDM is studied as a benchmark model for extended Higgs sectors and thought of as an effective theory at intermediate energy scales, describing the low energy limit of an ultraviolet-complete extension of the Standard Model. One of the most straightforward of these models is the Minimal Supersymmetric Standard Model (MSSM), which might result in an intermediate 2HDM of type II if the additional Higgs-bosons are lighter than the other supersymmetric partners.

2.1. The CP-conserving Two-Higgs-Doublet of type II

To fix the notation we will give a brief introduction to the 2HDM. In a generic 2HDM the only new field added is one additional Higgs doublet

$$\mathcal{L}_{2\text{HDM}} = \mathcal{L}_{\text{gauge}}^{\text{SM}} + \mathcal{L}_{\text{f}}^{\text{SM}} + (D_\mu \phi_2)^\dagger (D^\mu \phi_2) + (D_\mu \phi_1)^\dagger (D^\mu \phi_1) + \mathcal{V} + \mathcal{L}_{\text{Yuk}}^{2\text{HDM}}. \quad (2.1)$$

The gauge and fermionic parts of the Standard Model Lagrangian $\mathcal{L}_{\text{gauge}}^{\text{SM}}$ and $\mathcal{L}_{\text{f}}^{\text{SM}}$ are unchanged. The potential term \mathcal{V} will be defined in Equation (2.5) below. The Yukawa sector is given by

$$\mathcal{L}_{\text{Yuk}}^{2\text{HDM}} = - \sum_{j,k=1}^3 \left[y_{jk}^u \bar{Q}_j \tilde{\phi}_1 u_{Rk} + y_{jk}^d \bar{Q}_j \phi_1 d_{Rk} + \tilde{y}_{jk}^u \bar{Q}_j \tilde{\phi}_2 u_{Rk} + \tilde{y}_{jk}^d \bar{Q}_j \phi_2 d_{Rk} + h.c. \right] \quad (2.2)$$

This extension of the Yukawa sector bears a problem, as it introduces flavour changing neutral currents at tree level. In the standard model the couplings of the Higgs boson are diagonal in the mass eigenbasis of the fermionic fields, hence implying the absence of flavour changing neutral Higgs couplings. In the 2HDM this is not possible, as we briefly explain in the following. If we for the sake of this argument assume that only one of the scalar fields, e.g. ϕ_1 , gets a vacuum expectation value, going to the mass eigenbasis for the fermions means diagonalizing the coupling matrix to this scalar field ϕ_1 . As the entries of the two coupling matrices are in general just free parameters, the second coupling matrix will not be diagonal in this basis. In general these induce flavour-changing neutral-Higgs couplings at tree level and the high precision in flavour experiments tightly constrains these couplings. While the strength of this constraint varies, some of the off-diagonal elements are constrained to be smaller than 10^{-6} . [28] Hence one promotes the absence of flavour-changing neutral couplings to a feature of the model and implements it via a symmetry.

In the 2HDM of type II we will investigate in this thesis, a Z_2 symmetry is introduced for the fields such that

$$\begin{aligned} \phi_2 &\rightarrow -\phi_2 & \phi_1 &\rightarrow \phi_1 \\ u_{R,k} &\rightarrow -u_{R,k} & d_{R,k} &\rightarrow d_{R,k}. \end{aligned} \quad (2.3)$$

This ensures that ϕ_2 and ϕ_1 interact only with the up-type quarks and down-type

quarks respectively, as the Yukawa sector takes the form

$$\mathcal{L}_{\text{Yuk}}^{2\text{HDM-II}} = - \sum_{j,k=1}^3 \left[y_{jk}^d \bar{Q}_j \phi_1 d_{Rk} + \tilde{y}_{jk}^u \bar{Q}_j \tilde{\phi}_2 u_{Rk} + h.c. \right]. \quad (2.4)$$

Diagonalizing the Yukawa matrix to go to the mass basis, then leaves no additional non-diagonal couplings, since y_{jk}^d can be diagonalised by rotations of the down-type quarks and $\tilde{\phi}_{jk}^u$ by rotations of the up-type quarks.

We now come back to discuss the structure of the potential, given by

$$\begin{aligned} \mathcal{V} = & m_{11}^2 \phi_1^\dagger \phi_1 + m_{22}^2 \phi_2^\dagger \phi_2 - \left(m_{12}^2 \phi_1^\dagger \phi_2 + h.c. \right) \\ & + \frac{1}{2} \lambda_1 \left(\phi_1^\dagger \phi_1 \right)^2 + \frac{1}{2} \lambda_2 \left(\phi_2^\dagger \phi_2 \right)^2 + \frac{1}{2} \lambda_3 \left(\phi_2^\dagger \phi_2 \right) \left(\phi_1^\dagger \phi_1 \right) + \frac{1}{2} \lambda_4 \left(\phi_2^\dagger \phi_1 \right) \left(\phi_1^\dagger \phi_2 \right) \\ & + \left[\frac{1}{2} \lambda_5 \left(\phi_1^\dagger \phi_2 \right)^2 + h.c. \right]. \end{aligned} \quad (2.5)$$

Note that the m_{12} term is a soft breaking term of the Z_2 symmetry. A priori both Higgs doublets ϕ_1 and ϕ_2 might acquire a vacuum expectation value (vev), giving masses to the respective quarks. It is more convenient, however, to transform into the so called Higgs basis, in which the complete vacuum expectation value appears in one of the doublets. This can be done by a rotation in field space

$$\begin{pmatrix} \Phi \\ \Phi' \end{pmatrix} = \begin{pmatrix} \cos \beta & \sin \beta \\ -\sin \beta & \cos \beta \end{pmatrix} \begin{pmatrix} \phi_1 \\ \phi_2 \end{pmatrix} \quad (2.6)$$

where β is defined by

$$\tan \beta \equiv \frac{v_2}{v_1} \quad (2.7)$$

with

$$v^2 \equiv v_1^2 + v_2^2 = \frac{4M_W^2}{g^2} = (246\text{GeV})^2. \quad (2.8)$$

Regarding the electroweak symmetry breaking, we have a situation analogous to the SM, as all the vacuum expectation value is concentrated in one doublet while the other acquires no vev. This means that in the doublet Φ the charged field becomes the longitudinal degree of freedom of the W^\pm as the pseudo Goldstone boson and the pseudoscalar field is absorbed as the longitudinal degree of freedom of the Z . This leaves us with two neutral scalars h and H , one pseudoscalar A_0 and the charged component of Φ' H^\pm as physical scalar fields.

2. The Two-Higgs-Doublet model

After the rotation in Equation (2.6) it is still possible for the two neutral CP-even Higgs-bosons to mix, as they have the same quantum numbers. The angle diagonalizing this mass matrix is called α . In this thesis we imply that the lighter of the two neutral scalars h is the observed SM-like Higgs-boson. Following [7] we choose

$$v, \quad M_{h_0}, \quad \tan \beta, \quad \beta - \alpha, \quad m_{12}, \quad M_H, \quad M_A, \quad M_{H^\pm} \quad (2.9)$$

as independent parameters of the model.

As the exclusion limits for searches of additional scalars become more stringent with better collider data, implying larger masses [67, 37, 4] and the also constraints from measurements of the Higgs couplings get stronger [7], two physically interesting limits arise. The first is reached by letting the masses of the heavy scalars M_{H^\pm}, M_H and M_A go to infinity. This is called the decoupling limit and has been studied in [42]. As $\cos(\beta - \alpha) = \mathcal{O}(\frac{v^2}{M_A^2}) \rightarrow 0$, also the Higgs-couplings is affected. If constraints from the h couplings and unitarity bounds are taken into account, as done in [7], one realizes that not all free parameters of the model can be chosen freely. Instead the model is pushed towards the alignment limit, which is characterised by $c_{\beta-\alpha} = 0$.

In Section 3.3.4 we consider contributions from triple scalar couplings. When expressing the triple scalar couplings in the parameters listed in Equation (2.9), we encounter a $\tan \beta$ enhancement of the couplings. Two important triple Higgs coupling that exhibit this $\tan \beta$ enhancement are given as

$$C_{H_0 H^+ H^-} = \frac{c_{\beta-\alpha} M_{H_0}^2 s_\beta^2 + 2c_{\beta-\alpha} M_{H^\pm}^2 s_\beta^2 - m_{12}^2 s_\beta^2 s_{\beta-\alpha} + m_{12}^2 s_{\beta-\alpha}}{3M_{h_0}^2 s_\beta^2} \quad (2.10)$$

$$C_{h_0 H^+ H^-} = \frac{\tan \beta \left(2c_{\beta-\alpha} m_{12}^2 - M_{H_0}^2 s_\beta^2 s_{\beta-\alpha} \right)}{3M_{h_0}^2 s_\beta^2} - \frac{m_{12}^2 s_{\beta-\alpha} \tan^2 \beta}{3M_{h_0}^2} - \frac{M_{H_0}^2 s_{\beta-\alpha}}{3M_{h_0}^2 \tan \beta},$$

$$C_{h_0 H^+ H^-} = \frac{c_{\beta-\alpha} m_{12}^2 s_\beta^2 - c_{\beta-\alpha} m_{12}^2 + M_{h_0}^2 s_\beta^2 s_{\beta-\alpha} + 2M_{H^\pm}^2 s_\beta^2 s_{\beta-\alpha}}{3M_{h_0}^2 s_\beta^2} \quad (2.11)$$

$$- \frac{\tan \beta \left(c_{\beta-\alpha} M_{h_0}^2 s_\beta^2 + 2m_{12}^2 s_{\beta-\alpha} \right)}{3M_{h_0}^2 s_\beta^2} + \frac{c_{\beta-\alpha} m_{12}^2 \tan^2 \beta}{3M_{h_0}^2} + \frac{c_{\beta-\alpha}}{3 \tan \beta}.$$

Following [7] we normalised the couplings by the Standard Model triple Higgs coupling $C_{h_0 h_0 h_0}$. However, the $\tan \beta$ dependence is only an artefact of the chosen parameter basis. When expressing the triple scalar couplings by the couplings in the Higgs potential λ_i instead of the masses of the physical Higgs bosons the powers of $\tan \beta$ are not ex-

plicitly visible, as has been discussed in [63]. Performing the calculation in the λ_i basis is however not feasible. The important lesson from investigating the parameter space from the vantage point of different parametrisations is, that not all parameter choices in the mass basis lead to a physically meaningful prediction. It is therefore crucial to check the unitarity constraints when inserting values for the Higgs masses and the couplings, as the couplings get very large for randomly chosen values. We implement this by checking that $\lambda_i < 4$ for $i \in 1, 5$, which is the most straight forward way of implementing the check. The unitarity constraints have been used in [7] to constrain possible triple Higgs couplings and in [53], where a lower bound on the second lightest Higgs boson is derived from the unitarity requirement. The couplings λ_i are related to the set of free parameters given in Equation (2.9) as

$$\begin{aligned}
 \lambda_1 &= \frac{c_{\beta-\alpha}^2 M_{H_0}^2 + M_{h_0}^2 s_{\beta-\alpha}^2}{v^2} \\
 &\quad - \frac{2c_{\beta-\alpha}(M_{h_0}^2 - M_{H_0}^2)s_{\beta-\alpha}t_\beta}{v^2} + \frac{(c_{\beta-\alpha}^2 M_{h_0}^2 + M_{H_0}^2 s_{\beta-\alpha}^2)t_\beta^2}{v^2} - \frac{m_{12}^2 t_\beta^3}{s_\beta^2 v^2} \\
 \lambda_2 &= \frac{c_{\beta-\alpha}^2 M_{H_0}^2 + M_{h_0}^2 s_{\beta-\alpha}^2}{v^2} + \frac{c_{\beta-\alpha}^2 M_{h_0}^2 + M_{H_0}^2 s_{\beta-\alpha}^2}{t_\beta^2 v^2} \\
 &\quad - \frac{m_{12}^2 - 2c_{\beta-\alpha} M_{h_0}^2 s_\beta^2 s_{\beta-\alpha} + 2c_{\beta-\alpha} M_{H_0}^2 s_\beta^2 s_{\beta-\alpha}}{s_\beta^2 t_\beta v^2} \\
 \lambda_3 &= - \frac{(c_{\beta-\alpha}^2 - s_{\beta-\alpha}^2)M_{h_0}^2 - 2M_{H^\pm}^2 + M_{H_0}^2(s_{\beta-\alpha}^2 - c_{\beta-\alpha}^2)}{v^2} \\
 &\quad + \frac{c_{\beta-\alpha}(M_{h_0}^2 - M_{H_0}^2)s_{\beta-\alpha}}{t_\beta v^2} - \frac{(m_{12}^2 + c_{\beta-\alpha} M_{h_0}^2 s_\beta^2 s_{\beta-\alpha} - c_{\beta-\alpha} M_{H_0}^2 s_\beta^2 s_{\beta-\alpha})t_\beta}{s_\beta^2 v^2} \\
 \lambda_4 &= \frac{M_{A_0}^2 - 2M_{H^\pm}^2}{v^2} + \frac{m_{12}^2 t_\beta}{s_\beta^2 v^2} \\
 \lambda_5 &= - \frac{M_{A_0}^2}{v^2} + \frac{m_{12}^2 t_\beta}{s_\beta^2 v^2}.
 \end{aligned} \tag{2.12}$$

It will turn out in 3.3.4 that the contribution is linked to the quark contribution, since cancellation of ultraviolet divergences is only achieved when adding all $\tan^2 \beta$ enhanced terms. They also provide a well defined subset of the contributions due to the Higgs sector. Which ultimately provides the opportunity of studying the effect of large couplings to $b \rightarrow s\gamma$. In light of Equation (2.12) a remark is in order about the $\tan^2 \beta$ terms in Equation (2.12). Due to the unitarity requirement of λ_5 , m_{12} is pushed to small values in the region of large $\tan \beta$. Also λ_5 and m_{12} can be easily interchanged,

unlike $\lambda_1 - \lambda_4$ and the masses of the Higgs bosons which are intricately linked. Thus the $\tan^2 \beta$ enhancement does not necessarily equal a large coupling.

2.2. Renormalisation of the Two-Higgs-Doublet model

In this section we will proceed to evaluate the required counterterms for the calculations that will be presented in Sections 3.3.2 and 3.3.4. For the calculation of the $\tan \beta$ enhanced two-loop corrections to $b \rightarrow s\gamma$ only counterterms exhibiting this enhancement are needed, since the leading order amplitude is $\tan \beta$ independent. The masses of the light quarks are set to zero $m_u = m_d = m_s = m_c = 0$, while m_b is considered to be small. For the field and mass renormalisation the on-shell scheme was used. All self energies contributing to the renormalisation of the CKM matrix have to be evaluated for an equal value of the squared momentum [38]. We chose $p^2 = 0$ in the following derivation of the counterterms.

The complete list of required counterterms includes the LSZ factors (field renormalisation constants) for the b quark $\delta Z_{d,bb}^{L,os}$ and $\delta Z_{d,bb}^{R,os}$, the counterterms for the CKM matrix elements $\delta V_{tb}^{p^2=0}$ and $\delta V_{ts}^{p^2=0}$, and the mass counterterms δm_b^{os} , δM_t^{os} and $\delta M_{H^\pm}^2$. Their derivation and the results will be summarised in the following.

We do not include a tadpole counterterm to make sure we get gauge independent counterterms. While tadpole renormalisation does not automatically lead to gauge dependent counterterms, as has recently been shown for the 2HDM [56, 33], it is not required to obtain UV finite matrix elements. Tadpole renormalisation does, however, imply counterterms for vertices that are not included in the Lagrangian. One example is $H^\pm \rightarrow W^\pm \gamma$, a subprocess of $b \rightarrow s\gamma$. $H^\pm \rightarrow W^\pm \gamma$ is a loop induced process and thus yields a finite result when adding all the contributions. This statement crucially depends on the inclusion of the tadpoles. As there are no counterterms required, including tadpole renormalisation has to produce a completely new counterterm for the process. This has been investigated in [56] as well. To avoid such complications we did not include tadpole renormalisation.

The tadpoles appearing in the calculations include b quark and τ contributions and Higgs boson tadpoles proportional to the triple Higgs couplings. The top quark tadpoles however are not contributing to the $\tan^2 \beta$ term. Due to the leading order being independent of $\tan \beta$, the counterterm has to contain $\tan^2 \beta$, limits the number of diagrams we have to consider. All counterterms are calculated in the on-shell scheme and

2. The Two-Higgs-Doublet model

in Figure 2.1. The self-coupling tadpole only contributes when looking at the $y_b \tan \beta$ term, where one $\tan \beta$ is due to the triple Higgs coupling. In the matching calculation that will be presented in Section 3.3.4 an asymptotic expansion in small external momenta and masses m_b and m_τ is performed. To get consistent analytical result the same expansion is performed in the derivation of the counterterms. Details can be found in Section 4.3.

As a result we get

$$\begin{aligned}
\delta Z_{d,bb}^{L,os} = & \frac{e^2 m_b^2 \tan^2 \beta e^{-\gamma \epsilon} (4\pi)^\epsilon}{128\pi^2 M_W^2 s_W^2} \left[\frac{2}{\epsilon} + 1 - \ln \left(\frac{M_{A_0}^2}{\mu^2} \right) \right. \\
& - c_{\beta-\alpha}^2 \ln \left(\frac{M_{h_0}^2}{\mu^2} \right) - s_{\beta-\alpha}^2 \ln \left(\frac{M_{H_0}^2}{\mu^2} \right) \\
& + \frac{1}{6} \epsilon \left(3c_{\beta-\alpha}^2 \ln^2 \left(\frac{M_{h_0}^2}{\mu^2} \right) - 3c_{\beta-\alpha}^2 \ln \left(\frac{M_{h_0}^2}{\mu^2} \right) \right. \\
& + 3 \ln^2 \left(\frac{M_{A_0}^2}{\mu^2} \right) - 3 \ln \left(\frac{M_{A_0}^2}{\mu^2} \right) \\
& \left. \left. + 3s_{\beta-\alpha}^2 \ln^2 \left(\frac{M_{H_0}^2}{\mu^2} \right) - 3s_{\beta-\alpha}^2 \ln \left(\frac{M_{H_0}^2}{\mu^2} \right) + \pi^2 + 3 \right) \right], \tag{2.15}
\end{aligned}$$

$$\begin{aligned}
\delta Z_{d,bb}^{R,os} = & \frac{e^2 m_b^2 \tan^2 \beta e^{-\gamma \epsilon} (4\pi)^\epsilon}{128\pi^2 M_W^2 s_W^2} \left[\frac{4}{\epsilon} - \ln \left(\frac{M_{A_0}^2}{\mu^2} \right) - 2 \ln \left(\frac{M_{H^\pm}^2}{\mu^2} \right) + 2 \right. \\
& + \frac{2M_t^2 V_{tb} V_{tb}^*}{(M_{H^\pm}^2 - M_t^2)^2} \left(M_t^2 \ln \left(\frac{M_{H^\pm}^2}{M_t^2} \right) - M_{H^\pm}^2 + M_t^2 \right) \\
& - c_{\beta-\alpha}^2 \ln \left(\frac{M_{h_0}^2}{\mu^2} \right) - s_{\beta-\alpha}^2 \ln \left(\frac{M_{H_0}^2}{\mu^2} \right) \\
& + \frac{\epsilon}{6(M_{H^\pm}^2 - M_t^2)^2} \left[6M_t^2 V_{tb} V_{tb}^* \left(-M_t^2 \ln^2 \left(\frac{M_{H^\pm}^2}{\mu^2} \right) + 3(M_t^2 - M_{H^\pm}^2) \right. \right. \\
& + (2M_{H^\pm}^2 + M_t^2) \ln \left(\frac{M_{H^\pm}^2}{\mu^2} \right) + M_t^2 \ln^2 \left(\frac{M_t^2}{\mu^2} \right) - 3M_t^2 \ln \left(\frac{M_t^2}{\mu^2} \right) \\
& + (M_{H^\pm}^2 - M_t^2)^2 \left(3c_{\beta-\alpha}^2 \ln^2 \left(\frac{M_{h_0}^2}{\mu^2} \right) - 3c_{\beta-\alpha}^2 \ln \left(\frac{M_{h_0}^2}{\mu^2} \right) \right. \\
& + 3 \ln^2 \left(\frac{M_{A_0}^2}{\mu^2} \right) - 3 \ln \left(\frac{M_{A_0}^2}{\mu^2} \right) + 3s_{\beta-\alpha}^2 \ln^2 \left(\frac{M_{H_0}^2}{\mu^2} \right) \\
& \left. \left. - 3s_{\beta-\alpha}^2 \ln \left(\frac{M_{H_0}^2}{\mu^2} \right) + 6 \ln^2 \left(\frac{M_{H^\pm}^2}{\mu^2} \right) - 6 \ln \left(\frac{M_{H^\pm}^2}{\mu^2} \right) + 2\pi^2 + 6 \right) \right]. \tag{2.16}
\end{aligned}$$

The CKM renormalisation of [31, 32] leads to gauge dependent physical amplitudes, as has been shown in [38]. The counterterm for the CKM matrix elements is derived from the anti-Hermitian part of quark self energies, see Equation (2.17) below. The key point is that in [31, 32] all self energies used to derive the counterterms for the CKM matrix are evaluated on-shell. This is the cause of the gauge dependent amplitudes. To avoid gauge dependent amplitudes, the authors of [38] propose instead to evaluate all self energies at $p^2 = 0$. With this choice the counterterms can be extracted from

$$V_{ij}^0 + \delta V_{ij}^{p^2=0} = \left(\delta_{ik} + \frac{1}{2} \delta Z_{u, ik}^{AH\dagger} \right) V_{kn}^0 \left(\delta_{nj} + \frac{1}{2} \delta Z_{d, nj}^{AH} \right) \quad (2.17)$$

where

$$\delta Z_{ij}^{f, AH} = \frac{1}{2} \left(\delta Z_{f, ij}^{L, p^2=0} - \delta Z_{f, ij}^{L, p^2=0\dagger} \right) \quad (2.18)$$

are the anti-Hermitian parts of the field renormalisation constants δZ_{ij} and V^0 denotes the bare CKM matrix. All self energies are consistently evaluated at $p^2 = 0$, yielding

$$\begin{aligned} \delta Z_{f, ii}^{L, p^2=0} &= -\widetilde{Re} \Sigma_{ii}^{f, L} (0) - m_{f, i}^2 \frac{\partial}{\partial p^2} \widetilde{Re} \left[\Sigma_{ii}^{f, R} (p^2) + \Sigma_{ii}^{f, L} (p^2) + 2\Sigma_{ii}^{f, S} (p^2) \right] \Big|_{p^2=0} \\ \delta Z_{f, ij}^{L, p^2=0} &= \frac{2}{m_{f, i}^2 - m_{f, j}^2} \widetilde{Re} \left[m_{f, j}^2 \Sigma_{ij}^{f, L} (0) + m_{f, i} m_{f, j} \Sigma_{ij}^{f, R} (0) \right. \\ &\quad \left. + (m_{f, i}^2 + m_{f, j}^2) \Sigma_{ij}^{f, S} (0) \right], \quad i \neq j \end{aligned} \quad (2.19)$$

Only diagrams containing a H^\pm have to be considered, i.e. the diagram in the middle in Figure 2.1 for the respective external and arbitrary internal quarks. This results in the $\tan^2 \beta$ dependent terms of the CKM counterterms

$$\begin{aligned} \delta V_{ts} &= \frac{e^2 m_b^2 \tan^2 \beta V_{ts} V_{tb} V_{tb}^*}{256 \pi^2 M_W^2 s_W^2} \left(2 \log \left(\frac{M_{H^\pm}^2}{\mu^2} \right) + 2\gamma_E - 1 - 2 \log(4\pi) - \frac{2}{\epsilon} \right), \\ \delta V_{tb} &= \frac{e^2 m_b^2 \tan^2 \beta V_{tb} (V_{tb} V_{tb}^* - 1)}{256 \pi^2 M_W^2 s_W^2} \left(2 \log \left(\frac{M_{H^\pm}^2}{\mu^2} \right) + 2\gamma_E - 1 - 2 \log(4\pi) - \frac{2}{\epsilon} \right). \end{aligned} \quad (2.20)$$

When we consider an expansion in the Wolfenstein parameter λ , which is used to parametrise the hierarchy in the CKM matrix, δV_{tb} vanishes due to $V_{tb} V_{tb}^* = 1 + \mathcal{O}(\lambda^4)$. Hence only δV_{ts} contributes.

2. The Two-Higgs-Doublet model

The counterterms for the quark masses are derived as

$$\delta m_{f,i}^{os} = \frac{m_{f,i}}{2} \widetilde{Re} \left(\Sigma_{ii}^{f,L} (m_{f,i}^2) + \Sigma_{ii}^{f,R} (m_{f,i}^2) + 2\Sigma_{ii}^{f,S} (m_{f,i}^2) \right). \quad (2.21)$$

The result for δm_b^{os} is given by

$$\begin{aligned} \delta m_b^{os} = & \frac{e^2 m_b \tan^2 \beta e^{-\gamma \epsilon} (4\pi)^\epsilon}{128\pi^2 M_W^2 s_W^2} \left[\frac{3m_b^2}{\epsilon} + \frac{m_b^2 (-2M_t^2 V_{tb} V_{tb}^* + 3M_{H^\pm}^2 - 3M_t^2)}{2(M_{H^\pm}^2 - M_t^2)} \right. \\ & + \frac{m_{12}^2 \tan \beta}{M_{h_0}^2 M_{H_0}^2 \epsilon} (c_{\beta-\alpha}^2 M_{H_0}^2 + M_{h_0}^2 s_{\beta-\alpha}^2) (3c_{\beta-\alpha}^2 M_{h_0}^2 + M_{A_0}^2 + 3M_{H_0}^2 s_{\beta-\alpha}^2 + 2M_{H^\pm}^2) \\ & + \frac{1}{M_{h_0}^2 M_{H_0}^2 \epsilon} \left[-M_{A_0}^2 M_{h_0}^2 M_{H_0}^2 - M_{h_0}^2 M_{H_0}^2 (3M_{H_0}^2 s_{\beta-\alpha}^2 + 2M_{H^\pm}^2) \right. \\ & \quad \left. + c_{\beta-\alpha}^2 \left(-2M_{h_0}^6 s_{\beta-\alpha}^2 + M_{h_0}^4 M_{H_0}^2 (2s_{\beta-\alpha}^2 - 3) \right. \right. \\ & \quad \left. \left. + 2M_{h_0}^2 M_{H_0}^4 s_{\beta-\alpha}^2 - 2M_{H_0}^6 s_{\beta-\alpha}^2 \right) \right] \\ & + \frac{m_b^2}{(M_{H^\pm}^2 - M_t^2)^2} \left(M_t^2 V_{tb} V_{tb}^* \ln \left(\frac{M_{H^\pm}^2}{M_t^2} \right) - 3c_{\beta-\alpha}^2 M_{H^\pm}^4 \ln \left(\frac{M_{h_0}^2}{\mu^2} \right) \right. \\ & \quad + 6c_{\beta-\alpha}^2 M_{H^\pm}^2 M_t^2 \ln \left(\frac{M_{h_0}^2}{\mu^2} \right) - 3c_{\beta-\alpha}^2 M_t^4 \ln \left(\frac{M_{h_0}^2}{\mu^2} \right) \\ & \quad - 2M_{H^\pm}^2 M_t^2 \ln \left(\frac{M_{A_0}^2}{M_{H^\pm}^2} \right) + M_{H^\pm}^4 \ln \left(\frac{M_{A_0}^2}{M_{H^\pm}^2} \right) \\ & \quad + M_t^4 \ln \left(\frac{M_{A_0}^2}{M_{H^\pm}^2} \right) - 3M_{H^\pm}^4 s_{\beta-\alpha}^2 \ln \left(\frac{M_{H_0}^2}{\mu^2} \right) \\ & \quad \left. + 6M_{H^\pm}^2 M_t^2 s_{\beta-\alpha}^2 \ln \left(\frac{M_{H_0}^2}{\mu^2} \right) - 3M_t^4 s_{\beta-\alpha}^2 \ln \left(\frac{M_{H_0}^2}{\mu^2} \right) \right) \\ & - \frac{m_{12}^2 \tan \beta}{M_{h_0}^2 M_{H_0}^2} \left[(c_{\beta-\alpha}^2 M_{H_0}^2 + M_{h_0}^2 s_{\beta-\alpha}^2) \left(3c_{\beta-\alpha}^2 M_{h_0}^2 \ln \left(\frac{M_{h_0}^2}{\mu^2} \right) + M_{A_0}^2 \ln \left(\frac{M_{A_0}^2}{\mu^2} \right) \right. \right. \\ & \quad \left. \left. + 3M_{H_0}^2 s_{\beta-\alpha}^2 \ln \left(\frac{M_{H_0}^2}{\mu^2} \right) + 2M_{H^\pm}^2 \ln \left(\frac{M_{H^\pm}^2}{\mu^2} \right) \right) \right] \\ & + \frac{m_{12}^2 \tan \beta}{M_{h_0}^2 M_{H_0}^2} (c_{\beta-\alpha}^2 M_{H_0}^2 + M_{h_0}^2 s_{\beta-\alpha}^2) (3c_{\beta-\alpha}^2 M_{h_0}^2 + M_{A_0}^2 + 3M_{H_0}^2 s_{\beta-\alpha}^2 + 2M_{H^\pm}^2) \\ & + \frac{1}{M_{h_0}^2 M_{H_0}^2} \left[-2c_{\beta-\alpha}^2 M_{h_0}^2 M_{H_0}^4 s_{\beta-\alpha}^2 \ln \left(\frac{M_{H_0}^2}{\mu^2} \right) \right] \end{aligned}$$

$$\begin{aligned}
 & + c_{\beta-\alpha}^2 M_{h_0}^4 \ln \left(\frac{M_{h_0}^2}{\mu^2} \right) \left(2M_{h_0}^2 s_{\beta-\alpha}^2 + M_{H_0}^2 (3 - 2s_{\beta-\alpha}^2) \right) \\
 & + 2c_{\beta-\alpha}^2 M_{H_0}^6 s_{\beta-\alpha}^2 \ln \left(\frac{M_{H_0}^2}{\mu^2} \right) + M_{A_0}^2 M_{h_0}^2 M_{H_0}^2 \ln \left(\frac{M_{A_0}^2}{\mu^2} \right) \\
 & + 2M_{h_0}^2 M_{H_0}^2 M_{H^\pm}^2 \ln \left(\frac{M_{H^\pm}^2}{\mu^2} \right) + 3M_{h_0}^2 M_{H_0}^4 s_{\beta-\alpha}^2 \ln \left(\frac{M_{H_0}^2}{\mu^2} \right) \Big] \\
 & + c_{\beta-\alpha}^2 \left(-\frac{2M_{h_0}^4 s_{\beta-\alpha}^2}{M_{H_0}^2} - \frac{2M_{H_0}^4 s_{\beta-\alpha}^2}{M_{h_0}^2} + M_{h_0}^2 (2s_{\beta-\alpha}^2 - 3) + 2M_{H_0}^2 s_{\beta-\alpha}^2 \right) \\
 & - \left. M_{A_0}^2 - 3M_{H_0}^2 s_{\beta-\alpha}^2 - 2M_{H^\pm}^2 \right]
 \end{aligned} \tag{2.22}$$

For the on-shell renormalisation of the t quark δM_t^{os} the hierarchy of scales is different. The external momentum $p^2 = M_t^2$ has to be considered large in comparison with the b quark mass. The appropriate expansion is therefore a threshold expansion. For the on-shell counterterm we obtain

$$\begin{aligned}
 \delta M_t^{os} = \frac{e^2 M_t m_b^2 \tan^2 \beta V_{tb} V_{tb}^*}{128\pi^2 M_W^2 s_W^2} & \left(\frac{1}{\epsilon} - \gamma_E + 2 + \ln(4\pi) - \ln \left(\frac{M_{H^\pm}^2}{\mu_0^2} \right) \right. \\
 & \left. - \frac{M_{H^\pm}^2}{M_t^2} + \left(2\frac{M_{H^\pm}^2}{M_t^2} - \frac{M_{H^\pm}^4}{M_t^4} - 1 \right) \ln \left(1 - \frac{M_t^2}{M_{H^\pm}^2} \right) \right).
 \end{aligned} \tag{2.23}$$

The last counterterm required is $\delta M_{H^\pm}^{2,os}$. As in the t quark case, the momentum is considered to be large. The counterterm is extracted from

$$\delta M_{H^\pm}^{2,os} = \text{Re} \Sigma^{H^\pm} (M_{H^\pm}^2). \tag{2.24}$$

There are two types of contributions. First the contributions due to fermionic subloops. Here the case is the same as in the t quark renormalisation and an expansion in small m_b is applied. This ensures that the logarithms in m_b are of the same form as in the two-loop result. The relevant diagrams for the fermionic contributions can be found in Figure 2.2. The second contribution is due to Higgs loops, where the $\tan \beta$ originates in the Higgs couplings. In this contribution all particles in the loop have masses of the same scale. Therefore no expansion has been used for these diagrams. The relevant diagrams are shown in Figure 2.3. We used FormCalc [43] in combination with Package-X [71] to analytically check our results and LoopTools [43] for a numerical crosscheck of our FormCalc to Package-X interface.

2. The Two-Higgs-Doublet model

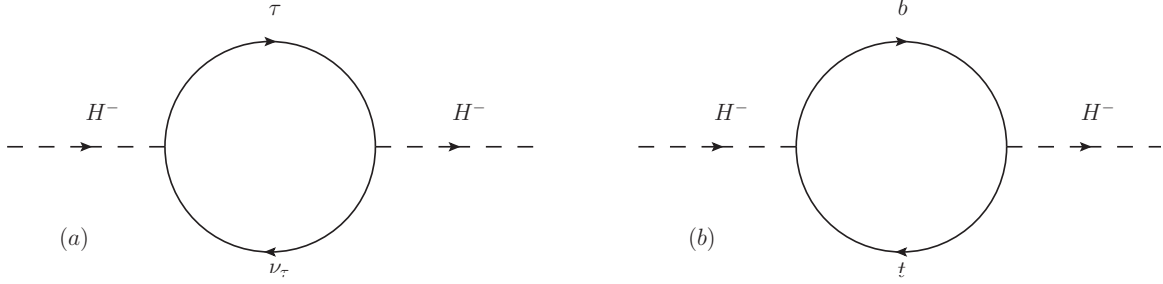


Figure 2.2.: Feynman diagrams contributing to the fermionic contributions of the charged Higgs mass counterterm $(\delta M_{H^\pm}^2)_\tau^{os}$ and $(\delta M_{H^\pm}^2)_b^{os}$.

We will list the final τ and b -quark contributions separately and therefore also write $\delta M_{H^\pm}^2 = (\delta M_{H^\pm}^2)_\tau^{os} + (\delta M_{H^\pm}^2)_b^{os} + (\delta M_{H^\pm}^2)_H^{os}$ for the contributions to the counterterm. The Higgs contribution $(\delta M_{H^\pm}^2)_H^{os}$ encompasses the $\tan^2 \beta$ terms due to Higgs couplings, which will also be important in the b quark result. The contributions to the counterterm are given by

$$(\delta M_{H^\pm}^2)_\tau^{os} = \frac{e^2 M_{H^\pm}^2 m_\tau^2 \tan^2 \beta}{32\pi^2 M_W^2 s_W^2} \left(\frac{1}{\epsilon} - \log \left(\frac{M_{H^\pm}^2}{\mu^2} \right) - \gamma_E + 2 + \log(4\pi) \right), \quad (2.25)$$

$$\begin{aligned} (\delta M_{H^\pm}^2)_b^{os} = & - \frac{3e^2 m_b^2 \tan^2 \beta V_{tb} V_{tb}^*}{32\pi^2 M_{H^\pm}^2 M_W^2 s_W^2} \left[\left(\frac{2}{\epsilon} - 2\gamma_E + 3 \right) M_{H^\pm}^4 x - M_{H^\pm}^4 (x^2 + 2) \ln(x) \right. \\ & + M_{H^\pm}^4 (x-1)^2 \ln(1-x) + 2M_{H^\pm}^4 x \ln(4\pi) - 2M_{H^\pm}^4 x \ln(M_{H^\pm}^2) \left. \right] \\ & - \frac{3e^2 m_b^2 M_{H^\pm}^2 \tan^2 \beta}{32\pi^2 M_W^2 s_W^2} \left(-\frac{1}{\epsilon} + \ln(M_{H^\pm}^2) + \gamma_E - 2 - \ln(4\pi) \right). \end{aligned} \quad (2.26)$$

As mentioned above the H contribution does not allow for an expansion. The contributing diagrams are shown in Figure 2.3. Thus we present the counterterm in terms of the Passarino-Veltman integrals [70]

$$\begin{aligned} (\delta M_{H^\pm}^2)_H^{os} = & \frac{e^2 \tan^2 \beta}{128 M_{h_0}^2 M_{H_0}^2 M_W^2 \pi^2 s_W^2} \left[\right. \\ & - 2 \left[2c_{\beta-\alpha}^2 m_{12}^2 M_{h_0}^2 + 2m_{12}^2 M_{H_0}^2 s_{\beta-\alpha}^2 \right. \\ & \left. \left. - c_{\beta-\alpha} (M_{h_0}^2 - M_{H_0}^2) (M_{A_0}^2 + M_{H^\pm}^2) s_{\beta-\alpha} \right] A_0(M_{A_0}^2) m_{12}^2 \right] \end{aligned}$$

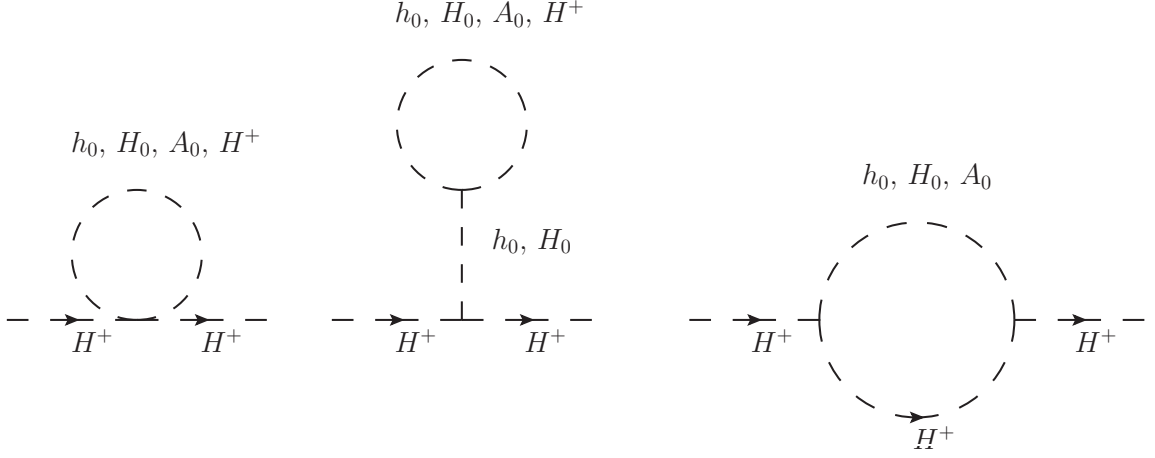


Figure 2.3.: Feynman diagrams contributing to the Higgs contribution of the charged Higgs mass counterterm $(\delta M_{H^\pm}^2)_H^{os}$. The $\tan \beta$ enhancement originates from the Higgs couplings.

$$\begin{aligned}
 & -c_{\beta-\alpha} \left[3c_{\beta-\alpha}^2 \left(-2M_{h_0}^4 + (M_{H_0}^2 - 2M_{H^\pm}^2) M_{h_0}^2 + 2M_{H_0}^2 M_{H^\pm}^2 \right) s_{\beta-\alpha} m_{12}^2 \right. \\
 & \quad + 6c_{\beta-\alpha}^3 M_{h_0}^2 m_{12}^4 + M_{h_0}^2 s_{\beta-\alpha} \left((11 - 5s_{\beta-\alpha}^2) M_{H_0}^2 + 2M_{h_0}^2 s_{\beta-\alpha}^2 \right) m_{12}^2 \\
 & \quad \left. - 2c_{\beta-\alpha} \left(m_{12}^4 \left(3s_{\beta-\alpha}^2 M_{h_0}^2 + M_{h_0}^2 - 6M_{H_0}^2 s_{\beta-\alpha}^2 \right) - M_{h_0}^4 M_{H_0}^2 \right) \right. \\
 & \quad \left. \right] A_0 \left(M_{h_0}^2 \right) \\
 & -s_{\beta-\alpha} \left[6c_{\beta-\alpha}^2 \left(2M_{h_0}^2 - M_{H_0}^2 \right) s_{\beta-\alpha} m_{12}^4 + c_{\beta-\alpha}^3 M_{H_0}^2 \left(5M_{h_0}^2 - 2M_{H_0}^2 \right) m_{12}^2 \right. \\
 & \quad + c_{\beta-\alpha} \left(6M_{H_0}^2 \left(M_{H_0}^2 + M_{H^\pm}^2 \right) s_{\beta-\alpha}^2 \right. \\
 & \quad \quad \left. \left. - M_{h_0}^2 \left(\left(3s_{\beta-\alpha}^2 + 11 \right) M_{H_0}^2 + 6M_{H^\pm}^2 s_{\beta-\alpha}^2 \right) \right) m_{12}^2 \right. \quad (2.27) \\
 & \quad \left. + 2M_{H_0}^2 s_{\beta-\alpha} \left(\left(3s_{\beta-\alpha}^2 - 1 \right) m_{12}^4 + M_{h_0}^2 M_{H_0}^2 \right) \right] A_0 \left(M_{H_0}^2 \right) \\
 & -2 \left[\left(4m_{12}^4 M_{h_0}^2 - M_{h_0}^4 M_{H_0}^2 \right) c_{\beta-\alpha}^2 + 4m_{12}^2 \left(M_{H_0}^2 - M_{h_0}^2 \right) M_{H^\pm}^2 s_{\beta-\alpha} c_{\beta-\alpha} \right. \\
 & \quad \left. + M_{H_0}^2 \left(4m_{12}^4 - M_{h_0}^2 M_{H_0}^2 \right) s_{\beta-\alpha}^2 \right] A_0 \left(M_{H^\pm}^2 \right) \\
 & + 2M_{h_0}^2 M_{H_0}^2 \left[\left(4s_{\beta-\alpha}^2 m_{12}^4 + c_{\beta-\alpha}^2 M_{h_0}^4 \right. \right. \\
 & \quad \left. \left. + 2c_{\beta-\alpha} \left(3M_{h_0}^2 + 2M_{H^\pm}^2 \right) s_{\beta-\alpha} m_{12}^2 \right) B_0 \left(M_{H^\pm}^2, M_{h_0}^2, M_{H^\pm}^2 \right) \right. \\
 & \quad \left. + \left[4c_{\beta-\alpha}^2 m_{12}^4 - 2c_{\beta-\alpha} \left(3M_{H_0}^2 + 2M_{H^\pm}^2 \right) s_{\beta-\alpha} m_{12}^2 \right. \right.
 \end{aligned}$$

$$+ M_{H_0}^4 s_{\beta-\alpha}^2 \left] B_0 \left(M_{H^\pm}^2, M_{H_0}^2, M_{H^\pm}^2 \right) \right] \Bigg],$$

which are defined as

$$A_0(m^2) = \frac{\mu^{2\epsilon}}{i\pi^{\frac{D}{2}} r_\Gamma} \int \frac{d^D q}{q^2 - m^2}, \quad (2.28)$$

$$B_0(p^2, m_0^2, m_1^2) = \frac{\mu^{2\epsilon}}{i\pi^{\frac{D}{2}} r_\Gamma} \int \frac{d^D q}{[q^2 - m_0^2][(q+p)^2 - m_1^2]}. \quad (2.29)$$

The analytic result has been evaluated with Package-X [71].

CHAPTER 3

$\tan \beta$ enhanced corrections to $b \rightarrow s\gamma$ in the Two-Higgs-Doublet Model of type II

The new matching calculation of the $\tan \beta$ enhanced contributions in the 2HDM will be presented in this chapter. The starting point is an introduction to effective field theory and the matching procedure for $b \rightarrow s\gamma$. Next we will review previous works on $b \rightarrow s\gamma$ starting with the standard model result. Here we will also present our first check of Medusa. The matching calculation of the next-to-leading order QCD contributions for $b \rightarrow s\gamma$ in the Standard Model, in which we found agreement with [12]. In Section 3.3 we will start investigating the 2HDMi, concentrating on the $\tan \beta$ enhanced contributions yet missing in the prediction of the branching ratio of $\bar{B} \rightarrow X_s\gamma$. As they are expected to be of the order of electroweak corrections, they become important only when the larger QCD corrections are already known. This is the case and we will start with reviewing previous works in the 2HDM. Next, the calculation of the $\tan \beta$ enhanced terms to $b \rightarrow s\gamma$ will be presented, starting with the τ contributions. The restriction to τ subloops simplifies the calculation and provides a gauge invariant subset of the complete $\tan \beta$ enhanced contribution. Based on this calculation we will remark on the treatment of γ_5 . In the last section, the b quark contributions will be discussed.

3.1. Introduction to effective field theory

3.1.1. A question of scales

Our understanding of physics relies on a chain of theories each valid for the description of a certain scale, i.e. energy region. We get a consistent picture of nature since the theories interlink and we can investigate limits in the border region to get redundant descriptions. To understand the properties of macroscopic objects, classical physics is a good approximation and we do not need to know about the position and interactions of each atom. Going to smaller and smaller length scales, i.e. higher energies, we first see the effects of quantum mechanics, for example in the energy levels of the atoms. The next link we encounter, when sufficient energy to create particle antiparticle pairs is available, is quantum field theory. Within quantum field theory the chain continues and is formalised in the concept of effective field theory.

When considering a physical problem at a certain scale it is enough to consider only the active degrees of freedom at that scale. This is possible since the effects of more massive particles are suppressed. An interesting case is when a process is forbidden at tree level in a low energy theory, which means that it will stand out as a rare event. If we want to keep only the active degrees of freedom in our theory, we can include these effects as new small interactions within the context of an effective field theory.

The first example of this was Fermi's theory of β decay. In quantum-electro-dynamics (QED) and quantum-chromo-dynamics (QCD), which govern the behaviour of quarks and electrons at energies below the electro-weak scale, there is no interaction that changes the flavour, i.e. the type of quark or lepton. Thus neither provides an explanation for the β -decay, $d \rightarrow ue^-\bar{\nu}_e$. Fermi thus introduced a new interaction to the Lagrangian to include this effect. Note that historically the theory was built from baryons and leptons. As we want to be able to describe the process in the full theory, the standard model, constituting of quarks and leptons, we will present the four fermion interaction on quark level.

$$\mathcal{L}_{\text{eff}} = -\frac{4G_F}{\sqrt{2}}V_{ud}(\bar{u}\gamma_\mu d_L)(\bar{e}\gamma^\mu\nu_{eL}) \quad (3.1)$$

Here the Fermi constant G_F is just a free parameter of the theory. The interaction in Equation (3.1) respects the symmetries of QED and QCD but is non-renormalisable,

since the coupling constant G_F has a negative mass dimension. To get the decay rate, the matrix element has to be calculated. For the process $d \rightarrow ue^- \bar{\nu}_e$ there is only the single vertex diagram with the operator above inserted. The tree level matrix element is given by

$$\mathcal{M}_{\text{eff}} = \frac{4G_F}{\sqrt{2}} V_{ud} (\bar{u}\gamma_\mu d_L) (\bar{e}\gamma^\mu \nu_{eL}) \quad (3.2)$$

As we understand today the β decay is mediated by a W boson with a much larger mass than the quarks and electrons involved. The part of the Standard Model responsible for the decay is

$$\mathcal{L}_W = \frac{g_2}{\sqrt{2}} V_{ij} \bar{u}_i \gamma^\mu \omega_- d_j W_\mu^- + \frac{g_2}{\sqrt{2}} \bar{l}_i \gamma^\mu \omega_- \nu_i W_\mu^+ + h.c., \quad (3.3)$$

which yields

$$\mathcal{M}_{\text{SM}} = \frac{g_2^2}{2} V_{ud} \frac{1}{p^2 - M_W^2} (\bar{u}\gamma_\mu d_L) (\bar{e}\gamma^\mu \nu_{eL}) \quad (3.4)$$

for the matrix element of the decay. Here p is much smaller than M_W and we can neglect it, hence obtaining

$$\mathcal{M}_{\text{SM}} = \frac{g_2^2}{2M_W^2} V_{ud} (\bar{u}\gamma_\mu d_L) (\bar{e}\gamma^\mu \nu_{eL}). \quad (3.5)$$

As the links of a chain overlap, so do the regions of viability of the effective theory and the standard model. Hence they have to yield the same result for predictions of measurable processes in this region, i.e. their results have to match. This matching is used to fix the coupling G_F of the effective theory, which is obtained by requiring the result in Equation 3.2 and Equation 3.4 are equal, yielding $\frac{4G_F}{\sqrt{2}} = \frac{g_2^2}{2M_W^2}$.

This is one example of a matching calculation. In general the couplings in the effective theory, like G_F in this example, are called Wilson coefficients. They contain all the information of the high scale in the problem. In the example above, these are the $SU(2)$ coupling g_2 and the mass M_W of the heavy degrees of freedom. The light degrees of freedom, i.e. the quark and lepton fields, are contained in the effective theory. They are part of the so called operator in the effective theory. This separation of scales is one of the advantages of treating problems within an effective field theory. In this case for example to get the actual decay rate we would have to calculate the matrix element of the quark current. The quarks are part of the nucleus and therefore strongly coupled, which means perturbation theory in small couplings breaks down. However in the

3. $\tan \beta$ enhanced corrections to $b \rightarrow s\gamma$ in the Two-Higgs-Doublet Model of type II

matching calculation perturbation theory is still viable since the matching is performed at the high scale where the strong coupling α_s is small enough. The separation of scales also prevents the appearance of large logarithms in the coefficient at the matching scale. When we are done with the matching at the high scale renormalisation group equations can be used to resum the large logarithms and evaluate the Wilson coefficient at the low scale. This improves the convergence of the perturbation series and thus the precision of our prediction.

The general approach can be summarised as follows. When investigating any low energy process in an effective field theory, first the order of the expansion of the high scale is fixed. This will constrain the mass dimension of the operators introduced into the Lagrangian. We then have to include all operators of up to this order, that respect the symmetries of the effective theory, with individual Wilson coefficients. Then there are two options. First the Wilson coefficients can be fixed from experiment. This approach is taken when considering the standard model as an effective theory and introducing higher dimensional operators to parametrize certain tensions in measurements. In the second approach, that we adapt, the Wilson coefficient is calculated in the matching with a proposed full theory.

3.1.2. Matching for $b \rightarrow s\gamma$

For the Lagrangian of the effective theory and the matching of $b \rightarrow s\gamma$ we follow the conventions of [12]. The Lagrangian is given by

$$\begin{aligned} \mathcal{L}_{eff} = & \mathcal{L}_{QCD \times QED}(u, d, s, c, b, e, \mu, \tau) \\ & + \frac{4G_F}{\sqrt{2}} [V_{us}^* V_{ub} (C_1^c Q_1^u + C_2^c Q_2^u) + V_{cs}^* V_{cb} (C_1^c Q_1^c + C_2^c Q_2^c)] \\ & + \frac{4G_F}{\sqrt{2}} \sum_{i=3}^{10} [(V_{us}^* V_{ub} + V_{cs}^* V_{cb}) C_i^c + V_{ts}^* V_{tb} C_i^t] Q_i \end{aligned} \quad (3.6)$$

The kinetic terms of the light quarks and leptons and their QED and QCD interactions are contained in $\mathcal{L}_{QCD \times QED}$. The operator basis Q_i is given by

$$\begin{aligned} Q_1^u &= (\bar{s}_L \gamma_\mu T^a u_L) (\bar{u}_L \gamma^\mu T^a b_L) \\ Q_2^u &= (\bar{s}_L \gamma_\mu u_L) (\bar{u}_L \gamma^\mu b_L) \\ Q_1^c &= (\bar{s}_L \gamma_\mu T^a c_L) (\bar{c}_L \gamma^\mu T^a b_L) \end{aligned}$$

$$\begin{aligned}
 Q_2^c &= (\bar{s}_L \gamma_\mu c_L) (\bar{c}_L \gamma^\mu b_L) \\
 Q_3 &= (\bar{s}_L \gamma_\mu b_L) \sum_q (\bar{q} \gamma^\mu q) \\
 Q_4 &= (\bar{s}_L \gamma_\mu T^a b_L) \sum_q (\bar{q} \gamma^\mu T^a q) \\
 Q_5 &= (\bar{s}_L \gamma_{\mu_1} \gamma_{\mu_2} \gamma_{\mu_3} b_L) \sum_q (\bar{q} \gamma^{\mu_1} \gamma^{\mu_2} \gamma^{\mu_3} q) \\
 Q_6 &= (\bar{s}_L \gamma_{\mu_1} \gamma_{\mu_2} \gamma_{\mu_3} T^a b_L) \sum_q (\bar{q} \gamma^{\mu_1} \gamma^{\mu_2} \gamma^{\mu_3} T^a q) \\
 Q_7 &= \frac{e}{g^2} m_b (\bar{s}_L \sigma^{\mu\nu} b_R) F_{\mu\nu} \\
 Q_8 &= \frac{1}{g} m_b (\bar{s}_L \sigma^{\mu\nu} T^a b_R) G_{\mu\nu}^a \\
 Q_9 &= \frac{e^2}{g^2} (\bar{s}_L \gamma_\mu b_L) \sum_l (\bar{l} \gamma^\mu l) \\
 Q_{10} &= \frac{e^2}{g^2} (\bar{s}_L \gamma_\mu b_L) \sum_l (\bar{l} \gamma^\mu \gamma_5 l).
 \end{aligned} \tag{3.7}$$

For the sake of the discussion of the next-to-leading-order QCD corrections to the matching, we will also need one of the equation of motion vanishing operators

$$Q_{35} = \frac{ie}{g^2} \left[\bar{s}_L \overleftarrow{\not{D}} \sigma^{\mu\nu} b_L F_{\mu\nu} - F_{\mu\nu} \bar{s}_L \sigma^{\mu\nu} \not{D} b_L \right] + Q_7. \tag{3.8}$$

The operators are normalised such that in the perturbative expansion of the Wilson coefficients

$$C_i^Q = \sum_{n=0}^{\infty} \left(\frac{g^2}{(4\pi)^2} \right)^n C_i^{Q(n)} \tag{3.9}$$

the order of the expansion corresponds with the loop order. This is why the operators that get their first contributions through an electroweak one-loop process are normalised by g^{-2} . In the expansion in the strong coupling in Equation (3.9) the second order terms have first been derived in [12] for the standard model while in the 2HDM they can be found in [15, 25, 24, 11]. The third order contributions, i.e. the next-to-next-to-leading-order QCD contributions, are also known and first presented in [66] in the standard model and in [45] for the 2HDM.

As the massless gluons are also part of the effective theory, their effects have to be taken into account on both sides of the matching. This leads to the need of renormalisation on the effective theory side. The Wilson coefficients, as the couplings of the

3. $\tan \beta$ enhanced corrections to $b \rightarrow s\gamma$ in the Two-Higgs-Doublet Model of type II

theory, are renormalised multiplicatively

$$C_i = Z_{ij} C_j. \quad (3.10)$$

Note that Z is a matrix that can mix the coefficients through renormalisation.

We however are looking at the $\tan \beta$ enhanced contributions in the Two-Higgs-Doublet Model of type II. This simplifies the situation, as to this order the operators above do not mix. It is therefore sufficient to calculate the Wilson coefficient $C_7^{Q(1)}$ to get a prediction, as it is the only operator contributing to $b \rightarrow s\gamma$ at leading order.

In the above notation the contributions we consider here are contributions to $C_i^{Q(1)}$, which can be written as

$$C_7^{Q(1)} = C_7^{Q(1,0)} + C_7^{Q(1,\tau)} + C_7^{Q(1,b)}. \quad (3.11)$$

We opted not to factorise the couplings, like for the QCD contribution in Equation (3.9), to make the $\tan \beta$ dependence in the final result explicit. The contribution $C_7^{Q(1,\tau)} \propto \frac{y_\tau^2}{(4\pi)^2}$ gets all $\tan \beta$ enhancement from the Yukawa coupling, $y_i = \frac{\tan \beta m_i}{v}$. The coefficient $C_7^{Q(1,b)} \propto \tan^2 \beta$ receives contributions purely due to the b quark Yukawa coupling as well as mixed contributions, where the $\tan \beta$ terms in the Higgs couplings provides one power of $\tan \beta$.

There are different possibilities to do the matching. The Wilson coefficient has only a dependence on the parameters of the high scale, it cannot depend on the kinematics chosen for the matching. The two notable possibilities are off-shell matching, as done in [12] and in Section 3.2 to check their results, and on-shell matching, as we will use for the matching of $C_7^{Q(1,i)}$ in Sections 3.3.2 and 3.3.4. This dictates the basis of Dirac structures used to describe the matrix elements, as we will see in Equation (3.12) and Equation (3.13).

The advantage of the off-shell basis is that no on-shell integrals have to be evaluated, thus making the calculation in the full theory less cumbersome. As a trade off the operator basis in the effective theory has to be extended by equation of motion vanishing operators. These operators do not contribute on-shell but describe the off-shell structure in the effective theory. As for higher loop calculations the additional complications by considering on-shell integrals outweigh the added complications in the matching this has been chosen references [12, 66, 45].

For our calculation, presented in Sections 3.3.2 and 3.3.4, we chose on-shell matching

however. Since it is possible to expand in small external momenta, the most complicated two-loop integral is a vacuum integral, independent of the external momenta. Through the asymptotic expansion [76] a small number of one-loop on-shell integrals are introduced. As the s quark is considered massless most of them have to be evaluated at $k^2 = 0$. A full list of required one-loop integrals, that have been solved in D dimensions, can be found in Section 4.4.1. In testing our approach was helpful as the full theory result is an on-shell amplitude and thus a physically meaningful object. Thus the cancellation of all divergences has to happen in the full theory result already. For the calculation of the Wilson coefficient in the matching this is not required as IR divergences can cancel by appearing both on the full theory side and the effective theory side of the matching equation.

Let us first review the off-shell basis. Again, we follow the notation of [12] to define the basis elements as

$$S_j = \left(\gamma_\mu \not{p} \not{k}, \gamma_\mu (p \cdot k), \gamma_\mu p^2, \gamma_\mu k^2, \not{p} k_\mu, \not{p} p_\mu, \not{k} p_\mu, \not{k} k_\mu, m_b \not{k} \gamma_\mu, m_b \gamma_\mu \not{k}, m_b \not{p} \gamma_\mu, m_b \gamma_\mu \not{p}, M_W^2 \gamma_\mu \right)_j. \quad (3.12)$$

Here p denotes the incoming b -quark momentum and k is the outgoing photon momentum. This basis is used to express both the result of the full theory and the effective theory off-shell Green's functions. We will elaborate in Section 3.2, where we confirmed the results of the unrenormalised off-shell Green's functions given in [12].

In the on-shell case, equations of motions can be used to reduce the number of basis elements. The resulting basis is defined as

$$U_j = \left(m_b^2 \gamma_\mu, m_b p_\mu \right). \quad (3.13)$$

We used this basis in the calculations presented in Sections 3.3.2 and 3.3.4.

Regardless of the basis, the matching is always between renormalised objects. For us this only means that the full theory result has to be renormalised as there are no corrections of the effective theory side to the order we investigate.

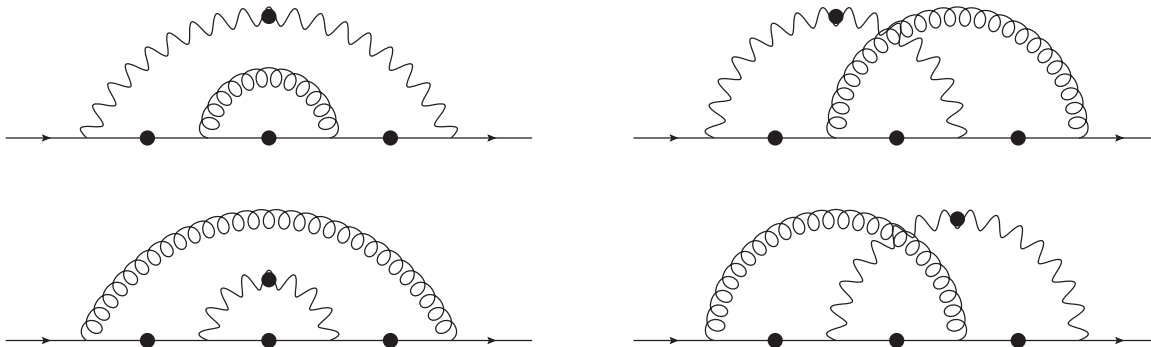


Figure 3.1.: Two-loop diagrams calculated in the check with [12]. The black dots are the points the external photon has to be attached. The loopy line represents the gluon, while the wavy line is the W.

3.2. Status of the SM predictions and first checks of Medusa

Due to the importance of $b \rightarrow s\gamma$ a lot of work went into the standard model prediction. A summary can be found in [65], where the authors present the current Standard Model prediction

$$\mathcal{B}_{s\gamma}^{SM} = (3.36 \pm 0.23) \times 10^{-4} \quad \text{for } E_0 = 1.6 \text{ GeV.} \quad (3.14)$$

where E_0 is the cut on the photon energy. The prediction includes the calculation of the matching up to next-to-next-to-leading order in the QCD corrections [66] and next-to-leading order in the EW corrections [39]. In the mixing NNLO corrections [29] are available as well.

On the experimental side there have been several measurements of the CP- and isospin-averaged $\bar{B} \rightarrow X_s\gamma$ branching ratio at CLEO [21], BaBar [61, 6, 60, 59] and Belle [2, 62, 1]. An average of these measurements has been provided by the Heavy Flavour Averaging Group [5], and reads

$$\mathcal{B}_{s\gamma}^{\text{exp}} = (3.32 \pm 0.15) \times 10^{-4} \quad \text{for } E_0 = 1.6 \text{ GeV.} \quad (3.15)$$

Because of the agreement between the prediction and measured value, investigating effects from the Two-Higgs-Doublet Model will result in a stringent lower bound on the mass of the charged Higgs boson.

As a first check of the Mathematica package Medusa, see Section 4, we calculated the

next-to-leading-order QCD matching corrections in the Standard Model and confirmed the result of [12], in which the two-loop result for the off-shell unrenormalised Green's function is presented explicitly. This provides the opportunity to directly check the result of the loop calculation, which makes an ideal first check of our method and implementation. The contributing diagrams are shown in Figure 3.1. We follow the notation of [12] and expressed the two-loop contributions $G^{(2)}$ to the off-shell Green's function as

$$G^{(2)} = i \frac{4G_F}{\sqrt{2}} \frac{eg^2\omega_+}{(4\pi)^4} N_\epsilon^{(2)} \left[(V_{us}^* V_{ub} + V_{cs}^* V_{cb}) \sum_{j=1}^{13} h_j^{(2)} S_j + V_{ts}^* V_{tb} \sum_{j=1}^{13} f_j^{(2)}(x) S_j \right]. \quad (3.16)$$

The S_j denote the elements of the off-shell basis defined in Equation (3.12), while e and g stand for the QED and QCD coupling respectively. $N_\epsilon^{(2)}$ is defined as

$$N_\epsilon^{(2)} = 1 - 2\epsilon\kappa + \epsilon^2 \left(\frac{\pi^2}{6} + 2\kappa^2 \right), \quad (3.17)$$

with $\kappa = \gamma_E - \ln(4\pi) + \ln(M_W^2/\mu_0^2)$.

The matching on Q_7 does not require calculating all coefficients h_i and f_i , since most of the Dirac structures describe only the off-shell structure and thus match on equation-of-motion-vanishing operators. When expressing the matrix element on the effective theory side by the off-shell basis in Equation (3.12) it becomes apparent that only the coefficients h_2 and h_{10} are required to fix C_7^c . They get contributions from only two operators

$$h_2 = -4A_{35}^c \quad h_{10} = A_7^c + A_{35}^c, \quad (3.18)$$

where A stand for the renormalised coefficients, i.e.

$$A_7^c = Z_\psi Z_g^{-2} \left[Z_m \sum_i C_i^c Z_{i7} + (Z_m - 1) \sum_i C_i^c Z_{i(35)} \right]. \quad (3.19)$$

We determined the two-loop coefficients h_i and f_i to be

$$\begin{aligned} h_2^{(2)} &= -\frac{272}{81\epsilon} - \frac{3740}{243}, & h_8^{(2)} &= -\frac{128}{81\epsilon^2} - \frac{1088}{243\epsilon} - \frac{314}{729} - \frac{128\pi^2}{243}, \\ h_{10}^{(2)} &= \frac{20}{9\epsilon} + \frac{92}{27}, \\ f_2^{(2)}(x) &= \frac{1}{\epsilon} \left[\frac{8x(-45x^3 - 34x^2 + 53x - 10)}{9(x-1)^5} \ln x + \frac{4(x^4 + 641x^3 - 501x^2 + 83x - 8)}{27(x-1)^4} \right] \end{aligned}$$

3. $\tan \beta$ enhanced corrections to $\mathbf{b} \rightarrow \mathbf{s}\gamma$ in the Two-Higgs-Doublet Model of type II

$$\begin{aligned}
& + \frac{8x(7x^3 - 69x^2 + 61x - 14)}{9(x-1)^4} \text{Li}_2\left(1 - \frac{1}{x}\right) \\
& + \frac{4x(45x^3 + 34x^2 - 53x + 10)}{3(x-1)^5} \ln^2 x \\
& + \frac{4(-6x^5 - 4497x^4 + 2622x^3 + 811x^2 - 638x + 88)}{81(x-1)^5} \ln x \\
& + \frac{2(-719x^4 + 35822x^3 - 35073x^2 + 11492x - 1802)}{243(x-1)^4}, \\
f_8^{(2)}(x) = & \frac{1}{\epsilon} \left[\frac{4(243x^4 + 486x^3 - 419x^2 + 130x - 8)}{81(x-1)^5} \ln x \right. \\
& \left. + \frac{2(-185x^4 - 3313x^3 + 369x^2 + 905x - 368)}{243(x-1)^4} \right] \\
& + \frac{4(32x^4 + 283x^3 - 135x^2 - 70x + 64)}{81(x-1)^4} \text{Li}_2\left(1 - \frac{1}{x}\right) \\
& + \frac{2(-243x^4 - 486x^3 + 419x^2 - 130x + 8)}{27(x-1)^5} \ln^2 x \\
& + \frac{2(370x^5 + 7933x^4 - 1370x^3 - 683x^2 + 238x - 8)}{243(x-1)^5} \ln x \\
& + \frac{2(-3301x^4 - 20714x^3 + 4182x^2 + 202x + 191)}{729(x-1)^4}, \\
f_{10}^{(2)}(x) = & \frac{1}{\epsilon} \left[\frac{2x(36x^2 + x - 10)}{9(x-1)^4} \ln x + \frac{11x^3 - 169x^2 + 132x - 28}{9(x-1)^3} \right] \\
& + \frac{2x(-15x^3 + 8x^2 - 21x + 10)}{9(x-1)^4} \text{Li}_2\left(1 - \frac{1}{x}\right) + \frac{x(-36x^2 - x + 10)}{3(x-1)^4} \ln^2 x \\
& + \frac{-22x^4 + 396x^3 - 377x^2 + 142x - 16}{9(x-1)^4} \ln x \\
& + \frac{31x^3 - 1071x^2 + 630x - 112}{54(x-1)^3}.
\end{aligned} \tag{3.20}$$

Our results are in agreement with those of [12, Eq. (65)]. Note that the diagrams relevant here, shown in Figure 3.1, lead to two-loop integrals with one massless propagator, due to the gluon. In this case our solution of the tensorial two-loop vacuum integral in Equation (4.32) does not contain any expansion. This fact enables us to analytically check the result.

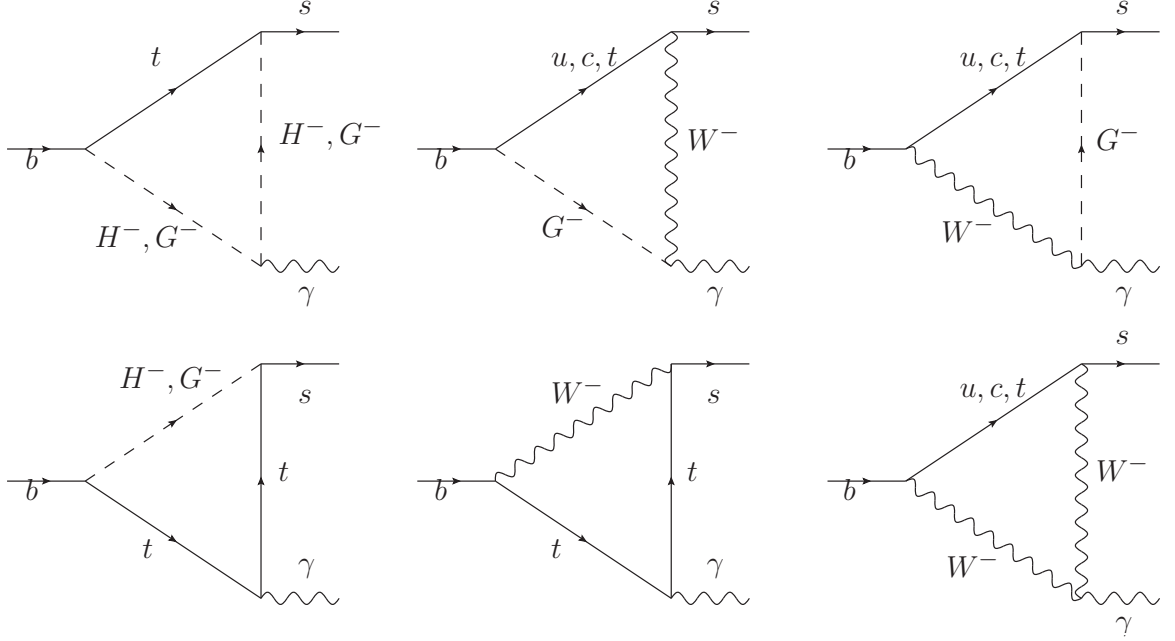


Figure 3.2.: The one-loop diagrams that constitute the leading order contribution to $b \rightarrow s\gamma$.

3.3. $b \rightarrow s\gamma$ in the Two-Higgs-Doublet Model

This section is devoted to the discussion of the $\tan^2 \beta$ enhanced contribution to $b \rightarrow s\gamma$. We will first review the current status of the theory prediction and its uncertainty. We then move on to presenting our result splitting it in two sections. In Section 3.3.2 we analyse the τ contributions, which we will use to investigate the dependence on the treatment of γ_5 in Section 3.3.3. In Section 3.3.4 we investigate the contribution coming from the b quark.

3.3.1. Status

The leading order contribution to $b \rightarrow s\gamma$ are the one-loop contributions shown in Figure 3.2. The result is given by

$$\begin{aligned}
 C_7^{c(1,0)} &= \frac{23}{36}, \\
 C_7^{t(1,0)} &= \frac{x_W(7 - 5x_W - 8x_W^2)}{24(x_W - 1)^3} + \frac{x_W^2(-2 + 3x_W) \ln x_W}{4(x_W - 1)^4}
 \end{aligned}$$

3. $\tan \beta$ enhanced corrections to $b \rightarrow s\gamma$ in the Two-Higgs-Doublet Model of type II

$$\begin{aligned}
& + \frac{x_{H^\pm}(3 - 5x_{H^\pm})}{12(x_{H^\pm} - 1)^2} + \frac{x_{H^\pm}(-2 + 3x_t)}{6(x_{H^\pm} - 1)^3} \ln x_{H^\pm} \\
& + \frac{x_{H^\pm}(7 - 5x_{H^\pm} - 8x_{H^\pm}^2)}{72 \tan^2 \beta (x_{H^\pm} - 1)^3} + \frac{x_{H^\pm}^2(-2 + 3x_{H^\pm})}{12 \tan^2 \beta (x_{H^\pm} - 1)^4} \ln x_{H^\pm},
\end{aligned}$$

where $x_i = \frac{M_t^2}{M_i^2}$. The light quark part C_7^c does not receive any contribution from diagrams with the charged Higgs-boson, since we neglect their masses $m_u = m_c = 0$. An important feature of this result in light of the following discussion is that the $\tan \beta$ dependence has the form $(\tan \beta)^{-2}$. This means that in the interesting case of large $\tan \beta$ the prediction is to a very good approximation independent of $\tan \beta$, since the $\tan \beta$ independent term dominates the prediction. Since the H^\pm contributions only enhance the prediction, this fact allows for a $\tan \beta$ independent lower bound on the charged Higgs mass, obtained by taking the limit $\tan \beta \rightarrow \infty$. In the Two-Higgs-Doublet Model the QCD corrections in the matching are known to next-to-next-to-leading order [45]. Due to this high precision this process is the source of the strongest bound on the charged Higgs mass $M_{H^\pm} > 570 - 800 \text{ GeV}$ [67], for intermediate to large $\tan \beta < 60$. In this region the bound is $\tan \beta$ independent in good approximation. For even larger values of $\tan \beta$, bounds from $B \rightarrow \tau\nu$ are stronger [4]. Our goal is to lift the $\tan \beta$ independence of the prediction by considering the $\tan^2 \beta$ enhanced terms due to the Yukawa couplings of the τ and the b quark and large Higgs self-couplings.

3.3.2. $m_\tau^2 \tan^2 \beta$ contributions to $b \rightarrow s\gamma$ in the 2HDM

The first contributions we calculated are characterised by τ -loops and yield a result proportional to $m_\tau^2 \tan^2 \beta$. The leading order result in Equation (3.21) does not have a $\tan^2 \beta$ term, since the $\tan \beta$ from the b quark Yukawa coupling and the $\cot \beta$ from the t quark Yukawa coupling cancel. When analysing the diagrams containing a τ sub-loop and contribute to the leading $\tan^2 \beta$ term, there are two classes to be considered. In the first class the sub-loop mixes H^- and W^- , hence avoiding the $\cot \beta$ of the t quark Yukawa coupling, while introducing one $\tan \beta$ through the τ Yukawa coupling. In the second class, both $\tan^2 \beta$ originate from the τ Yukawa coupling. This simplifies the calculation, since the τ sub-loop required to generate the m_τ^2 leaves us with only the 34 diagrams shown in Figure 3.3.

Diagrams with mixing self-energies on external lines, i.e. diagrams 6 – 15 in Figure 3.3, are taken into account as proper diagrams, as discussed in [63]. Even though

they are not one-particle irreducible diagrams, their contribution does not go into the LSZ factor. The reason is that the propagator to cut is not on-shell, due to the mass difference of the mixing quarks. Thus it does not contribute to the one-particle pole of the propagator and does not have to be resummed into the Dyson series.

It is also possible to entirely omit self-energy diagrams for the extraction of the Wilson coefficient $C_7^{(1,\tau)}$ if the amplitude is projected on the correct Dirac structure. For on-shell matching this is

$$m_b p_\mu \bar{s}_L(k_2, 0) \cdot b_R(p, m_b) \quad (3.21)$$

where p is the incoming momentum of the b quark. However, we chose to keep the self-energy diagrams, as the cancellation of contributions that do not match on Q_7 provides an important cross-check. This amounts to checking the Ward identity for the amplitude.

The restriction to τ contributions also simplifies the renormalisation. For the one-loop contribution the only $\tan\beta$ dependence drops off as $\tan^{-2}\beta$ and is a numerically irrelevant correction to the dominant constant term in the interesting region of large $\tan\beta$, see Equation (3.21). Therefore to contribute to the $\tan^2\beta$ term, the counterterm itself has to be proportional to $\tan^2\beta$. The only counterterm that fulfils this restriction is the mass counterterm to the charged Higgs boson mass $(\delta M_{H^\pm})_\tau^{os}$ given in Equation (2.25), which receives the $m_\tau^2 \tan^2\beta$ dependence through the Yukawa coupling in a $\tau - \nu_\tau$ loop.

This calculation provided the second test of our package Medusa, that will be presented in Section 4, where technical details of the calculation, as the solution of the two-loop integral and asymptotic expansion, will be addressed.

Due to the differences in scales of $M_i \in M_{H^\pm}, M_W, M_t$ and the external momenta $p \sim k \sim m_b \ll M_i$, with p denoting the incoming momentum of the b quark and k being the outgoing momentum of the photon, we can expand in small external momenta. It suffices to consider the leading order term of this expansion, since the expansion parameter $\bar{m}_b(M_W)^2/M_W^2 = 0.0012$ is very small. The effects of higher order corrections would be matched on dimension 8 operators, which are insignificant for $b \rightarrow s\gamma$. Thus the integrals to be considered are vacuum two-loop integrals for which a closed formula is given in Section 4.4. While we neglect the masses of the lighter u, d, s and c quarks, there is still the question of how to treat the particles that have a mass of the scale of

3. $\tan \beta$ enhanced corrections to $b \rightarrow s \gamma$ in the Two-Higgs-Doublet Model of type II

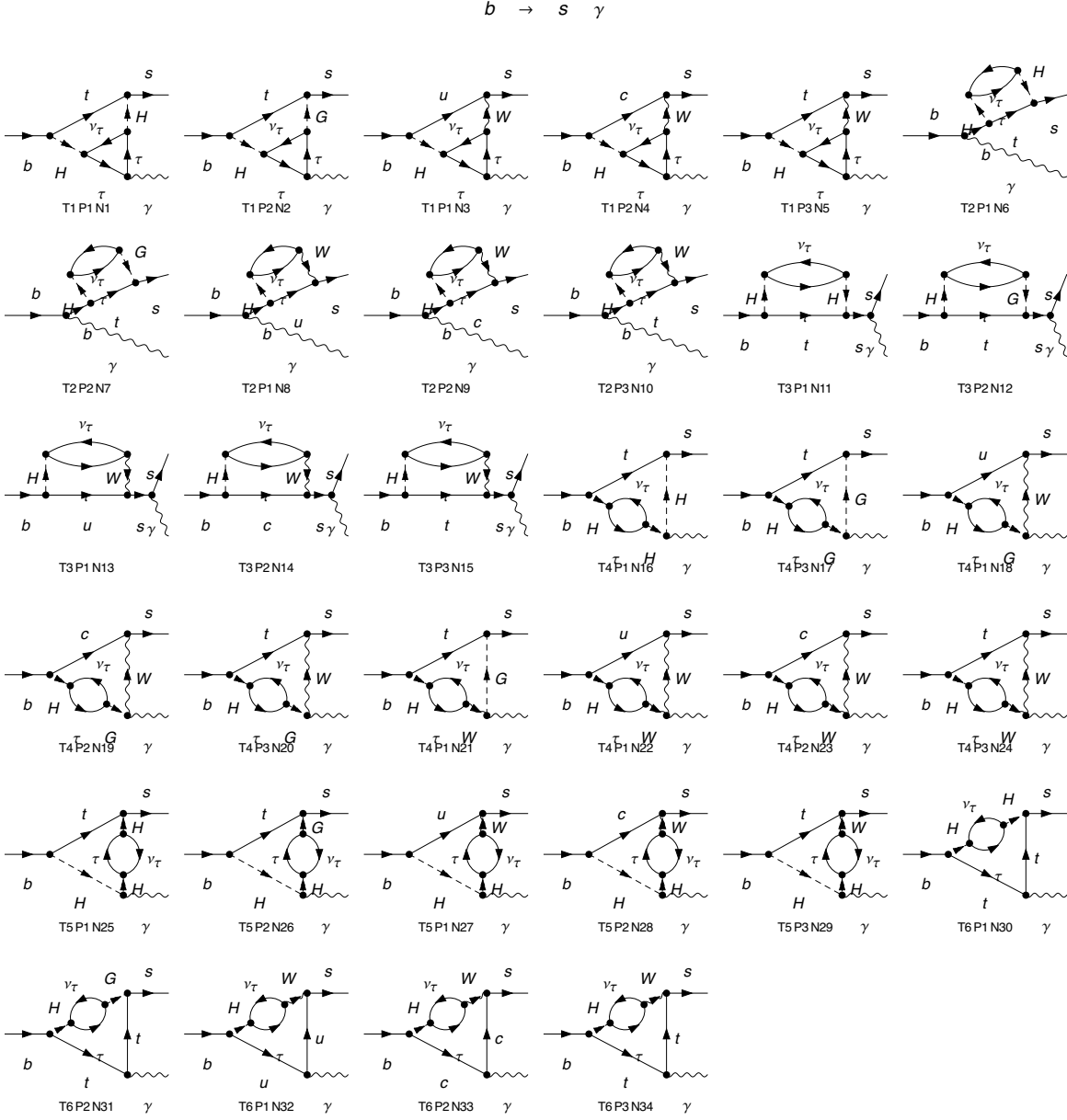


Figure 3.3.: All diagrams contributing to $m_\tau^2 \tan^2 \beta$. The leading order has no $\tan \beta$, since $\tan \beta$ from the bottom Yukawa and $\cot \beta$ from the top Yukawa cancels. There are two classes of diagrams involving $\tan \beta$. Firstly, the $\cot \beta$ associated with the top Yukawa coupling can be replaced by the insertion of a subloop mixing the H^\pm to W^\pm or G^\pm . This gives one $\tan \beta$ from the bottom Yukawa-coupling and one from the τ Yukawa-coupling. Secondly, one can just introduce two new powers of $\tan \beta$ by τ -Yukawa couplings to the H^\pm .

the external momenta: m_b and m_τ . To check our method, we performed this calculation in two ways.

First we set all instances of m_τ in loops to zero. Doing so produces infrared (IR) divergences in single diagrams, which we regularised dimensionally. A meaningful result for the physical on-shell matrix element needs to be free of any divergences. In our calculation all IR and ultraviolet (UV) divergences of single diagrams cancel in the sum, which constitutes a strong check for our result.¹

The second calculation has been done without setting $m_\tau = 0$. Since $m_\tau \sim m_b \sim p$ is of the same small scale as the momenta in which we expand, factors of m_τ have to be taken into account in the expansion as well. If the expansion is performed naively by Taylor expansion of the propagators, new IR divergences are introduced, which can be avoided by the utilisation of the asymptotic expansion with the large mass procedure [77]. An introduction of the basic idea and our implementation will follow in Section 4.3.

Since we get the $\tan\beta$ from one bottom- and one τ -Yukawa-coupling, which come with the respective masses, and we need one spinflip of the τ , the leading order in the masses is $m_b m_\tau^2$. For matching on Q_τ we also need one power of the incoming momentum. Thus we have to expand to fourth order. As we will elaborate in Section 4.3, the naive Taylor expansion introduces infrared divergences. In the asymptotic expansion this spurious IR divergence is compensated by considering the different limits in all possible regions of integration space. This cancels the dimensionally regularised IR divergence and reintroduces the logarithmic dependence on m_τ . Hence utilizing the asymptotic expansion has the effect that what appeared as a dimensionally regularised IR divergence in the first method now appears as $\ln m_\tau^2$. In this approach an IR divergence of the final result would consist of a logarithmic divergence when setting the small masses and momenta to zero. As before the final result has to be free of all infrared divergences. That is, all logarithms of m_τ that appear in intermediate steps drop out in the sum. Both the massless result and the asymptotically expanded result yield the same value for the Wilson coefficient.

One issue that surfaced in the calculation is the dependence of the result on the treatment of γ_5 . This will be more thoroughly discussed in Section 3.3.3, where we will present the different schemes, including our results obtained in their application. The

¹A priori the result could have IR divergences for $m_\tau \rightarrow 0$ which match onto corresponding divergent terms in the effective theory, represented by $\bar{b} - s - \bar{\tau} - \tau$ operators. We have checked that these operators have either zero coefficients or zero matrix elements.

3. $\tan \beta$ enhanced corrections to $\mathbf{b} \rightarrow \mathbf{s}\gamma$ in the Two-Higgs-Doublet Model of type II

conclusion of this discussion is that for this calculation it is justified to use anticommuting γ_5 for all traces with even number of γ_5 . For traces with exactly one γ_5 the four dimensional trace condition is inserted, see Equation (3.30). The case of three γ_5 does not occur since one coupling in the fermionic triangle is always the vector coupling to the Photon.

As a further check, We also verified the consistency with the Ward identity. For this check we used the on-shell conditions only for the external quarks and allowed for the Photon to be off-shell. Replacing the polarisation vector with the Photon momentum yields zero for the amplitude, confirming the Ward identity. This provides also a strong check for the finite parts of the result.

The calculation was performed in a generic 't Hooft gauge. Thus we could as a final check confirm independence of the final result on the gauge parameter ξ_W . We performed the matching on-shell, expressing both the effective theory matrix element and the full theory matrix element in the on-shell basis defined in Equation (3.13). For the τ contributions to the Wilson coefficient C_7 we get

$$C_7^{(1,\tau)} = \frac{G_F m_\tau^2 \tan^2 \beta}{16\sqrt{2}\pi^2} \left(\frac{x_t}{3(1-x_t)^2} - \frac{x_t^2(3-7x_t+x_w+3x_t x_w) \ln x_t}{3(1-x_t)^3(x_t-x_w)} + \frac{x_t(-2+2x_t+3x_t^2) \ln^2 x_t}{3(1-x_t)^4} + \frac{x_t x_w \ln x_w}{(x_t-x_w)(1-x_w)} \right), \quad (3.22)$$

where $x_i = \frac{M_i^2}{M_{H^\pm}^2}$.

This result shows two interesting properties. First of all its magnitude compared to the leading order is surprisingly small. The largest effect can be achieved by choosing a low mass for the charged Higgs boson just above the current exclusion bounds, $M_{H^\pm} = 600\text{GeV}$, and large $\tan \beta = 60$. The ratio of the $\tan^2 \beta$ enhanced contribution compared to the leading order is

$$\frac{C_7^{(1,\tau)}}{C_7^{1,0}} = 5.2 \cdot 10^{-4} \quad (3.23)$$

This implies that when the Yukawa couplings are pushed to the unitarity limit, which is approximated by $y_b \sim y_\tau \sim 2$ and corresponds to $\tan \beta \sim 120$, its relative importance is still sub-percent, $\frac{C_7^{(1,\tau)}}{C_7^{1,0}} = 0.0025$.

When estimating the size of the contributions from the couplings and the $(16\pi^2)^{-1}$ suppression factor from the additional loop the result was expected to be much larger.

$M_W = 80.385 \pm 0.015 \text{GeV}$ [72]
$G_F = 1.1663787(6) \times 10^{-5} \text{GeV}^{-2}$ [72]
$M_{h_0} = 125.1 \pm 0.2 \text{GeV}$ [72]
$m_\tau = 1776.86 \pm 0.12 \text{MeV}$ [72]
$V_{ts} = 0.04 \pm 0.0027$ [72]
$V_{tb} = 1.021 \pm 0.032$ [72]
$\bar{m}_b(M_W) = 2.8767 \pm 0.0096 \text{GeV}$ [46, 23]

Table 3.1.: List of the values of the Standard Model parameters inserted.

Considering the three diagrams of Figure 3.4, the ratio of the couplings summarised in c , which also includes the suppression factors $(16\pi^2)^{-1}$ of the two-loop and the one-loop diagrams is given by

$$\begin{aligned} \frac{c_a}{c_b} &= \frac{y_\tau}{y_t} \frac{\alpha}{8\pi s_W^2} = \frac{m_\tau t_\beta^2}{M_t} \frac{\alpha}{8\pi s_W^2} = 0.05, \\ \frac{c_a}{c_c} &= \frac{y_\tau y_b}{16\pi^2} = \frac{m_\tau m_b t_\beta^2}{16\pi^2 v^2} = 0.0038, \end{aligned} \tag{3.24}$$

for $\tan\beta = 60$. When considering single diagrams this estimation turns out to be accurate and there are contributions in the percent level. However due, to cancellations, we remain with the very small result above.

It should be noted that the diagrams with mixing self-energy on external lines are up to 6 orders of magnitude larger than the final result. This is due to the cancellation of the m_b dependence due to the b quark propagator. If the analytical cancellation of these contributions is spoiled the remaining contribution has numerically large effects. With an incorrect treatment of γ_5 , for example, the cancellation is spoiled, leading to % level corrections of the one-loop prediction.

The other interesting property of the result is that the Barr-Zee type diagrams, that have the triangle subloop, are contributing less significantly than the diagrams with self-energy subloops.

3.3.3. Treatment of γ_5

In this section we give an overview of the problem of γ_5 in dimensional regularisation and present some of the proposed prescriptions to handle it. We used several schemes proposed in the literature to evaluate the leptonic contributions presented in Section 3.3.2.

3. $\tan \beta$ enhanced corrections to $b \rightarrow s\gamma$ in the Two-Higgs-Doublet Model of type II

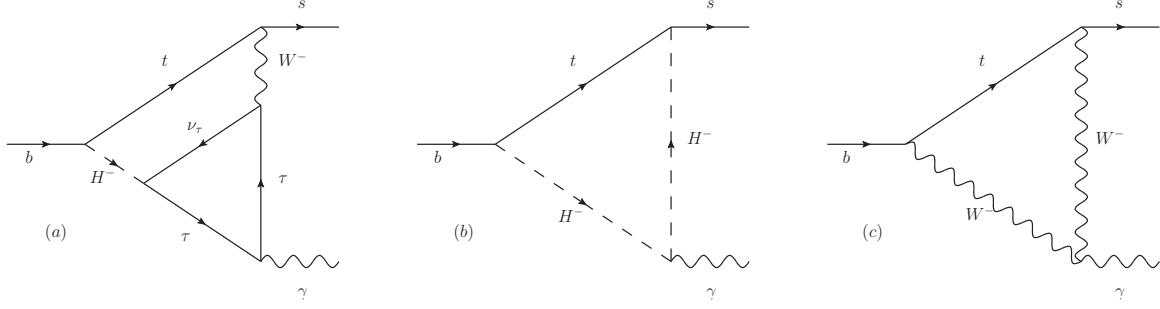


Figure 3.4.: Example diagrams from two- and one-loop level to discuss the relative importance of their contribution.

For the open fermion chain we use anticommuting γ_5 , which always yields the same result as using the 't Hooft Veltman [48] scheme with the inclusion of proper finite counter terms, as has been shown in [79].

For the closed fermion loops we checked several prescriptions. The main difference is the anti-commutation relations of γ_5 . In the anticommuting schemes

$$\{\gamma_\mu, \gamma_5\} = 0 \quad (3.25)$$

is used in D dimensions. With this definition an inconsistency arises, since it can be shown that all traces containing an odd number of γ_5 vanish. The necessary steps, following [26], can best be shown for the case of two γ matrices. The step-by-step derivation is given by

$$\begin{aligned} D \operatorname{tr} \gamma_5 \gamma_\mu \gamma_\nu &= \operatorname{tr} \gamma_5 \gamma_\mu \gamma_\nu \gamma_\lambda \gamma^\lambda \\ &= \operatorname{tr} \gamma^\lambda \gamma_5 \gamma_\mu \gamma_\nu \gamma_\lambda \\ &= -\operatorname{tr} \gamma_5 \gamma^\lambda \gamma_\mu \gamma_\nu \gamma_\lambda \\ &= -2g_\mu^\lambda \operatorname{tr} \gamma_5 \gamma_\nu \gamma_\lambda + 2g_\nu^\lambda \operatorname{tr} \gamma_5 \gamma_\mu \gamma_\lambda - D \operatorname{tr} \gamma_5 \gamma_\mu \gamma_\nu \\ &= -2\operatorname{tr} \gamma_5 \{\gamma_\mu, \gamma_\nu\} + (4 - D)\operatorname{tr} \gamma_5 \gamma_\mu \gamma_\nu \\ &= (4 - D)\operatorname{tr} \gamma_5 \gamma_\mu \gamma_\nu. \end{aligned} \quad (3.26)$$

First cyclicity of the trace is used. In the second step the anticommutation relation defined in Equation (3.25) is applied. Next the γ_μ have to be anticommutated back to the starting order. In the last step we used $\operatorname{tr} \gamma_5 = 0$, which can be proved analogously to Equation (3.26). This implies $(2 - D)\operatorname{tr} \gamma_5 \gamma_\mu \gamma_\nu = 0$. Since a result obtained in

dimensional regularisation has to be a meromorphic function in D , a stepwise definition of the trace for $D = 2$ and $D \neq 2$ is not possible and $\text{tr}\gamma_5\gamma_\mu\gamma_\nu = 0$ must hold for all D .

Using the same steps, namely cyclicity of the trace, anticommutivity of γ_5 and the anticommutation relations of the γ_μ , one can analogously show $(4 - D)\text{tr}\gamma_5\gamma_\mu\gamma_\nu\gamma_\lambda\gamma_\kappa = 0$. Requiring that the result of the trace is meromorphic implies $\text{tr}\gamma_5\gamma_\mu\gamma_\nu\gamma_\lambda\gamma_\kappa = 0$ for all D , which is inconsistent with the 4-dimensional result in Equation (3.30). To fix this inconsistency one has to drop one of the properties used. One choice is to drop the cyclicity property of the trace [55]. This results in the need to clarify how to read fermion traces.

In [48] 't Hooft and Veltman proposed to change the anticommutation relations of γ_5 , resulting in a scheme which has been proven to be consistent by Breitenlohner and Maison [16]. In this treatment, γ_5 is defined as an inherently 4-dimensional object

$$\gamma_5 = \frac{i}{4!}\epsilon^{\mu\nu\kappa\lambda}\gamma_\mu\gamma_\nu\gamma_\kappa\gamma_\lambda, \quad (3.27)$$

where ϵ is the 4-dimensional Levi-Civita Tensor.

For the commutation relations this means that γ_5 anticommutes only in 4-dimensions and commutes with the $(D - 4)$ -dimensional part of γ_μ

$$\begin{aligned} \{\tilde{\gamma}_\mu, \gamma_5\} &= 0, \\ [\hat{\gamma}_\mu, \gamma_5] &= 0. \end{aligned} \quad (3.28)$$

Here and in the following, \hat{T} denotes $(D - 4)$ -dimensional tensors while \tilde{T} denotes 4-dimensional tensors. Tensors $T = \hat{T} + \tilde{T}$ without any marks are considered to be D -dimensional. Since ϵ and γ_5 only exist in 4-dimension the $\tilde{}$ is implied. One important property to note is that the 4-dimensional tensors can be seen as projectors on the physical dimensions.

$$\begin{aligned} g_{\mu\nu}\tilde{g}^\nu{}_\lambda &= \tilde{g}_{\mu\lambda} \\ g_{\mu\nu}\hat{g}^\nu{}_\lambda &= \hat{g}_{\mu\lambda} \end{aligned} \quad (3.29)$$

For traces with γ_5 the 4-dimensional result is retained

$$\text{tr}\gamma_5\gamma_\mu\gamma_\nu\gamma_\lambda\gamma_\kappa = 4i\epsilon_{\mu\nu\lambda\kappa}. \quad (3.30)$$

3. $\tan \beta$ enhanced corrections to $b \rightarrow s\gamma$ in the Two-Higgs-Doublet Model of type II

The downside of the solution in Equation (3.28) of the inconsistency problem is that it violates Ward identities [16]. This can be fixed by introducing an appropriate finite renormalisation [26]. The QCD contributions to this finite renormalisation are considered up to three loops in [58], while in [17] contributions due to Higgs bosons in a Two Higgs Doublet Model are considered.

It is instructive to explicitly consider the form of the counterterms for the finite renormalisation. For the example of the non-singlet axial current, following the notation of [58], is given by

$$J_\mu^{5a}(x) = \bar{\psi}(x)\gamma_\mu\gamma_5 t^a\psi(x). \quad (3.31)$$

The renormalised axial vector current is given by

$$(J_\mu^{5a})_R = Z_5^{ns}(a)Z_{MS}^{ns}(a)(J_\mu^{5a})_B, \quad (3.32)$$

where Z_{MS}^{ns} encompasses the normal field renormalisation and Z_5 is the new counterterm. The subscripts B and R denote the currents of bare fields and renormalised fields respectively. The counterterm is fixed by the renormalisation condition

$$Z_5^{ns}R_{MS}\langle\bar{\psi}J_\mu^{5a}(0)\psi\rangle = R_{MS}\langle\bar{\psi}J_\mu^a(0)\psi\rangle\gamma_5. \quad (3.33)$$

The form of this possible counterterm should be kept in mind in the following.

After reviewing the basic ideas, we will look specifically at widely used schemes, remarking on their differences and presenting the results obtained for the calculation at hand.

Naive Dimensional Regularisation

Naive Dimensional Regularisation (NDR) implies using anticommuting γ_5 in D -dimensions, see Equation (3.25). While this is not a consistent scheme, it is sufficient for a lot of circumstances, namely those with even number of γ_5 in the traces. As pointed out in [52] truly anomalous cases have to be considered separately in 4-dimensions.

Note that the Tracer [51] implementation of NDR still uses the non zero trace of γ_5 in Equation (3.30). For the τ contributions to $b \rightarrow s\gamma$ presented in Section 3.3.2, this yields a finite and gauge parameter independent result that respects the Ward identity. Even though this is not a consistent treatment, the fact that it yields a sensible result can be understood when considering the traces that appear in the calculation. In

the triangle subloop one of the vertices is always a vector current. This means the maximum number of γ_5 in one trace is two. As has been pointed out in [79], it is always possible to use anticommuting γ_5 for traces with an even number of γ_5 . It is actually advisable to do so, since in the 't Hooft Veltman scheme, even for these cases, spuriously anomalous terms are created, which have to be removed by finite renormalisation. In [79] it is shown that using anticommuting γ_5 from the beginning yields the same result as in the 't Hooft Veltman scheme including the correct finite renormalisation. The remaining traces have just one γ_5 , meaning they can be solved by Equation (3.30) without using anticommutation relations.

Naive 't Hooft-Veltman scheme

In the 't Hooft Veltman prescription for γ_5 , the remaining issue is the definition of the vector and axial vector current. With the naive 't Hooft-Veltman scheme we denote the scheme that implements the usual 4-dimensional currents, i.e. $\bar{\psi}\gamma_\mu\psi$ and $\bar{\psi}\gamma_\mu\gamma_5\psi$ as the d dimensional currents. This is inconsistent since in the derivation of the Feynman rules for the axial vector current from the Lagrangian anticommutation relations are used to bring them in their usual form. It is instructive to look at an explicit example, following [52]. The leptonic part of the SM Lagrangian is given by

$$\mathcal{L}_l = \bar{l}_R i\gamma^\mu (\partial_\mu + ig'B_\mu) l_R + \bar{L}_l i\gamma_\mu \left(\partial^\mu + i\frac{g'}{2}B_\mu - ig\frac{\tau_a}{2}W_{\mu a} \right) L_l, \quad (3.34)$$

where L denotes the left-handed SU(2) doublet and l_R the right-handed SU(2) singlet

$$l_R = \omega_+ l, \quad L_l = \begin{pmatrix} \nu \\ l \end{pmatrix}_L = \omega_- \begin{pmatrix} \nu \\ l \end{pmatrix}. \quad (3.35)$$

The right- and left-handed projectors are given by

$$\omega_+ = \frac{1}{2}(1 + \gamma_5), \quad \omega_- = \frac{1}{2}(1 - \gamma_5). \quad (3.36)$$

Thus when reading off the Feynman rules we obtain

$$\bar{\psi}\omega_+\gamma_\mu\omega_-\psi = \bar{\psi}\gamma_\mu\omega_-\psi + \frac{1}{2}\bar{\psi}\{\gamma_\mu, \gamma_5\}\omega_-\psi, \quad (3.37)$$

which is just the standard left-handed current only if the anticommutator is set to zero.

3. $\tan \beta$ enhanced corrections to $\mathbf{b} \rightarrow \mathbf{s}\gamma$ in the Two-Higgs-Doublet Model of type II

In our calculation, all schemes based on the 't Hooft-Veltman prescription for γ_5 yield similar results. Therefore, we will jointly evaluate them in the end of this section.

The chirally improved 't Hooft-Veltman scheme

In [52] the chirally improved 't Hooft-Veltman scheme is defined as using the 't Hooft Veltman prescription given in Equation (3.28) in combination with consistent currents. When inserting the anticommutator of the 't Hooft-Veltman prescription, see Equation (3.28), $\{\gamma_\mu, \gamma_5\} = 2\hat{\gamma}_\mu\gamma_5$ we get

$$\bar{\psi}\omega_+\gamma_\mu\omega_-\psi = \bar{\psi}\gamma_\mu\omega_-\psi + \bar{\psi}\hat{\gamma}_\mu\gamma_5\omega_-\psi = \bar{\psi}\tilde{\gamma}_\mu\omega_-\psi. \quad (3.38)$$

Since the Lagrangian is consistently defined using chiral fields, this amounts to replacing both the axial vector as well as the vector current by the currents projected on the 4-dimensional subspace. This scheme has also been used in [20], where no closed Fermion loops appear. The authors also checked the NDR scheme for which they get the same results, consistent with the opening statement that for open fermion chains NDR and 't Hooft-Veltman yield the same results when including the finite renormalisation.

By considering the kinetic term one can also easily see the need for finite renormalisation, since there too the vector current is replaced by the 4-dimensional one.

$$i\bar{\psi}\hat{\gamma}_\mu\partial^\mu\psi = i\bar{\psi}\gamma_\mu\partial^\mu\psi - i\bar{\psi}\tilde{\gamma}_\mu\partial^\mu\psi \quad (3.39)$$

This points out a problem. When using 4-dimensional fermion propagators, dimensional regularisation does no longer work for fermion loops. Thus in order to regularize fermion loops dimensionally, the D -dimensional propagator has to be used and the $(D - 4)$ -dimensional term has to be included in the Lagrangian as an evanescent operator, vanishing in 4-dimensions. If this operator occurs in a divergent subgraph it will contribute to the finite result. The problem is that the $(D - 4)$ -dimensional operator is not of order ϵ but a tensor of rank $D - 4 = -2\epsilon$. To be properly considered as a counterterm a perturbative treatment has to be possible. This means, while this scheme works in practice, it cannot be seen as the last word as it too has conceptual issues.

Larin scheme

Another widely used scheme is the **Larin scheme** first applied in [58]. In this scheme the γ_5 definition of Equation (3.27) of 't Hooft and Veltman is used. Rather than an independent scheme for γ_5 it might be more fitting to refer to it as a technique to solve the traces, since the main idea is to replace all γ_5 by the following prescriptions for the axial vector and pseudoscalar currents

$$\begin{aligned} J_\mu^5 &= \frac{1}{2} \bar{\psi} (\gamma_\mu \gamma_5 - \gamma_5 \gamma_\mu) = \frac{i}{3!} \epsilon_{\mu\nu_1\nu_2\nu_3} \bar{\psi} \gamma_{\nu_1} \gamma_{\nu_2} \gamma_{\nu_3} \psi, \\ J^5 &= \bar{\psi} \gamma_5 \psi = \frac{i}{4!} \epsilon_{\nu_1\nu_2\nu_3\nu_4} \bar{\psi} \gamma^{\nu_1} \gamma^{\nu_2} \gamma^{\nu_3} \gamma^{\nu_4} \psi. \end{aligned} \quad (3.40)$$

Note that the symmetrisation in the axial vector current amounts to using the 4-dimensional current when seen in the 't Hooft-Veltman notation

$$J_\mu^5 = \frac{1}{2} \bar{\psi} (\gamma_\mu \gamma_5 + \tilde{\gamma}_\mu \gamma_5 - \hat{\gamma}_\mu \gamma_5) = \bar{\psi} \tilde{\gamma}_\mu \gamma_5 \psi. \quad (3.41)$$

The benefit of replacing the γ_5 is mostly that the trace can be solved using standard methods without the need to implement 4 and $(D-4)$ -dimensional objects. Instead the ϵ -tensors are regarded as projectors onto the 4-dimensional subspace to be evaluated after the loop integrals and their divergences have been taken care of. Note that in contrast to the chirally-improved 't Hooft-Veltman scheme, the vector currents are not touched.

In our test of different prescriptions, the usage of the replacement rules in Equation (3.40) and a 't Hooft Veltman prescription with the symmetrised axial vector current yielded the same result. It should also be stressed that the pure Larin scheme has therefore the same need for finite renormalisation than the 't Hooft Veltman schemes.

The Larin replacement rules, i.e. Equation (3.40), are also used in hybrid schemes, where traces of even numbers of γ_5 are treated naively. The replacement rule in Equation (3.40) is then only inserted for the last γ_5 , as in [83]. Note that in their treatment it is crucial to consistently choose the same reading point for all diagrams that appear. As shown in [9] there is an ambiguity when choosing different reading points. Since it is not obvious which reading point choice leads to the correct result, this scheme is dangerous. Effectively they choose to keep anticommutivity and the trace condition in Equation (3.30) and choose instead to give up the cyclicity of the trace, which causes the reading point ambiguity.

3. $\tan \beta$ enhanced corrections to $\mathbf{b} \rightarrow \mathbf{s}\gamma$ in the Two-Higgs-Doublet Model of type II

In the evaluation of the τ contributions the hybrid Larin scheme yielded the same result as the hybrid NDR scheme. This is due to the fact that the most complicated traces with odd number of γ_5 only involve exactly one γ_5 . For these traces the two schemes give the same result, since the difference of replacing the D -dimensional current with the 4-dimensional current is $(D - 4)$ -dimensional. As the trace results in an ϵ -tensor, a projector on the 4-dimensional subspace,

$$\text{tr}\gamma_\mu\gamma_\nu\gamma_\kappa\gamma_\lambda\gamma_5 - \text{tr}\gamma_\mu\gamma_\nu\gamma_\kappa\tilde{\gamma}_\lambda\gamma_5 = \text{tr}\gamma_\mu\gamma_\nu\gamma_\kappa\hat{\gamma}_\lambda\gamma_5 = 4i\epsilon_{\mu\nu\kappa\rho}\hat{g}^\rho_\lambda = 0 \quad (3.42)$$

the difference between the schemes is zero.

Evaluation of the 't Hooft-Veltman schemes

Next we will discuss the pure 't Hooft-Veltman schemes, that never use anticommuting γ_5 : naive, chirally improved 't Hooft-Veltman and Larin. For the purpose of this discussion it is implied to use the replacement rules defined in Equation (3.40) for all appearing γ_5 when we say Larin scheme. The Ward identity for the external Photon was not satisfied, regardless of the definition of the current in the Feynman rules. This is equivalent to saying that the result does not match on the operator Q_7 of Equation (3.8), since the Ward identity holds in the EFT. To understand this mismatch it is helpful to track the contributions of single diagrams. When setting the contributions of single diagrams to zero we found that the mismatch of all other diagrams vanishes if the $H^- - G^-$ -bubbles shown in Figure 3.5 are set to zero.

While it is true that without proper finite renormalisation the Ward identities can be violated in the 't Hooft Veltman schemes it is unclear that this is the case here. In [58, 17] counterterms for the axial current are introduced. They are of the form shown in Equation (3.32). These however cannot help us here since in this calculation we are only interested in the terms $\propto m_\tau^2 \tan^2 \beta$, which cannot be produced in a one-loop correction to a quark current. This issue can be investigated at one-loop level in $H^- \rightarrow \bar{t}b$. The important property to look at is the independence of the gauge parameter ξ in 't Hooft gauge of the $H^\pm - G^\pm$ and $H^\pm - W^\pm$ mixing diagrams.

When investigating the gauge dependence of the diagrams shown in Figure 3.6, the only remaining gauge dependence originates from the non-zero anticommutator in the

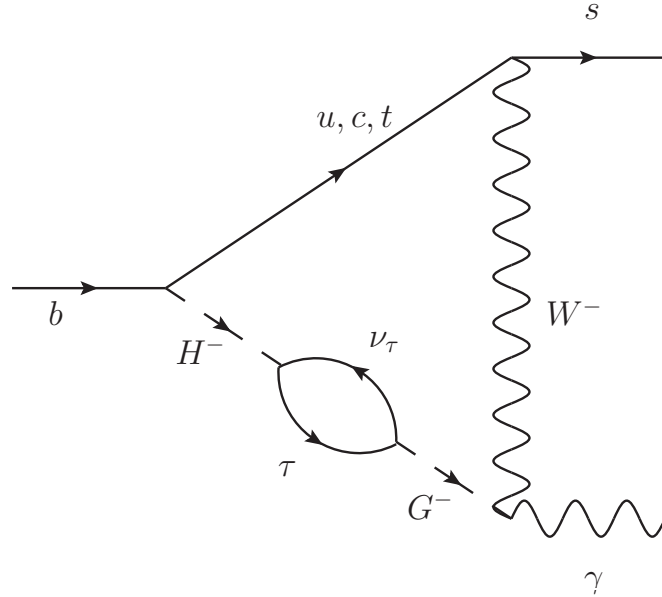


Figure 3.5.: Problematic diagram in the 't Hooft Veltman schemes.

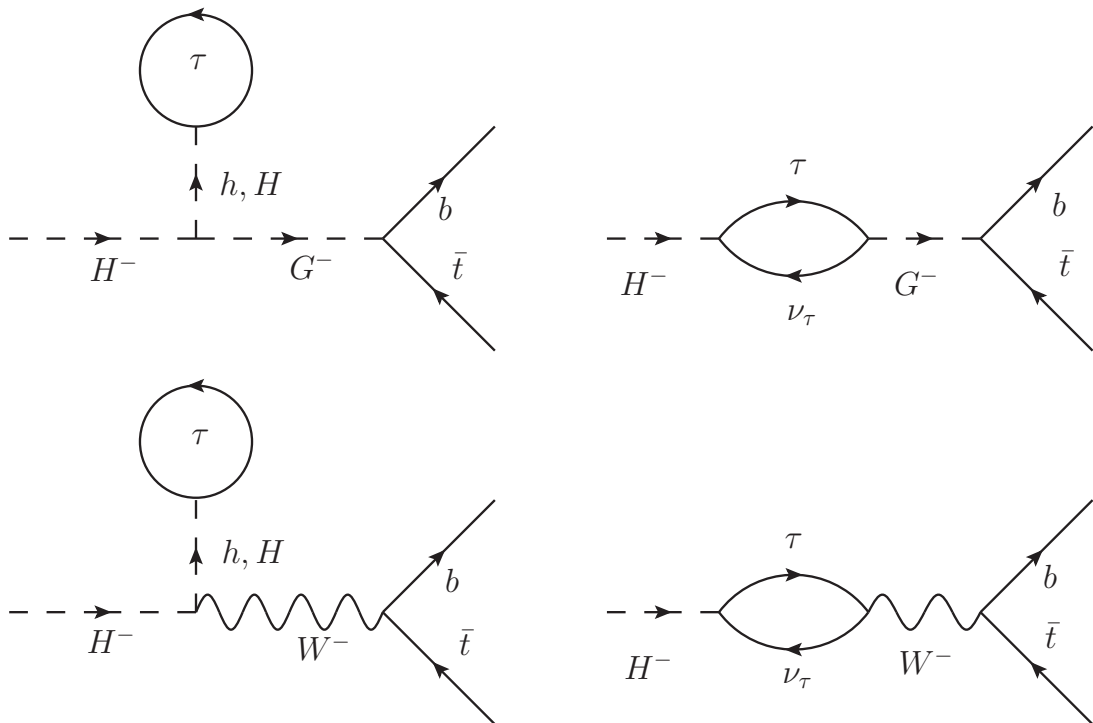


Figure 3.6.: Diagrams to investigate the gauge dependence of $H^- \rightarrow \bar{t}b$.

3. $\tan \beta$ enhanced corrections to $b \rightarrow s\gamma$ in the Two-Higgs-Doublet Model of type II

't Hooft-Veltman scheme:

$$A_\xi = \frac{e^3 \tan \beta V_{tb}^* m_\tau^2}{96\sqrt{2}M_W^3 \pi^2 s_W} \left(3m_\tau^2 - M_{H^\pm}^2\right) \frac{1}{p^2 - M_W^2 \xi_W} (m_b \bar{u} \cdot \omega_- \cdot v - m_t \bar{u} \cdot \omega_+ \cdot v) \quad (3.43)$$

Following [79], where the difference of 't Hooft-Veltman scheme and anticommuting γ_5 is explicitly investigated for bubbles, we also tried to introduce a mixing counterterm for HG.

$$\delta Z_{HG} = -\frac{e^2 m_\tau^2 (M_{H^\pm}^2 - 3m_\tau^2) \tan \beta}{96M_W^2 \pi^2 S_W^2} \quad (3.44)$$

While it is obviously possible to get rid of the gauge dependence at one-loop, since the problematic term is solely produced by the HG mixing diagram, the same counterterm does not fix the mismatch in the two-loop case. This is not surprising since the HG bubble appears as a subloop in other diagrams as well, see Figure 3.3.

To construct all necessary counterterms in the 't Hooft-Veltman scheme a more systematic investigation of the sub processes and their Slavnov Taylor identities would be required. Since the hybrid Larin and the hybrid NDR scheme yield consistent results, that respect the Ward identity, are finite and gauge parameter independent, all results given in this thesis are derived in these schemes.

3.3.4. The $\tan^2 \beta$ enhanced quark contributions to $b \rightarrow s\gamma$ in the 2HDM

A more important part of the $\tan^2 \beta$ enhanced contributions is due to the Yukawa coupling of the bottom quark. We split the contribution in two parts CKM suppressed and unsuppressed. As we are dealing with small corrections to the leading order already, additional CKM suppression renders the contributions numerically insignificant. Thus we will consider only the unsuppressed contributions. The contribution has two parts. First the part proportional to y_b^2 , i.e. both powers of $\tan \beta$ originate in the Yukawa coupling of the b quark. The 167 diagrams belonging to this part are presented in Appendix A. Compared to the leptonic case there are more classes of diagrams, since the restriction to closed fermionic subloops is lifted. This has the notable consequence that diagrams with triple scalar couplings from the Higgs-potential can occur. As mentioned in Section 2.1 the triple Higgs coupling can also be $\tan \beta$ enhanced in our parametrisation. The 410 diagrams corresponding to this case can be found in Ap-

pendix B.

It is not possible to split the self-coupling contributions from the pure Yukawa contributions, as the separate parts are not finite on their own. Due to the possible $1/\epsilon^2$ pole in single diagrams both the pure Yukawa contribution and the contribution due to triple Higgs couplings produce a non-trivial $1/\epsilon$ term containing logarithms. This term only cancels when adding both parts. It should be reiterated, that the $\tan\beta$ enhancement in the triple Higgs couplings is possibly an artefact of the parametrisation of the Two Higgs Doublet Model by masses and $\tan\beta$. We covered this in more detail in Section 2.1. However, once we choose the set of parameters we have to consider all $\tan\beta$ contributions in a consistent way. It is also not obvious whether this problem can be avoided by choosing a different set of parameters, since the parametrisation with λ_i is only concise in the interaction basis. Once we consider the mass eigenstates of the Higgs bosons we automatically get a non-trivial dependence of the masses to λ_i .

Another new class of contributions are the one-loop self-energy contributions, see Figure A.3. As stated in Section 2.2 the mixing self-energies are taken as proper diagrams with a factor of 1. For the b quark non-mixing self-energy wave function renormalisation has to be introduced. The counterterm has been derived in Section 2.2 and is given in Equation (2.16) and Equation (2.15). The integrals relevant for this class are one-loop tadpole integrals, since the momentum dependence is eliminated by asymptotic expansion.

Furthermore diagrams with two self-energy contributions appear. They are depicted in Figure A.4. They are considered as proper diagrams as well. The non-mixing self-energy contributions are considered by including diagonal field renormalisation.

In comparison with the τ contributions also additional counterterms have to be considered. These are the counterterm for the b quark mass δm_b , see Equation (2.22), t quark mass δM_t , given in Equation (2.23), and the CKM matrix elements δV_{tb} and δV_{ts} , see Equation (2.20), are required. For their derivation we refer to Section 2.2. The counterterm for the charged Higgs mass δM_{H^\pm} gets additional contributions due to b - t loops, which are given in Equation (2.26), and contributions due to Higgs couplings .

As a result of the discussion presented in Section 3.3.3 anticommuting γ_5 is used. This is possible, since there is no new class of diagram with a more complicated fermion trace than in the τ calculation. Again the maximum number of γ_5 in any given trace is two, which occurs precisely in the pseudoscalar pseudoscalar vector trace of the loop induced vertex of $H^-H^-\gamma$ and $H^-G^-\gamma$ in diagrams 34-37 of Figure A.1 and the

3. $\tan \beta$ enhanced corrections to $\mathbf{b} \rightarrow \mathbf{s}\gamma$ in the Two-Higgs-Doublet Model of type II

pseudoscalar axial-vector vector trace of the loop induced vertex $H^-W^-\gamma$ in diagrams 42-45 of Figure A.1.

While all divergences cancel, we do not get a gauge invariant result. The interesting property of the gauge invariance check, done via checking the Ward identity, is, that it does not hold for the correctly cancelling UV poles either. This suggests that the origin is of conceptual nature.

We performed the calculation keeping m_b as a small mass in the asymptotic expansion. Thus the IR behaviour is expressed in logarithms of m_b . Like in the τ case all the logarithms of m_b drop out when adding all diagrams. This implies, that we do not have to consider additional loop induced contributions on the effective theory side. The cancellation of IR divergences is also a check for the result.

As the contributions due to triple Higgs couplings and the y_b contributions cannot be split, the result cannot be given in a concise form as Equation (3.22). This is in part due to the expansion in the solution of the two-loop integral in Equation (4.32), which now becomes relevant as it is evaluated for three different scales. For the numeric evaluation the expansion order was varied around 10, i.e. keeping terms up to $(m^2/(M_1^2 + M_2^2))^{10}$, to ensure it has no large effect on the result. It is also important to insert viable values for the parameters of the Two Higgs Doublet Model. As we discussed in Section 2.1 they are not unconstrained and can easily be chosen in a way to render the theory non-perturbative or non-unitary. We therefore check the unitarity constraints, given by requiring $\lambda_i < 4$. It is more convenient to check the constraints for the couplings defined in the potential defined in Equation (2.5), as the chosen parameters $\tan \beta$, $\beta - \alpha$, M_{H^\pm} , M_{A_0} , M_{H_0} and m_{12} obscure the unitarity property. The λ_i are related to the parameters we chose for the Two Higgs Doublet model by Equation (2.12). For each set of the Two Higgs Doublet Model parameters, $\tan \beta$, $\beta - \alpha$, M_{H^\pm} , M_{A_0} , M_{H_0} and m_{12} we insert here, this check has been performed.

The numerical result for $\tan \beta = 60$, $\beta - \alpha = \pi/2$, $M_{H^\pm} = 600\text{GeV}$, $M_{A_0} = 601\text{GeV}$, $M_{H_0} = 643\text{GeV}$ and $m_{12} = 83\text{GeV}$ is

$$\frac{C_7^{(1,b)}}{C_7^{(1,0)}} = 82.7 \quad (3.45)$$

The correction to the Wilson coefficients $C_7^{(1,b)}$ includes all couplings from the two-loop contribution and is defined in Equation (3.11). The result is unrealistically large, pointing towards a spoiled cancellation of contributions. We saw in Section 3.3.2 that

numerically the first six digits of the contributions of single self-energy diagrams cancel. In Section 3.3.2 we observed non-cancellation before the treatment of γ_5 was investigated more thoroughly. As we consistently applied anticommuting γ_5 , which provided a finite, gauge invariant in the τ case, and with the contribution due to fermion chains being analogous to the τ contribution, this cannot be the case here. The finiteness of the result also restricts possible solutions like adding new diagrams or counterterms.

CHAPTER 4

The Mathematica package Medusa for two loop calculations in flavour physics

In this chapter, we will give a quick overview of the Mathematica package **Medusa** developed for the calculation presented in Chapter 3. The package is designed to calculate two-loop contributions to processes in flavour physics. This includes rare decays and contributions to Meson mixing. In flavour physics the typical problem is to calculate cross sections and decay rates of hadronic processes that are mediated by heavy gauge bosons. This creates a natural separation of scales. The scale of the hadronic process $\mathcal{O}(\Lambda_{\text{QCD}})$ or $\mathcal{O}(m_b)$ and the scale of the bosons mediating the process $\mathcal{O}(M_W)$. Possible new physics contributions are also considered to be of the high scale in the context of this thesis. This characteristic physical situation gives us the opportunity to simplify the calculation, as it enables us to expand in the ratio of the two scales. This is not only true for the masses themselves but also for the momenta of the external particles. In a light meson like the Pion the order of magnitude of the momentum of the constituent quarks is given by $\mathcal{O}(\Lambda_{\text{QCD}})$. For heavy mesons like the B meson the characteristic energy scale of the momenta is $\mathcal{O}(m_b)$. As both are much smaller than M_W the expansion in m_b/M_W converges quickly and the first order is already a good approximation. On the technical side the expansion simplifies the calculation as the loop integrals that have to be solved are reduced to vacuum integrals.

In `Medusa` this simplification is crucial, since at the heart of `Medusa` is only one two loop integral, which will be presented in Section 4.4.

`Medusa` encompasses an implementation of all steps for the calculation of two-loop amplitudes. The goal is to facilitate the calculation of possible enhanced two-loop effects in a wide range of new physics models. As for one-loop processes FeynArts [44] and FormCalc [43] are widely used to make predictions, the FeynArts interface gives the possibility to reuse the same model files. The calculation can be carried out in an fully automated fashion or semi automatic, allowing for more user control. Furthermore Mathematica as a front-end offers a powerful set of functions to work with the result and customize the calculation to the specific problem at hand in a convenient way. The results are produced fully D -dimensional and can therefore also be expanded to higher orders in ϵ if required.

While `Medusa` can be used to calculate SM contributions, many of which are already known to high precision, i.e. [65, 13, 18, 19], the main application will be to calculate contributions due to heavy unobserved particles in the loops. The two-loop contributions due to new particles can in some cases even be the leading contribution. For example in the Barr Zee [8] diagrams in the neutrino magnetic moments. They appear in Two Higgs Doublet models with flavour changing neutral Higgs couplings. The basic idea is that a small Yukawa coupling to leptons can be avoided by replacing it by a quark Yukawa coupling. This is possible by introducing a second loop, which mixes the Higgs with the flavour changing coupling to a Goldstone boson or a gauge boson. The large hierarchy of the Yukawa couplings then compensates for the additional loop suppression. The enhancement of Barr Zee diagrams opens a gateway of studying new physics in fermionic electromagnetic dipole moments, which have been investigated in Two Higgs Doublet Models for example in [3, 27, 50].

`Medusa` can also be used to study the internal dynamics of models. Since in flavour physics all external particles are Standard Model particles, the leading effect of the Higgs-selfcouplings enters at two-loop. We encountered this in the calculation presented in Section 3.3.4, as the Higgs-selfcouplings enter the problem due to their spurious $\tan\beta$ dependence. Bounds on the couplings in the Higgs potential of the Two Higgs Doublet Model are constrained mainly by unitarity bounds and perturbativity bounds [7]. A notable exception of course are the couplings of the light Standard Model like Higgs, which are directly constrained by experiment and are pushed towards the Standard Model value. As the perturbativity bounds allow for sizeable couplings their effects

could be investigated through their contribution to two-loop processes. The Higgs-selfcouplings and the Barr-Zee diagrams provide additional incentive to study precisely the two-loop contribution. `Medusa` has been designed to facilitate these studies.

We presented the ground work, like the derivation of the tensorial two-loop vacuum integral, for the package `Medusa` in [81]. We will first outline the general structure and then emphasise some of the important extensions of the functionality since [81].

4.1. Overview of the structures and used packages

The generation of the Feynman amplitudes is done in `FeynArts` [44]. The fermion traces are evaluated with `Tracer` [51], which can handle both the anticommuting and 't Hooft-Veltman scheme [48, 16] for γ_5 . Still, there is one caveat when using the 't Hooft-Veltman scheme or any scheme besides anticommuting γ_5 and `FeynArts` in combination, which will be elaborated on in Section 4.2. The implementation of the open fermion chains uses anticommuting γ_5 , which is always sufficient as discussed in Section 3.3.3. It is also possible to influence this simplification by defining custom rules to arrive at the desired basis for the Dirac structure.

A larger addition is the implementation of the large mass expansion of [76], while in [81] only naive expansion was possible. We will elaborate on the technique and implementation in Section 4.3 below. Since we consider processes in flavour physics in the context of heavy new physics, it is always justified to expand in small momenta, as they are of the order of the mass of Mesons or leptons.

After the expansion is complete the most complicated loop integral remaining is a tensorial two-loop vacuum integral with some powers of propagators raised due to the expansion. At this point there are two options to proceed. The standard method is to first use projection to get rid of the tensor structure and proceed using integration-by-parts identities to reduce it down to the scalar vacuum master-integral with all powers of propagators equal to one [30]. For this special case however it is also possible to use directly a closed formula for the tensorial two-loop integral with arbitrary powers of propagators, that will be shown in Section 4.4 and has first been derived in [68]. We generalised the solution to arbitrary indices in [81]. While the reduction procedure is scalable and can be used for higher loop orders as well, we restrict ourselves to this special case and can therefore use our knowledge of the closed solution shown in Equation (4.32). The restriction to this special case allows us to have all steps

implemented in Mathematica, while keeping the memory requirement manageable.

This was encountered when comparing the closed solution in Equation (4.32) with the solution of the scalar integral in [30]. The latter solution is given in terms of the master-integral with all powers of propagators equal to one. To solve a generic two-loop integral integration-by-parts identities are used recursively to express it in terms of the two-loop and possible one-loop master-integrals. For our naive implementation of the recursion relations given in [30] this check was only possible with manageable resource requirement in Mathematica for integrals where the sum of the powers was smaller than ten. The result is also fully D dimensional and can therefore be expanded to higher powers in ϵ , which are required for the computation of higher loop orders.

Another advantage of the tensorial master-integral is that there is no need to project out the tensor structure. The inclusion of the tensor structure in fact does not make the derivation of the solution in Equation (4.32). This is made possible by the use of symbolically symmetrised products of metric tensors and four-vectors. As can be seen in Equation (4.32) they are naturally produced by the solution of the loop integral. If one expresses them explicitly by metric tensors and four-vectors the number of terms grows factorially with the rank of the tensors, $(2g - 1)!(1 + 2g)_p$ where g denotes the number of metrics, p the number of four-vectors in the product and $(a)_b = \Gamma(a+b)/\Gamma(a)$ denotes the Pochhammer symbol. Using the symmetry property however it is possible to avoid the factorial growth of terms. For the simplification of the Lorentz structure rules are defined to simplify the symbolic representations of the symmetrised products. Examples will be discussed in Section 4.5. This also is a necessary requirement for doing this calculation in Mathematica.

The two-loop integral, see Equation (4.32), and some of the one-loop integrals in D dimensions, see Section 4.4.1, are expressed in terms of hypergeometric functions, which are then expanded in ϵ by using HypExp [49]. In the implementation at first only the divergent parts are expressed explicitly and the finite parts are expressed as the functions TL, to make intermediate results more compact. This will be examined in more detail in Section 4.5. Thus it is possible to handle the divergent part first and insert the finite parts after adding all diagrams to make use of cancellations without generating large expressions in intermediate steps.

We close this overview with a comment on considering higher loop orders with this method. The core of the package **Medusa** is the closed solution of the tensorial two-loop vacuum integral, which is not known on three loop order. While there is a conjecture

[69] that the necessary manipulations of the contour integral used in the derivation of Equation (4.32) might also be applicable to the three loop integral, we did not consider it further. Due to the increase in the number of diagrams the implementation in Mathematica would be tedious and could be tackled with a FORM [57] back-end, which can more easily deal with larger expressions. In closing this discussion it should be pointed out that the two-loop order is distinguished since the parametrically enhanced contributions we were considering in Section 3 first appear at two-loop. This is also true for Barr-Zee diagrams [8] discussed above. We are unaware of enhanced contribution at three-loop level that could be of the same order of magnitude of the one-loop results. Thus for phenomenological applications the three-loop calculations are less relevant.

4.2. The treatment of γ_5 in FeynArts

One issue that has to be kept in mind when using the 't Hooft-Veltman prescription for γ_5 in conjunction with FeynArts is the usage of flipping rules, which will be introduced in the following. In the following we will start with an explicit example of the inconsistency in the evaluation of fermion traces that arises. Afterwards we will elaborate what causes the issue and how it can be solved.

The issue is relevant in the calculation of the τ contributions to the $\tan^2 \beta$ enhanced corrections presented in Section 3.3.2. Two of the diagrams relevant for this discussion are shown in Figure 4.1. Both include the same fermionic subloop yet FeynArts constructs two different fermion traces. The reason is the application of the so called "flipping rules". This feature of FeynArts allows for an unambiguous construction of fermion traces containing Majorana fermions [34, 44]. However the algorithm to construct the fermion traces uses the flipping rules in general. Thus it also affects the diagrams in Figure 4.1. In the diagram on the left in Figure 4.1 the trace is constructed to be

$$\text{tr} \left[(q_1 + q_2) \left(-\frac{ie}{\sqrt{2}s_W} \gamma_\mu \omega_- \right) (m_\tau + q_2) \frac{iem_\tau \tan \beta}{\sqrt{2}M_W s_W} \omega_- \right], \quad (4.1)$$

while in the diagram on the right the flipping rules are applied yielding

$$\text{tr} \left[(-q_1 - q_2) \frac{iem_\tau \tan \beta}{\sqrt{2}M_W s_W} \omega_- (m_\tau - q_2) \frac{ie}{\sqrt{2}s_W} \gamma_\mu \omega_+ \right] \quad (4.2)$$

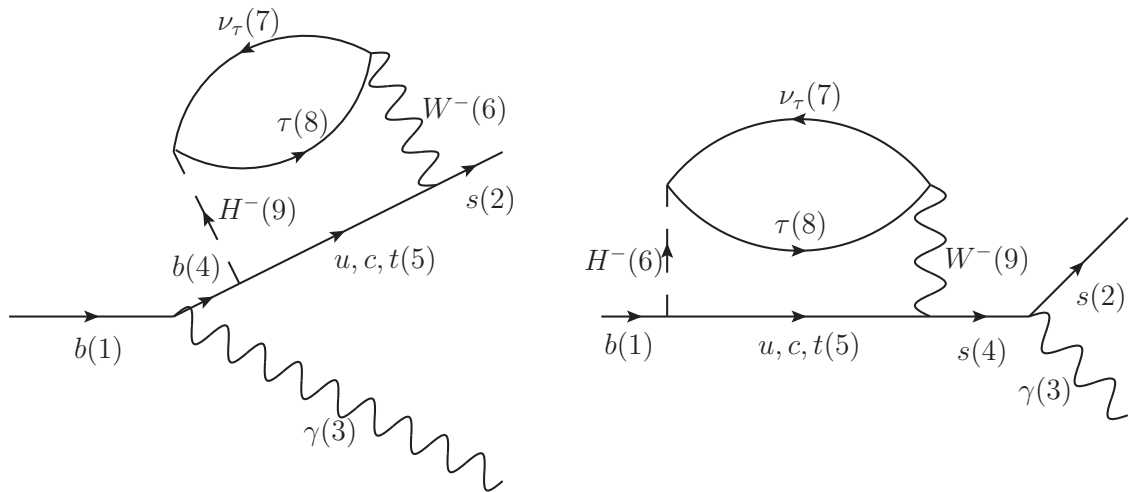


Figure 4.1.: Sample diagrams for which FeynArts produces an amplitude inconsistent with the 't Hooft-Veltman prescription for γ_5 . Alongside the particles we also denote the internal field numbers in brackets. Note that the trace of the fermion subloop is the same. Due to the different field numbers of the external H and W, flipping rules are applied for the diagram on the right.

The right- and left-handed projectors are given by

$$\omega_+ = \frac{1}{2}(1 + \gamma_5), \quad \omega_- = \frac{1}{2}(1 - \gamma_5). \quad (4.3)$$

When evaluating the trace in Equation (4.1) only the term proportional to m_τ contributes, since traces over odd numbers of gamma matrices vanish. Thus the projection operators are next to each other and no commutation relations have to be used. This means that there can be no dependence on the γ_5 treatment, as the evaluation is trivial. In the flipped case this is no longer the case, since γ_5 was anticommutated in the flipping rules. If the 't Hooft-Veltman scheme is applied in the calculation and the flip is reversed using a different prescription for γ_5 an error of order ϵ is introduced. After introducing the algorithm that is used by FeynArts and explaining the crucial step that causes the error, a replacement rule, defined in Equation (4.11), will be introduced to fix the error.

FeynArts is designed to be applicable to a wide range of models. To this end it can also handle Majorana fermions. This is achieved by the usage of flipping rules [34, 44] Instead of constructing fermion traces and open chains following the direction of fermion number flow backwards, which is inconsistent when fermion number violating

Majorana fermions are involved, FeynArts internally chooses a direction of fermion flow and uses the flipping rules for couplings when the chosen direction is going against the fermion number flow. This can be a problem, since in the implementation of the flipping rules anticommuting γ_5 is used. The usage of flipping rules is the general prescription to construct traces and is applied in cases where no Majorana fermions appear as well. It should be pointed out that in the most common usage of FeynArts, in conjunction with FormCalc [43] to calculate one-loop diagrams, this is unproblematic, as anticommuting γ_5 is used consistently in both construction and evaluation of the fermion traces.

The flipping rules are derived in [34] and amount to a charge conjugation of the coupling.

$$\Gamma_{\text{flip}} = C\Gamma^T C^\dagger \quad (4.4)$$

Where $\Gamma_i = 1, i\gamma_5, \gamma_\mu\gamma_5, \gamma_\mu, \sigma_{\mu\nu}$ are the elementary Dirac structures that need to be considered. Using the properties of the charge conjugation matrix

$$C^\dagger = C^{-1}, \quad C^T = -C \quad (4.5)$$

the result is expressed in [34] in terms of

$$C\Gamma_i^T C^{-1} = \eta_i \Gamma_i \quad (4.6)$$

with

$$\eta_i = \begin{cases} 1 & \text{for } \Gamma_i = 1, i\gamma_5, \gamma_\mu\gamma_5, \\ -1 & \text{for } \Gamma_i = \gamma_\mu, \sigma_{\mu\nu}. \end{cases} \quad (4.7)$$

It is easy to see that for $\gamma_\mu\gamma_5$ anticommuting γ_5 was used, i.e.

$$(\gamma_\mu\gamma_5)_{\text{flip}} = C(\gamma_\mu\gamma_5)^T C^{-1} = C\gamma_5^T \gamma_\mu^T C^{-1} = \gamma_5 C\gamma_\mu^T C^{-1} = -\gamma_5\gamma_\mu. \quad (4.8)$$

If we want to express the result of $(\gamma_\mu\gamma_5)_{\text{flip}}$ in Equation (4.8) in terms of the basic structures Γ_i , like in Equation (4.7), one has to anticommute once. In [34] this step is implemented with anticommuting γ_5 . Since the SM and the 2HDM are defined in terms of chiral fields, the axial vector coupling in Equation (4.8) does not appear in the generic model files FeynArts uses. The chiral basis is Γ_i^X : $1, \omega_\pm, \gamma_\mu\omega_\pm$. Therefore

the implemented chiral flipping rule in the default generic model file of FeynArts is

$$\gamma_\mu \omega_\pm \xrightarrow{\text{flip}} -\gamma_\mu \omega_\mp. \quad (4.9)$$

Where we followed the notation of [34] to denote the chiral projectors as $\omega_\pm = \frac{1}{2} (1 \pm \gamma_5)$.

The issue cannot be solved with replacing the flipping rule with $\omega_\pm \gamma_\mu$, were no anticommuting γ_5 was used, as this structure is not part of the chiral basis Γ_i^X used to describe generic couplings. When the flipping rule produces different structures not represented in the basis they are not replaced when creating the amplitude, leaving a generic placeholder in the expression. If on the other hand new structures are introduced in the generic coupling, i.e. $\omega_\pm \gamma_\mu$, they will be inserted in every occurrence of the generic coupling. This creates additional terms for all insertions of the coupling instead of just fixing the flipped couplings. Note that this problem cannot be solved by using the chirally improved 't Hooft-Veltman scheme, presented in Section 3.3.3, as the projectors change sign and are therefore not mapped on themselves either, see

$$\omega_\mp \gamma_\mu \omega_\pm \xrightarrow{\text{flip}} -\omega_\pm \gamma_\mu \omega_\mp. \quad (4.10)$$

The solution we chose when utilizing the 't Hooft-Veltman scheme is to tag the terms generated using this rule, which can easily be done in the generic model file. Next the Dirac structure of the coupling is replaced by the structure obtained without anticommuting. The explicit replacement rule is given by

$$-\gamma_\mu \omega_\mp \rightarrow -\omega_\pm \gamma_\mu. \quad (4.11)$$

4.3. Asymptotic expansion in small momenta

Since we are interested in new physics contributions in flavour physics, there is always a clear separation of scales. There is the low scale of the masses and momenta of external Standard Model particles and the high scale of the masses of new physics particles. Hence for the considered cases an expansion in $\frac{k_i^2}{M_{NP}^2}, \frac{m^2}{M_{NP}^2}$ the ratio of these scales is always possible. This significantly simplifies the problem as the loop-integrals to be computed reduce to a single integral, which is presented in Equation (4.32).

For this section we follow [76], since they give a very thorough introduction to the topic. Here we briefly review the basic ideas using one diagram of the calculation

presented in Figure 3.3.2 as an example. At the end of this section we will remark also on the implementation and the role of asymptotic expansion in the package.

The example diagram of Figure 4.2 leads, when for simplicity disregarding the numerator to

$$A = \iint d^D q_1 d^D q_2 I = \iint \frac{d^D q_1 d^D q_2}{(q_1 + k_1)^2 - M_t^2} \frac{1}{(q_1 + k_2)^2 - M_{H^\pm}^2} \frac{1}{q_1^2 - M_W^2} \frac{1}{(q_1 + q_2)^2} \frac{1}{q_2^2 - m_\tau^2} \frac{1}{(q_2 + k_2)^2 - m_\tau^2}. \quad (4.12)$$

The naive approach is to apply the Taylor expansion

$$\mathcal{T}_x^n f(x) = \sum_{j=0}^n \mathcal{T}_x^{(j)} f(x) = \sum_{j=0}^n \frac{1}{j!} \left. \frac{d^j f(x)}{dx^j} \right|_{x=0} x^j \quad (4.13)$$

to the integrand. Here x stands for one of the small momenta or masses. In the following \mathcal{T} is understood as an operator acting on all terms to the right. In the integral above the small scale is represented by the external momenta and the τ mass. Thus the expansion is given by

$$A = \iint d^D q_1 d^D q_2 \mathcal{T}_{m_\tau, p, k}^n I \quad (4.14)$$

where the Taylor operator of multiple variables is simplified with

$$\mathcal{T}_{x,y}^n = \sum_{j=0}^n \mathcal{T}_x^{(j)} \mathcal{T}_y^{n-j} = \sum_{j=0}^n \mathcal{T}_x^j \mathcal{T}_y^{(n-j)} \quad (4.15)$$

The expansion parameter is the small external momentum or mass divided by one of the large masses k_i^2/M_{large}^2 , m^2/M_{large}^2 . While propagators with large masses M_i are regular as k_i goes to zero a problem arises when expanding the last two terms in Equation (4.12), as there is no large mass present to regularize the propagators when the small scales are set to zero. Instead one has to assume that the external momentum is small compared to the only other scale in this propagator, the loop momentum. This however is not true for all values of the infinite integration domain. If the naive Taylor expansion is used anyway new infrared divergences are introduced. Note that in this diagram this situation cannot be avoided by rerouting the flow of external momenta. The solution of this problem of the naive expansion is the asymptotic expansion with

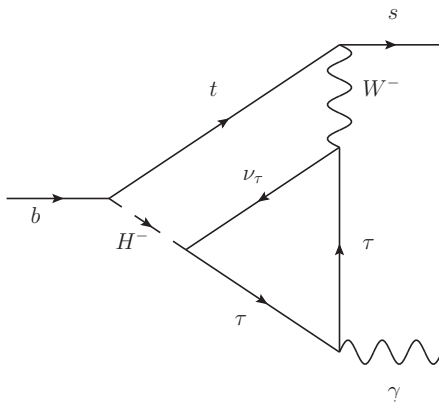


Figure 4.2.: Example diagram to consider the basics of asymptotic expansion. The hierarchy of scales is given by $m_\tau^2 \sim m_b^2 \sim p^2 \ll M_W^2 < M_t^2 < M_{H^\pm}^2$.¹

the large mass procedure in described in [76].

The basic idea is that the integration domain is split into regions. For the discussion at hand it is sufficient to split the integration domain in two. The value of the cut off Λ is dictated by the structure of the integrand. The term yielding the contribution of the naive Taylor expansion is the region in which the loop momentum is considered to be large. In Equation (4.16) this will be the first term. For the above example in Equation (4.12) Λ has to be chosen such that $q_1, q_2 > \Lambda \sim k_i \sim m_\tau$. For this example the only other contributing limit is defined by $q_2 \sim k_i < \Lambda < q_1 \sim M_i$, yielding the second term in Equation (4.16). In the generic two-loop case there are other limits to consider, i.e. $q_1 < \Lambda < q_2 \sim M_i$ and $q_1 \sim q_2 < \Lambda < M_i$. In the example at hand these limits will result in scaleless integrals, which vanish in dimensional regularisation. In the specified regions

$$A = \int_{|q_1| > \Lambda} d^D q_1 \int_{|q_2| > \Lambda} d^D q_2 \mathcal{T}_{k_i, m_\tau} I + \int d^D q_1 \int_{|q_2| < \Lambda} d^D q_2 \mathcal{T}_{k_i, m_\tau, q_2} I \quad (4.16)$$

it is justified to perform the appropriate expansions.

Instead of evaluating the integrals with the cutoff Λ , the integration domain for each integral is now extended over all loop momenta again. This means that in Equation (4.16) we drop the restrictions of the integration domains and get

$$A = \int d^D q_1 \int d^D q_2 \mathcal{T}_{k_i, m_\tau} I + \int d^D q_1 \int d^D q_2 \mathcal{T}_{k_i, m_\tau, q_2} I. \quad (4.17)$$

¹Like many of the Feynman diagrams in this thesis this has been created with the help of [10]

This is a non-trivial step and in [76] there is only one basic example where this is presented step by step, since as they state it is very difficult to give rigorous proofs that the extension of the integration domain is possible. A plausibility argument is that the integrals we obtain in this procedure are regulated by a cut-off. The method of regularisation however is a choice and the regularisation parameter has to vanish in physically meaningful results. If we disregard that the integrals resulted from splitting the domain, the freedom of choice of the regularisation method gives a hint as to why it is possible to apply dimensional regulation for the integrals of the expanded integrands.

While it is instructive to look at the regions explicitly, for a systematic generation of all needed terms in the expansion the expansion by subgraphs will be presented as a general prescription. The implementation in **Medusa** closely follows the way the procedure is presented here. A subgraph consists of a subset of the propagators. A propagator is called a heavy line if the mass of the propagator is considered to be large compared to the external momenta. To systematically include all possible contributions we have to identify the so called asymptotically irreducible (AI) subgraphs. A subgraph is AI if:

1. it contains all the heavy lines
2. it is one particle irreducible with respect to the light lines

The task then is to find all AI subgraphs and expand them in the small masses and all momenta that are external to the respective subgraph.

Constructing all AI subgraphs will ensure that all relevant regions are taken into account. When constructing the subgraphs one loop is always cut open, rendering the respective loop momentum an external momentum with respect to the subgraph. It is therefore considered small and expanded. This case corresponds to the second term in Equation (4.16), where the region of small loop momentum is considered.

To illustrate these steps we turn back to our example given in Equation (4.12). The identified AI subgraphs are also shown in Figure 4.3. Certainly the whole diagram satisfies the AI condition. The other subgraphs can be found by removing light lines from the graph. Due to the second condition there are three possibilities. Remove both of the τ propagators, since by removing only one the result would not be 1PI with respect to the remaining τ line and therefore violate the second condition. Secondly the ν_τ propagator can be removed. This gives us the two subgraphs in the middle of Figure 4.3. The last AI subgraph comprises the heavy lines only.

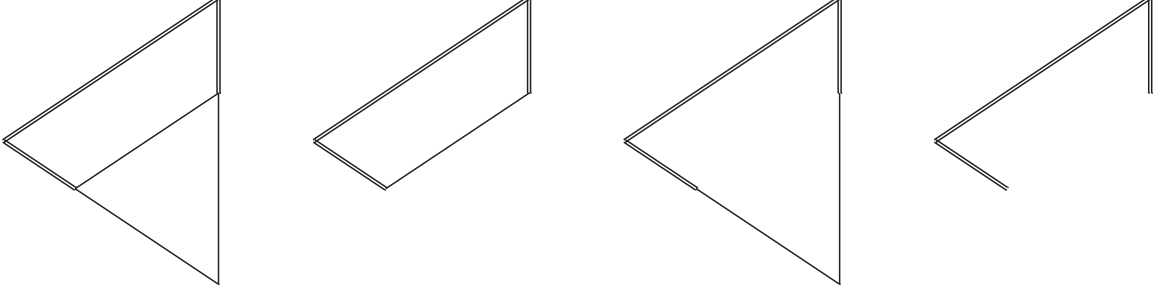


Figure 4.3.: Possible AI subgraphs of Figure 4.2. We follow the convention to denote heavy lines by a double line.

Now that we identified the subgraphs we need to expand them in the appropriate parameters. As stated above this means all small masses and all momenta external to the subgraph. For the first subgraph we retrieve the naive Taylor expansion.

$$I_{\gamma_1} = \iint d^D q_1 d^D q_2 T_{k_1, k_2, m_\tau} \frac{1}{(q_1 + k_1)^2 - M_t^2} \frac{1}{(q_1 + k_2)^2 - M_{H^\pm}^2} \frac{1}{q_1^2 - M_W^2} \frac{1}{(q_1 + q_2)^2} \frac{1}{q_2^2 - m_\tau^2} \frac{1}{(q_2 + k_2)^2 - m_\tau^2} \quad (4.18)$$

For the second subgraph in Figure 4.3, the loop momentum q_2 is considered to be external, since it is flowing through the subgraph. Thus it is included in the expansion. This will result in genuine two-loop integrals that can be solved with Equation (4.32). One finds

$$I_{\gamma_2} = \int d^D q_2 \frac{1}{q_2^2 - m_\tau^2} \frac{1}{(q_2 + k_2)^2 - m_\tau^2} \int d^D q_1 T_{k_1, k_2, m_\tau, q_2} \frac{1}{(q_1 + k_1)^2 - M_t^2} \frac{1}{(q_1 + k_2)^2 - M_{H^\pm}^2} \frac{1}{q_1^2 - M_W^2} \frac{1}{(q_1 + q_2)^2}. \quad (4.19)$$

This will leave us with the product of two one loop integrals, a massive tadpole and a B_0 -function. These are the two non-zero contributions we mentioned earlier.

For the third subgraph the roles of the light lines are reversed.

$$\begin{aligned}
 I_{\gamma_3} = & \int d^D q_2 \frac{1}{q_2^2} \\
 & \int d^D q_1 T_{k_1, k_2, m_\tau, q_2} \frac{1}{(q_1 + k_1)^2 - M_t^2} \frac{1}{(q_1 + k_2)^2 - M_{H^\pm}^2} \frac{1}{q_1^2 - M_W^2} \\
 & \frac{1}{(q_2 - q_1)^2 - m_\tau^2} \frac{1}{(q_2 - q_1 + k_2)^2 - m_\tau^2}
 \end{aligned} \tag{4.20}$$

Note that we changed the flow of loop momenta, since effectively only one loop momentum has to flow out of this subgraph, as it is topologically the same as the previous one. Although in this diagram we could have circumvented this from the beginning by choosing the loop momenta such that only the massive propagators carry both loop momenta, in general this is a required step. This will lead to a massless tadpole integral for q_2 and thus vanishes.

In the fourth subgraph only the massive lines are expanded and both loop momenta are external, since the diagram is not a closed loop itself. We get

$$\begin{aligned}
 I_{\gamma_4} = & \int \frac{d^D q_1}{q_1^2} \int \frac{d^D q_2}{q_2^2 - m_\tau^2} \frac{1}{(q_2 + k_2)^2 - m_\tau^2} \\
 & T_{k_1, k_2, m_\tau, q_1, q_2} \frac{1}{(q_1 - q_2 + k_1)^2 - M_t^2} \frac{1}{(q_1 - q_2 + k_2)^2 - M_{H^\pm}^2} \frac{1}{(q_1 - q_2)^2 - M_W^2}.
 \end{aligned} \tag{4.21}$$

The expansion will leave us with a prefactor of large masses multiplied with a massless tadpole and a B_0 -function. Thus this subgraph also vanishes in this example. Note that we shifted $q_1 \rightarrow q_1 - q_2$ to make the massless tadpole obvious.

The last two vanishing contributions exemplify that in general the loop momenta might have to be shifted, which is important to note in the implementation of the algorithm. If the masses in the diagram are different, there could have been one additional subgraph. To arrive at this case the top quark is replaced by a up quark or charm quark. If m_u or m_c are not set to zero to start with, but taken into account in the expansion, the additional subgraph would include the leptonic subloop and the two remaining massive lines, excluding only the light quark propagator.

The implementation in Medusa follows the algorithm presented here step by step very closely. With exp [78] there is also an older more general implementation in Fortran with interfaces to FORM. First the set of propagators is split into heavy propagators,

which are included in the expansion of all subgraphs, and light propagators. Then the light propagators are categorised by the loop momenta passing through, i.e. only q_1 , only q_2 or $q_1 + q_2$. The subgraphs are then constructed by removing one of the categories from the graph. Due to the second condition for AI subgraphs, only a complete category can be removed to create a subgraph.

The only subgraph that might not be covered yet contains no closed loops and constitutes of only heavy lines. In the example considered above this case is represented by the diagram on the right in Figure 4.3. Thus in the end we check whether the subgraph containing only heavy lines is already covered in the previous construction or has to be added. This amounts to removing all three categories from the diagram. Note that if propagators from all three categories are present and we take out two categories, the resulting graph cannot be 1PI with respect to the light lines, since there cannot be a closed loop. Therefore with this procedure all combinations have been accounted for. The loop momentum that needs to be expanded is always the loop momentum defining the category removed from the subgraph or both in the case of the purely massive subgraph.

Finally we want to comment on the role of the asymptotic expansion in matching calculations, for example the one presented in Section 3. As has been stated in Section 3.1.1, the matching comprises of one calculation of the amplitude in the full theory, containing the heavy degrees of freedom, which has to be equal to the result of the calculation in the effective theory, where all heavy scales have been integrated out. This equation is used to solve for the Wilson coefficient of the effective theory, encompassing all information of the heavy scale.

The extra terms generated by the large mass procedure, compared to the naive Taylor expansion, describe the physics of the low energy scale, for example the m_τ -dependence of the B_0 -function in I_{γ_2} in Equation (4.19). The latter gives rise to logarithms of m_τ . They cannot be part of the Wilson coefficient in the end, as it is a function purely of the heavy masses. Therefore contributions from the small scale either have to cancel when adding up all the diagrams of the full theory or the same dependence on the small scale has to appear on the side of the effective theory describing the low scale physics. The latter would be the case if there are loop diagrams on the side of the effective theory. In the calculation of Section 3.3.2, from which the example diagram Figure 4.2 is extracted, a cancellation of all contributions from the light degrees of freedom occurs, since the four fermion operators cannot mix into Q_7 at the considered order.

The difference between asymptotic expansion and the naive Taylor expansion is in this context the treatment of infrared divergences. In the naive Taylor expansions, when the small masses are set to zero new infrared divergences can arise, which are then regularised dimensionally. When using the asymptotic expansion for the same process there will be logarithmic divergence when considering the limit of the small mass approaching zero. This has been investigated in detail for the calculation presented in Section 3.3.2. In both pictures the infrared divergence has to cancel either in the matrix element of the full theory itself or in the matching if there is an equal contribution on the effective theory side. The advantage of using the asymptotic expansion is that it allows a clear distinction of infrared and ultraviolet and therefore enables us to understand the origin of the contributions. It also increases the applicability of the package and allows quick checks for one-loop processes.

4.4. The loop Integrals

In this section we will present the loop integrals used. We start with some brief remarks about the one-loop case, as we recalculated several integrals in D dimensions, and subsequently present the solution of the tensorial two-loop vacuum integral with three masses. We close the section by presenting the checks used to verify the solutions.

4.4.1. One-loop integrals in D dimensions

Among the diagrams at two-loop level there will be some containing products of two one-loop integrals. Due to the asymptotic expansion in small momenta they will be reduced to simple tadpole diagrams. The asymptotic expansion however produces also one-loop diagrams with one or two external momenta. They have to be evaluated to first order in ϵ , as the other integral in the product can be divergent, resulting in a finite term where the ϵ^{-1} term and the ϵ^1 term in the expansion cancel.

For all diagrams needed in the calculations presented in Section 3 we opted to evaluate the tensorial one-loop integrals fully in D dimensions. The solutions will be listed below. The only exception is the $B_0(k^2, m_0, m_1)$ function with three different scales, for which only the first order in ϵ has been implemented. When evaluating the amplitude on-shell, several different cases have to be considered. Whenever possible we compared our results with [75, 76] and found agreement.

The integrals will be listed in the following. First, some notation has to be introduced. Symmetric products of metric tensors and four vectors of different powers will be expressed as $(g^\lambda p^n)^{\{\mu_1 \dots \mu_{2\lambda+n}\}}$, i.e.

$$(gp^2)^{\{\mu\nu\kappa\lambda\}} = g^{\mu\nu} p^\kappa p^\lambda + g^{\mu\kappa} p^\nu p^\lambda + g^{\mu\lambda} p^\nu p^\kappa + g^{\kappa\nu} p^\mu p^\lambda + g^{\kappa\lambda} p^\mu p^\nu + g^{\lambda\nu} p^\mu p^\kappa. \quad (4.22)$$

The Beta function is expressed as $B(a, b) = \frac{\Gamma(a)\Gamma(b)}{\Gamma(a+b)}$. Finally the Pochhammer symbol $(a)_b$ is defined as $(a)_b = \frac{\Gamma(a+b)}{\Gamma(a)}$.

$$B_{ab}^r(k, k^2, m_0, m_1) = \int d^D q \frac{\prod_{i=1}^r q^{\mu_i}}{(q^2 - m_0^2)^a ((q+k)^2 - m_1^2)^b} \quad (4.23)$$

$$\begin{aligned} B_{ab}^r(k, k^2, 0, 0) &= \frac{i\pi^{\frac{D}{2}}}{\Gamma(a)\Gamma(b)} \sum_{\lambda=0}^{\lfloor \frac{r}{2} \rfloor} (-1)^{r+a+b-\lambda} 2^{-\lambda} (-k^2)^{-a-b+\lambda+\frac{D}{2}} \\ &\quad (g^\lambda k^{r-2\lambda})^{\{\mu_1 \dots \mu_r\}} \Gamma\left(a+b-\lambda-\frac{D}{2}\right) \\ &\quad B\left(-b+\lambda+\frac{D}{2}, -a+r-\lambda+\frac{D}{2}\right) \end{aligned} \quad (4.24)$$

$$\begin{aligned} B_{ab}^r(k, k^2, 0, m_1) &= \frac{i\pi^{\frac{D}{2}}}{\Gamma(b)} \sum_{\lambda=0}^{\lfloor \frac{r}{2} \rfloor} (-1)^{r+a+b-\lambda} 2^{-\lambda} (m_1^2)^{-a-b+\lambda+\frac{D}{2}} \\ &\quad (g^\lambda k^{r-2\lambda})^{\{\mu_1 \dots \mu_r\}} \Gamma\left(a+b-\lambda-\frac{D}{2}\right) \\ &\quad \frac{\Gamma(-a+r-\lambda+\frac{D}{2})}{\Gamma(r-\lambda+\frac{D}{2})} \\ &\quad {}_2F_1\left(a, a+b-\frac{D}{2}-\lambda, r-\lambda+\frac{D}{2}, \frac{k^2}{m_1^2}\right) \end{aligned} \quad (4.25)$$

$$\begin{aligned} B_{ab}^r(k, 0, 0, m_1) &= \frac{i\pi^{\frac{D}{2}}}{\Gamma(b)} \sum_{\lambda=0}^{\lfloor \frac{r}{2} \rfloor} (-1)^{r+a+b-\lambda} 2^{-\lambda} (m_1^2)^{-a-b+\lambda+\frac{D}{2}} \\ &\quad (g^\lambda k^{r-2\lambda})^{\{\mu_1 \dots \mu_r\}} \Gamma\left(a+b-\lambda-\frac{D}{2}\right) \\ &\quad \frac{\Gamma(-a+r-\lambda+\frac{D}{2})}{\Gamma(r-\lambda+\frac{D}{2})} \end{aligned} \quad (4.26)$$

$$\begin{aligned}
 B_{ab}^r(k, 0, m_1, m_1) &= \frac{i\pi^{\frac{D}{2}}}{\Gamma(b)} \sum_{\lambda=0}^{\lfloor \frac{r}{2} \rfloor} (-1)^{r+a+b-\lambda} 2^{-\lambda} (m_1^2)^{-a-b+\lambda+\frac{D}{2}} \\
 &\quad (g^\lambda k^{r-2\lambda})^{\{\mu_1 \dots \mu_r\}} \Gamma\left(a+b-\lambda-\frac{D}{2}\right) \\
 &\quad \frac{\Gamma(b+r-2\lambda)}{\Gamma(a+b+r-2\lambda)}
 \end{aligned} \tag{4.27}$$

$$\begin{aligned}
 B_{ab}^r(k, 0, m_0, m_1) &= \frac{i\pi^{\frac{D}{2}}}{\Gamma(a)\Gamma(b)} \sum_{\lambda=0}^{\lfloor \frac{r}{2} \rfloor} (-1)^{r+a+b-\lambda} 2^{-\lambda} (m_1^2)^{-a-b+\lambda+\frac{D}{2}} \\
 &\quad (g^\lambda k^{r-2\lambda})^{\{\mu_1 \dots \mu_r\}} \Gamma\left(a+b-\lambda-\frac{D}{2}\right) \left[\right. \\
 &\quad \frac{\Gamma(a)\Gamma(-a+\frac{D}{2}+r-\lambda)}{\Gamma\left(\frac{D}{2}+r-\lambda\right)} \\
 &\quad {}_2F_1\left(a, a+b-\frac{D}{2}-\lambda, 1+a-\frac{D}{2}-r+\lambda, \frac{m_0^2}{m_1^2}\right) \\
 &\quad + \left(\frac{m_0^2}{m_1^2}\right)^{-a+\frac{D}{2}+r-\lambda} \frac{\Gamma(b+r-2\lambda)\Gamma\left(a-\frac{D}{2}-r+\lambda\right)}{\Gamma\left(a+b-\frac{D}{2}-\lambda\right)} \\
 &\quad \left. {}_2F_1\left(b+r-2\lambda, \frac{D}{2}+r-\lambda, 1-a+\frac{D}{2}+r-\lambda, \frac{m_0^2}{m_1^2}\right) \right]
 \end{aligned} \tag{4.28}$$

The tadpole integral is given as

$$\begin{aligned}
 \int d^D q \frac{\prod_{i=1}^r q^{\mu_i}}{(q^2 - m^2)^a} &= \frac{i\pi^{\frac{D}{2}} (-1)^a}{(d+r-2)!!\Gamma(a)} \left(-\frac{D}{2} - \frac{r}{2} + 1\right)_{\frac{r}{2}} \left(g^{\frac{r}{2}}\right)^{\{\mu_1 \dots \mu_r\}} \\
 &\quad (m^2)^{-a+\frac{r}{2}+\frac{D}{2}} \Gamma\left(a - \frac{r}{2} - \frac{D}{2}\right)
 \end{aligned} \tag{4.29}$$

completing the list of one-loop integrals implemented in D dimensions.

4.4.2. The tensorial two-loop vacuum integral with three masses

The most complicated integral implemented in Medusa is the tensorial two-loop vacuum integral with three different masses. A solution based on tensor reduction and subsequent reduction to master-integrals by integration-by-parts identities was first

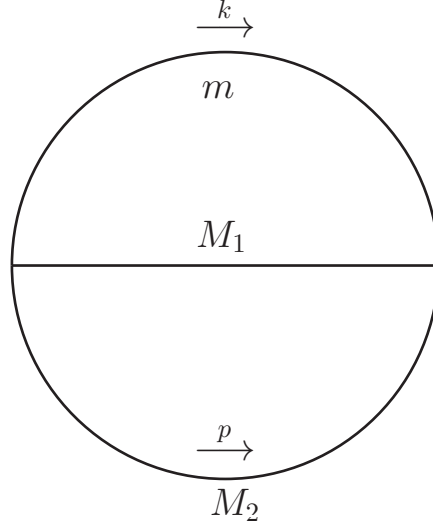


Figure 4.4.: The topology of the two-loop vacuum integral. In the solution the powers of the three propagators can be raised to arbitrary powers.

obtained in [30]. In the following we will present the solution implemented in **Medusa**, which is a closed form solution for arbitrary tensor orders and powers of the denominators. The topology is shown in Figure 4.4. The generic tensorial two-loop vacuum integral is defined by

$$T_{\alpha\beta\gamma}^{\nu_1\dots\nu_s;\mu_1\dots\mu_r}(m, M_1, M_2) = \frac{\mu^{4\epsilon} e^{2\gamma_E\epsilon}}{[i\pi^{\frac{D}{2}}]^2} \iint d^D k d^D p \frac{p^{\nu_1} \dots p^{\nu_s} \cdot k^{\mu_1} \dots k^{\mu_r}}{(m^2 - k^2)^\gamma \cdot (M_1^2 - p^2)^\alpha} \frac{1}{(M_2^2 - (p+k)^2)^\beta}. \quad (4.30)$$

A closed form solution has first been obtained in [68]. The solution is expressed in terms of a set of functions h , introduced to simplify the result and its evaluation. They are defined in Equation (4.33) and were first evaluated using a reduction approach. We later extended the solution to arbitrary powers, α, β and γ , of the propagators in [81]. Note that integrals with additional propagators of different masses can always be simplified to the form of Equation (4.30) by partial fractioning. The form in Equation (4.30) is therefore the most general case that needs to be considered.

The Lorentz structure of the result is expressed in terms of

$$G_\lambda^{\nu_1\dots\nu_s\mu_1\dots\mu_r} = \sum_{\{\rho_1\dots\rho_{2\lambda}\} \cap \{\rho_{2\lambda+1}\dots\rho_s\} = \{1\dots s\}} (g^\lambda)^{\{\nu_{\rho_1}\dots\nu_{\rho_{2\lambda}}\}} \left(g^{\frac{r+s}{2}-\lambda}\right)^{\{\nu_{\rho_{2\lambda+1}}\dots\nu_{\rho_s}\mu_1\dots\mu_r\}}. \quad (4.31)$$

The indices ν_1, \dots, ν_s are divided into all possible subsets of length λ . The sum goes over all subsets of $\{1, 2 \dots s\}$ and defines the possible values of ρ_i . $(g^n)^{\mu_1 \dots \mu_{2n}}$ is the symmetric sum of products of n metric tensors. The functions h and T_{IR} will be defined in Equation (4.33) and Equation (4.34) respectively. The solution of the integral reads [81]

$$\begin{aligned}
 T_{\alpha\beta\gamma}^{\nu_1 \dots \nu_s; \mu_1 \dots \mu_r}(m, M_1, M_2) = & \\
 & \frac{e^{2\gamma E\epsilon} (-1)^{\frac{s-r}{2}}}{\Gamma(\alpha)\Gamma(\beta)} \sum_{\lambda=0}^{\lfloor \frac{s}{2} \rfloor} G_{\lambda}^{\nu_1 \dots \nu_s \mu_1 \dots \mu_r} \left(\frac{1}{2}\right)^{\frac{r+s}{2}} \left[T_{\alpha\beta\gamma, IR}^{s, r, \lambda}(m, M_1, M_2) \right. \\
 & + \sum_{k=0}^{\kappa} \frac{(1-\gamma-k)_k}{k!} (m^2)^k \frac{\Gamma\left(-4+\alpha+\beta+\gamma-\frac{r+s}{2}+k+2\epsilon\right)}{\left(2-\gamma+\frac{r+s}{2}-\lambda-k-\epsilon\right)_{\gamma+k}} \\
 & \left. h_{-3+\beta+\gamma+\frac{s-r}{2}-\lambda+k, -3+\alpha+\gamma-\frac{s+r}{2}+\lambda+k}^{4-\alpha-\beta-\gamma+\frac{r+s}{2}-k}(M_2, M_1) \right], \tag{4.32}
 \end{aligned}$$

where h contains the hypergeometric function and is defined as

$$\begin{aligned}
 h_{k n}^p(M_i, M_j) & := \mu^{4\epsilon} \int_0^1 dx x^{k+\epsilon} (1-x)^{n+\epsilon} \left(x(M_i^2 - M_j^2) + M_j^2 \right)^{p-2\epsilon} \\
 & = (M_j^2)^p \left(\frac{M_j^2}{\mu^2} \right)^{-2\epsilon} B(1+k+\epsilon, 1+n+\epsilon) \\
 & \quad {}_2F_1\left(-p+2\epsilon, 1+k+\epsilon, 2+k+n+2\epsilon, 1 - \frac{M_i^2}{M_j^2}\right). \tag{4.33}
 \end{aligned}$$

B denotes the Beta function $B(x, y) = \Gamma(x)\Gamma(y)/\Gamma(x+y)$ The function T_{IR} contains possible infrared poles and is given by

$$\begin{aligned}
 T_{\alpha\beta\gamma, IR}^{s, r, \lambda}(m, M_1, M_2) = & \\
 & \frac{(-1)^{r-\lambda+\gamma}}{\Gamma(\gamma)} \frac{\Gamma(-2+\alpha+\beta-\lambda+\epsilon)}{\Gamma\left(2+\frac{r+s}{2}-\lambda-\epsilon\right)} \frac{\pi\mu^{4\epsilon}}{\sin(\pi\epsilon)} \sum_{k=0}^{L-2-\frac{r+s}{2}+\lambda+\kappa} \frac{(-1)^k}{k!} \\
 & \left(3+\frac{r+s}{2}-\lambda-\gamma+k-\epsilon\right)_{\gamma-1} (m^2)^{2+\frac{r+s}{2}-\lambda-\gamma+k-\epsilon} \\
 & \sum_{i=0}^{-1+\alpha+k} \binom{-1+\alpha+k}{i} \frac{(-1)^i}{(3-\alpha-\beta+\lambda-\epsilon)_{\beta+i+s-2\lambda}} \\
 & \frac{\partial^{-1+\beta+s-2\lambda+k+i}}{\partial(M_2^2)^{-1+\beta+s-2\lambda+k+i}} \frac{(M_1^2)^{2-\alpha+s-\lambda+i-\epsilon} - (M_2^2)^{2-\alpha+s-\lambda+i-\epsilon}}{M_1^2 - M_2^2} \tag{4.34}
 \end{aligned}$$

In the derivation of Equation (4.32) an expansion in $\frac{m^2}{(M_1+M_2)^2}$ was performed. In the above formula the expansion order has been denoted with κ . Note that this is a regular expansion in the sense that it does not introduce new dimensionally regulated singularities. It is also converging rather fast, while extending the expansion order to high values, i.e. ≥ 10 , is feasible on a regular desktop.

As has been already mentioned in Section 4.1, T and T_{IR} are not functions accessible to the user in the implementation of **Medusa**. Instead the total result is split in the finite part, represented by **TLFin**, and the divergent part, which is automatically inserted. This gives the opportunity to raise the expansion order after the calculation is otherwise complete to achieve the desired precision. While obviously it would be preferable to have the result without any expansions, due to this setup the expansion is of no issue in practical calculations. To facilitate this **Medusa** builds a database of solved and simplified instances of the loop integral.

One special case is if one mass is zero $m = 0$. This leads to a simplified result

$$\begin{aligned}
 T_{\alpha\beta\gamma}^{\nu_1\dots\nu_s;\mu_1\dots\mu_r}(0, M_1, M_2) = & \\
 & \frac{(i\pi^{\frac{D}{2}})^2}{\Gamma(\alpha)\Gamma(\beta)} \sum_{\lambda=0}^{\lfloor \frac{s}{2} \rfloor} 2^{-\frac{r+2}{2}} (-1)^{\frac{r}{2}+\frac{3}{2}s} G_{\lambda}^{\nu_1\dots\nu_s;\mu_1\dots\mu_r} (M_1^2)^{4+\frac{r+s}{2}-\alpha-\beta-L-2\epsilon} \\
 & \frac{\Gamma(2-\epsilon+\frac{r+s}{2}-\lambda-L)\Gamma(-4+2\epsilon-\frac{r+s}{2}+\alpha+\beta+L)}{\Gamma(2-\epsilon+\frac{r+s}{2}-\lambda)} \\
 & B(-2+\epsilon-\frac{r-s}{2}-\lambda+\beta+L, -2+\epsilon-\frac{r+s}{2}+\lambda+\alpha+L) \\
 & {}_2F_1\left(-2+\epsilon-\frac{r-s}{2}-\lambda+\beta+L, -4+2\epsilon-\frac{r+s}{2}+\alpha+\beta+L, \right. \\
 & \left. -4+2\epsilon-r+\alpha+\beta+2L, 1-\frac{M_2^2}{M_1^2}\right). \tag{4.35}
 \end{aligned}$$

Especially the solution for the case $m = 0$, $M_1 = M_2$ is in agreement with [22].

4.4.3. Checks

Since no reduction with integration-by-parts (IBP) relations has been performed, they are a useful tool to crosscheck the result. They give us relations between different tensor orders and indices of the integral, which we used as consistency checks of the

solution. We used the following two relations for crosschecks

$$\begin{aligned}
 0 &= \iint d^D q_1 d^D q_2 \frac{\partial}{\partial q_1^\mu} \frac{\prod_{i=1}^s q_1^{\sigma_i} q_1^\mu}{(q_1^2 - m_1^2)^a} \frac{1}{((q_1 + q_2)^2 - m_2^2)^b} \frac{\prod_{j=1}^r q_2^{\rho_j}}{(q_2^2 - m_3^2)^c} \\
 &= (D + s)I_{s,r}(a, b, c) - 2aI_{s+2,r}(a + 1, b, c) \\
 &\quad - 2b(I_{s+2,r}(a, b + 1, c) + I_{s+1,r+1}(a, b + 1, c)),
 \end{aligned} \tag{4.36}$$

$$\begin{aligned}
 0 &= \iint d^D q_1 d^D q_2 \frac{\partial}{\partial q_2^\mu} \frac{\prod_{i=1}^s q_1^{\sigma_i}}{(q_1^2 - m_1^2)^a} \frac{1}{((q_1 + q_2)^2 - m_2^2)^b} \frac{\prod_{j=1}^r q_2^{\rho_j} q_2^\mu}{(q_2^2 - m_3^2)^c} \\
 &= (D + r)I_{s,r}(a, b, c) - 2cI_{s,r+2}(a, b, c + 1) \\
 &\quad - 2b(I_{s,r+2}(a, b + 1, c) + I_{s+1,r+1}(a, b + 1, c)).
 \end{aligned} \tag{4.37}$$

Where I is given by

$$I_{s,r}(a, b, c) = \iint d^D q_1 d^D q_2 \frac{\prod_{i=1}^s q_1^{\sigma_i}}{(q_1^2 - m_1^2)^a} \frac{1}{((q_1 + q_2)^2 - m_2^2)^b} \frac{\prod_{j=1}^r q_2^{\rho_j}}{(q_2^2 - m_3^2)^c}. \tag{4.38}$$

The addition of 1 and 2 to the q_i tensor rank, s and r , means that the contracted μ appear with the respective loop momentum of the category s and r .

These relations allow for a fully analytic consistency check of our solution. We implemented an automatic check of all index combinations used in the calculations, presented in this thesis, and obtained agreement. We also numerically compared to the result of [30] for low powers of propagators and tensor ranks. Note that the IBP relations always relate $I_{s,r}(a, b, c)$ with integrals of increased tensor order and powers of the propagators. Comparing the starting point numerically and consistently rising to arbitrary orders by the IBP recurrence relation, poses a strong check of the result and implementation of the integral.

In fact we also applied similar IBP checks to all solutions of one loop integrals we implemented.

4.5. Functions and structures of Medusa

In this section we will take a closer look at the implementation of the Mathematica package Medusa. We will shortly present the two ways to use it for calculations: fully

automatic and semi automatic. The necessary steps for a calculation with Medusa only change slightly for different cases, which is why we implemented an optimised, via options customizable function to handle one diagram or a list of diagrams. In some cases however one might be interested to see and manipulate intermediate expressions, which is why all functions for specific tasks are also made accessible. Where adequate we will give complete lists of conceptually linked structures as quick references.

Fully automatic calculation of amplitudes

The outline of the steps has been already given in Section 4.1. Now we will discuss the implementation and the options it offers.

$$\text{ComputeAmplitudes}[OutputDir, Name, Range, ExpansionOrder, OSrules, MassHierarchy, Amplitude]$$

Since at two loop the number of diagrams can reach $\mathcal{O}(1000)$, the parameters *OutputDir* and *Name* have been introduced. This gives the possibility to structure the output by contributions. For simple calculations one can set the *OutputDir* to False which will return the results directly as Mathematica output. *Range* is a list of the diagram numbers to calculate and allows to split a calculation into several parts, for example when naive parallelisation is used. The *ExpansionOrder* = $\{a, b\}$ is supposed to be a list where the first integer *a* dictates the order of the asymptotic expansion in small momenta, while the second integer *b* is the order to which the integrals of Section 4.4 are expanded. The required order in the expansion in small momenta is small in the applications to be considered with the package. The recommended expansion order for the integral depends on the masses in question. Tested values reach up to 20. It is important to correctly take into account possible small masses, that are of the scale of the external momentum, in the asymptotic expansion. This is done by specifying the *MassHierarchy*, i.e. $MassHierarchy = \{\{0, m_b\}, M_W, M_t, M_{H^\pm}\}$, which categorises the masses into small, list of masses in the first element, i.e. m_b , and large M_W, M_t, M_{H^\pm} , whose hierarchy is dictated by their order in the subsequent elements. The hierarchy will be automatically used to evaluate the expansion in the two-loop solution accordingly. The *OSrules*, i.e. $OSrules = \{\text{Scalp}[\text{FourMomentum}[\text{Outgoing}, 1], \text{FourMomentum}[\text{Outgoing}, 1]] \rightarrow 0\}$, are used if a process is to be evaluated on-shell and are expected to be a list of rules replacing scalar products of external momenta. The *Amplitude* has to be given in

FeynArts notation. It is important to keep this in mind when performing custom manipulations on the amplitude beforehand.

There are a wide range of options falling into two categories: functional and diagnostic. First we will briefly review the functional options to influence the flow of the calculation.

The most important one is **OptionsDir**(file name), which can be set either to a directory containing the files `FCRules.m` and `hooks.m` or to a list of the explicit file names in the order given here.

`FCRules` can contain custom rules to change the handling of open fermion chains. A default set of rules is defined based on anticommuting γ_5 , which just sorts the chains to reduce the number of terms. Often there is the need to customize these rules. As discussed in Section 3.1.2 different basis can be chosen for matching calculations. This applies to the choice of on-shell and off-shell basis discussed in Section 3.1.2 as well as different basis for other processes. As the desired basis varies from calculation to calculation the definition of the basis via Mathematica replacement rules, has to be user defined.

In `hooks.m` functions can be defined that give the possibility to include user defined code during the calculation. The first is `PreProd`, that can be used to modify the parts of the amplitude before the calculation. The second one, `hook1`, is called right before the asymptotic expansion, i.e. right before the first non-trivial task. It takes two arguments. The first is the global factor of the diagram containing all the couplings. The second is a sum containing the rest. At this point of the calculation the structure of the amplitude has been simplified from the original FeynArts formatting. Most importantly all the factors are extracted out of the trace and fermion chain, which makes it the ideal point to select the desired contributions. For example we selected only the $\tan^2 \beta$ enhanced terms in the calculation detailed in Section 3.3.2. This corresponds to the definition

```
hook1[GlobalFactor_, MainTerm_] := {GlobalFactor, TB2Coefficient[MainTerm, TB2]}
```

This reduces the number of terms and can lead to a considerable speed up. The last function `HookFunkEnd` is called after `ComputeAmplitudes` is finished and can be used to simplify the output. It receives the final result of `ComputeAmplitudes` as first argument, the specified output directory as second argument and the number of

the considered diagram as third argument. It can be useful to split the result into contributions on this level, producing different output files for each.

UseHypExp (Boolean) and **UseHypExpLib**(Boolean) control whether HypExp and its built in database is used. While it is strongly suggested to use HypExp, there exists also a considerably slower reduction based method to evaluate the hypergeometric functions in Equation (4.32). By default HypExp starts to build a library of known functions, which can speed up the calculation noticeably, thus this too is recommended. Medusa comes with a modification of HypExp replacing the functions controlling the library to extend the range of possible parameters, which by default cannot surpass single digit numbers. This means that when using this feature an old library created without the modification will not be compatible. As the modification does not touch the functionality and just extends the reach of the library it can be consistently used whenever using HypExp for other applications.

UseTLFin (Boolean) determines whether to directly insert the full result of two loop integrals or to keep the final part as the Head **TLFin**. Also this is strongly recommended as cancellations mostly happens when adding all diagrams, which makes it more efficient to first add and then simplify.

AutoOptimizeMomenta (Boolean) has been introduced, since the momentum flow of the FeynArts amplitudes is most of the times not optimal. When set to **True** **ComputeAmplitudes** tries to minimize the number of propagators with external momentum dependence to preemptively simplify the asymptotic expansion and minimize the number of terms. As there are no negative effects and it speeds up the calculation this too is recommended.

Finally the options for the asymptotic expansion: **UseLargeMassExpansion** (Boolean) can be set to **False** when a naive expansion is sufficient. **NoExpansion** (Boolean) cannot be used on two-loop, since Medusa can only handle vacuum integrals. On one-loop it should be considered experimental, as not all one-loop integrals are implemented as of now. Furthermore there are specialised programs and packages to handle one-loop calculations [64, 74, 43], which will be faster. We used this mainly for crosschecks with the mentioned programs when calculating the counterterms.

Next we review the diagnostic options.

RunLog (Boolean or file name) specifies if and where to write a log during runtime. The content of the log are both the tasks last completed and key parameters of the calculation. These are: time expired for the specified step, memory required, maximum

memory used and the leaf count of the intermediate expression.

ReapIntermediate (Boolean) can be used to get a list of intermediate results at key points of the calculation, i.e. in between the important steps.

TagAsExpContributions (Boolean) controls whether the extra terms due to the asymptotic expansion, as compared to the naive expansion, should be tagged.

To use the maximum potential of a Mathematica implementation care has been taken to make sure user defined objects are not touched, while making sure that automated steps are robust. When investigating the γ_5 dependence of the amplitude, see Section 3.3.3, for example this idea was very helpful. The order of steps in **ComputeAmplitudes** is to solve traces in the before the asymptotic expansion to make use of simplifications early on. To test many schemes with one result however it is much more useful to return the result with the traces unevaluated. This is easily possible by introducing a custom Head for the trace, while making sure the loop momenta are explicitly separated, i.e. the object replaced consists only of γ -matrices. The implemented automatic calculation then just ignores the custom Head. Since everything is built to handle open Lorentz indices, the missing trace leads to no errors and can be treated, by hand in a number of schemes, after the rest of the calculation is taken care of automatically.

Next we will shortly review the structures that will constitute the result.

For the Lorentz structure we kept mostly to the FeynArts notation, with the notable exception of the symbolically symmetrised products. As stated in Section 4.1 they are crucial to the handling of tensorial integrals. All structures are summarised in Table 4.1.

Global contraction rules are defined only for the symmetric products, as they are introduced in the expression in a controlled way through the solution of the loop integrals. As both the Lorentz structure and the solution of the integral can include a number of terms, it is very inefficient to expand the product to contract all indices. Thus the Lorentz structure of the prefactor is contracted directly with the symmetric product of metrics that constitutes the tensorial part of the solution of the loop integral, while the rest is factored out.

The functions **LorentzContract**, **MetricElim** and **LCTElim** are used to contract all Lorentz structures or metrics and ϵ tensors respectively. We did not include global rules for the elementary structures for metric, four-vector and Levi-Civita tensor, as they often can't be further simplified. This is the case when they are contracted with a tensor integral or in the fermion chain for example/ Choosing when to contract, by

$g_{\mu\nu}$ p_μ $(g^\lambda)^{\{\mu_1, \mu_2, \dots, \mu_{2\lambda}\}}$ $\rho_1! \rho_2! (g^\lambda p_1^{\rho_1} p_2^{\rho_2})^{\{\mu_1, \dots, \mu_{2\lambda + \rho_1 + \rho_2}\}}$ $\epsilon_{\alpha\beta\mu\nu}$ $p \cdot k$ $\hat{g}_{\mu\nu}$ $\tilde{g}_{\mu\nu}$	$\text{Metric}[\mu, \nu]$ $\text{FourVector}[p, \mu]$ $\text{SymbSymMetric}[\mu_1, \dots, \mu_{2\lambda}]$ $\text{SymbSymProd}[\mu_1, \dots, \mu_{2\lambda + \rho_1 + \rho_2}][\lambda, \{\{\rho_1, p_1\}, \{\rho_2, p_2\}\}]$ $\text{LCT}[\{\alpha, \beta, \mu, \nu\}]$ $\text{Scalp}[p, k]$ $\text{H}[\text{Metric}[\mu, \nu]]$ $\text{T}[\text{Metric}[\mu, \nu]]$
LorentzContract MetricElim LCTElim	Contract all indices Contract metrics only Contract Levi-Civita Tensors only

Table 4.1.: The basic Lorentz structures and functions to manipulate them. The ϵ tensor is considered 4-dimensional, as is \tilde{g} . \hat{g} is the metric in $(D - 4)$ -dimensions. All other objects are defined in D -dimensions.

calling the above function, therefore speeds up the calculation, as the rules are only applied when needed.

It should also be pointed out that the metrics of the subspaces are viewed as projectors onto the respective subspace. Thus we do not create $(D - 4)$ and 4-dimensional scalar products in the loop integration. They are simplified only when contracting with other metrics or when resulting in zero, when projectors on two different subspaces are contracted. Following Tracer $\tilde{g} = g - \hat{g}$ is used in the fully automatic calculation, but \tilde{g} can be handled also explicitly.

As pointed out before, another important structure in the output is **TLFin**, denoting the finite part of a two-loop integral. They can be inserted explicitly via **InsertTLFin**. It is best used after adding different diagrams to keep the terms small in intermediate steps and use cancellation between diagrams in one simplification step.

Functions for single tasks

If more control over the calculation is required, it can also be carried out step by step. To properly set up certain global variables **InitializeFreeFire** is the first step. Next the amplitude has to be translated in Medusa notation via **GetFeynAmp**. This splits it into parts: *IntegralPart*, *FactorPart*, *TracePart* and *FermionChain*. The parts are accessed via **GetParts** to then manipulate with the appropriate functions. For the trace and fermion chain these are the respective prepare functions, listed in Table 4.2.

<p>MatrixTrace TraceHead TraceList FermionChain FermionChainHead ChainList</p>	<p>Trace of γ kept in FeynArts notation Placeholder for unevaluated Trace List of definitions of TraceHead Open chain of γ kept in FeynArts notation Placeholder for unevaluated open chain List of definitions of FermionChainHead</p>
<p>PrepareFermionChain InsertSimpFermionChain PrepareTrace InsertTraceSol</p>	<p>Splits kinematic variables and couplings off the chain Custom rules can be defined to match a wanted operator base Splits kinematic variables and couplings off the chain Handling of γ_5 can be controlled by options</p>

Table 4.2.: Overview over the basic Dirac-structures and the functions to manipulate them.

The introduced Placeholders can then be solved or simplified right away with the Insert functions or after the other steps.

The next step is the asymptotic expansion via `AsExp`. The result is still given in terms of propagators `SerProp`. To collect all propagators to loop integrals `GlueLoopInts` is used. At this point the loop integrals are represented with `LoopInt` and `Loop2Int`. The solutions of the loop integrals are inserted via `SolveLoopIntegrals`. The last step is the expansion in ϵ which is done with `ϵ Exp`.

CHAPTER 5

Conclusion

In this thesis we presented the calculation of the $\tan\beta$ leading contributions to the inclusive radiative B decay $\bar{B} \rightarrow X_s \gamma$ in the Two Higgs Doublet Model of type II. To this end we calculated the two-loop corrections to the Wilson coefficients due to Barr-Zee type diagrams containing $b-t$ quark and $\tau-\nu_\tau$ subloops.

The leptonic result turned out to be unexpectedly small due to cancellations between the leading diagrams. An upper bound on the relative size of the two-loop contributions due to τ subloops is only $\frac{C_7^{(1,\tau)}}{C_7^{(1,0)}} = 5.2 \cdot 10^{-4}$. This in turn means that the $\tan\beta$ independent bound on the charged Higgs mass from [67] is proven to be valid for all values of $\tan\beta$.

We investigated the $\tan\beta$ enhanced quark contributions to $b \rightarrow s \gamma$ and found that they are inseparable from the contributions due to Higgs self-couplings. Once a set of minimal parameters for the model is chosen both types contribute to the $\tan\beta$ enhanced term and do not yield finite results if they are considered separately. We also found that it is crucial to include the charged Higgs contributions to the CKM renormalisation. Thus we considered the leading $\tan\beta$ contributions to the counterterm of the CKM matrix elements, which acquire $\tan\beta$ enhanced contributions due to the flavour changing self-energies containing H^\pm . We obtain a finite but gauge variant result, hinting at a conceptual problem with the mixing self-energy contributions.

For the sake of these calculations the new Mathematica package **Medusa** has been

5. Conclusion

developed, that can be used for applications in flavour physics. This includes matching calculations for rare decays, as has been presented in this thesis, as well as the calculation of contributions to neutral meson mixing. With the presented calculations in the Two Higgs Doublet Model and the Standard Model we showed the viability of our method and implementation. The package `Medusa` provides a fully automatic implementation of two-loop calculations and is primarily aimed to enable fast calculation of two-loop contributions in a variety of models. It is being applied presently to calculate Higgs self energies at two loop in the MSSM [35].

Since in the near future the experimental landscape gets expanded by Belle II, the new package comes at an opportune time, as high precision predictions are required to make the most of the increased precision of the experiment.

APPENDIX A

Feynman diagrams of the y_b induced $\tan \beta$ enhanced terms in $b \rightarrow s\gamma$

In this appendix the relevant Feynman diagrams for the discussion of the y_b^2 contribution in Section 3.3.4 are depicted. The diagrams are split into the triangle diagrams, the class with one external mixing self energy and the class with two external self energies. Non mixing external self energy contributions are considered by renormalisation of the fields. As explained in Section 2.2 the mixing self energies are considered as proper diagrams.

A. Feynman diagrams of the y_b induced $\tan \beta$ enhanced terms in $b \rightarrow s\gamma$

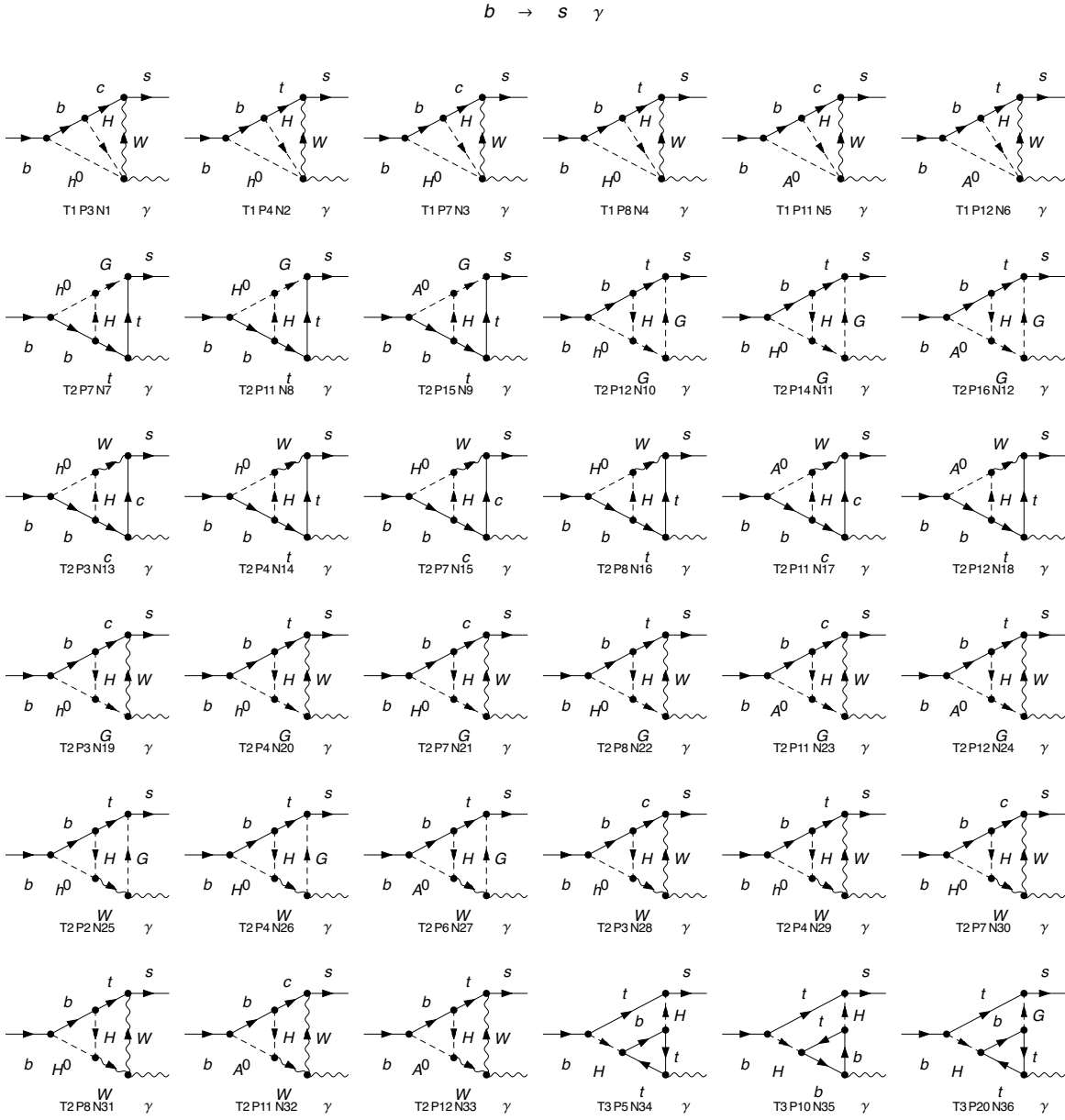


Figure A.1.: First part of the diagrams contributing to the leading y_b^2 terms.

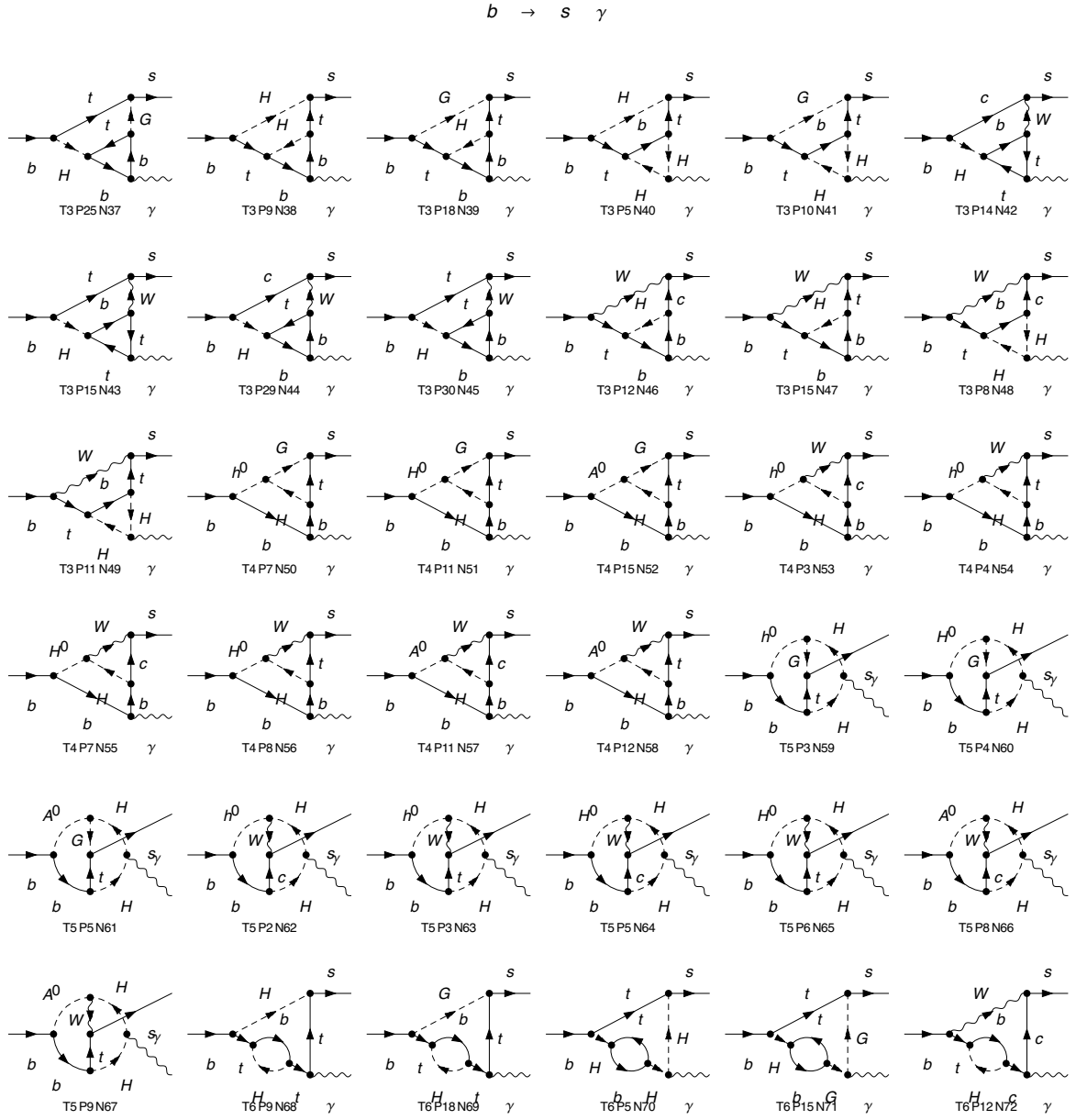


Figure A.2.: Second part of the diagrams contributing to the leading y_b^2 terms.

A. Feynman diagrams of the y_b induced $\tan \beta$ enhanced terms in $b \rightarrow s\gamma$

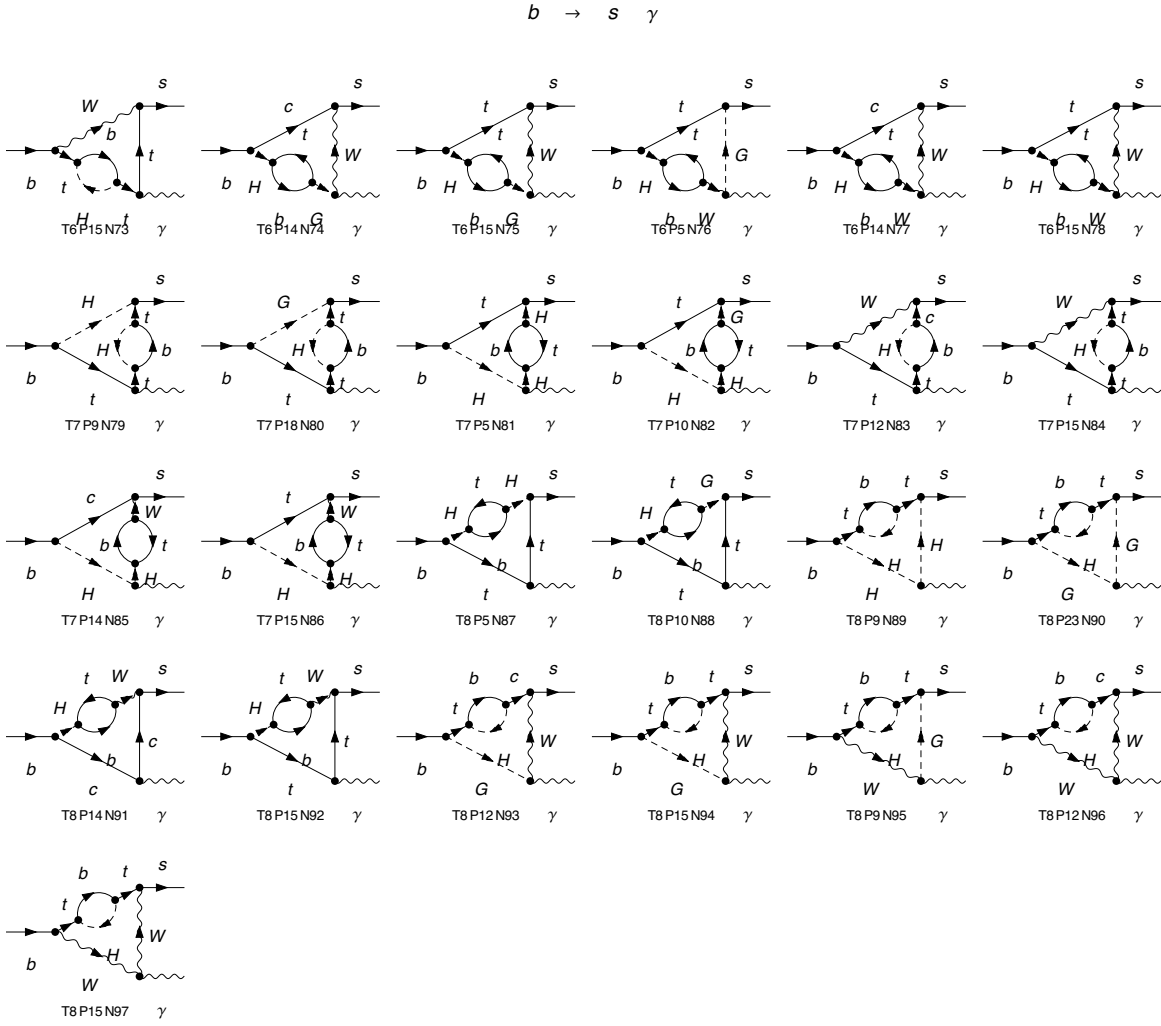


Figure A.3.: Third part of the diagrams contributing to the leading y_b^2 terms.

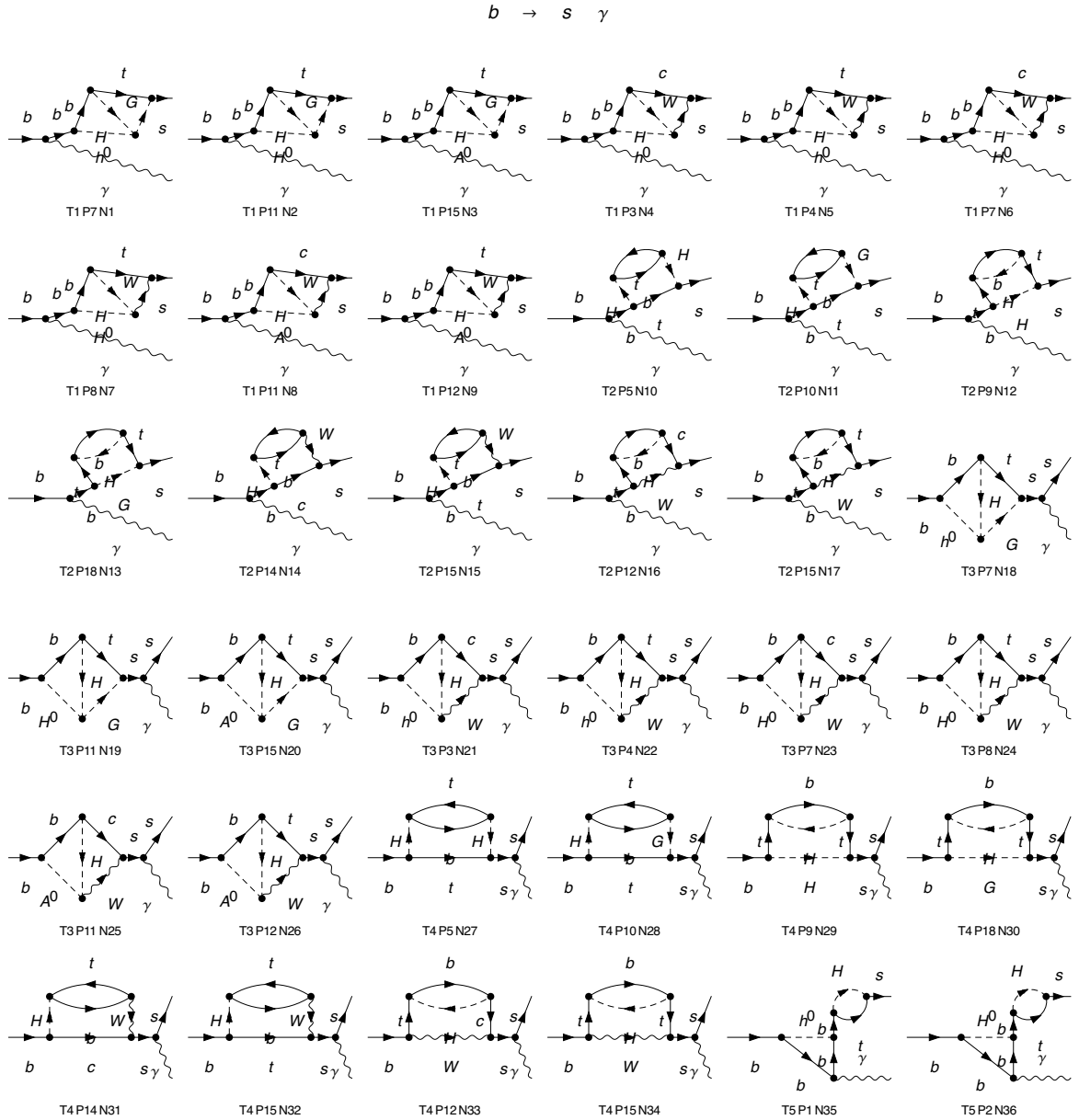


Figure A.4.: Fourth part of the diagrams contributing to the leading y_b^2 terms. Here contributions containing one external mixing self-energy are depicted.

A. Feynman diagrams of the y_b induced $\tan \beta$ enhanced terms in $b \rightarrow s \gamma$

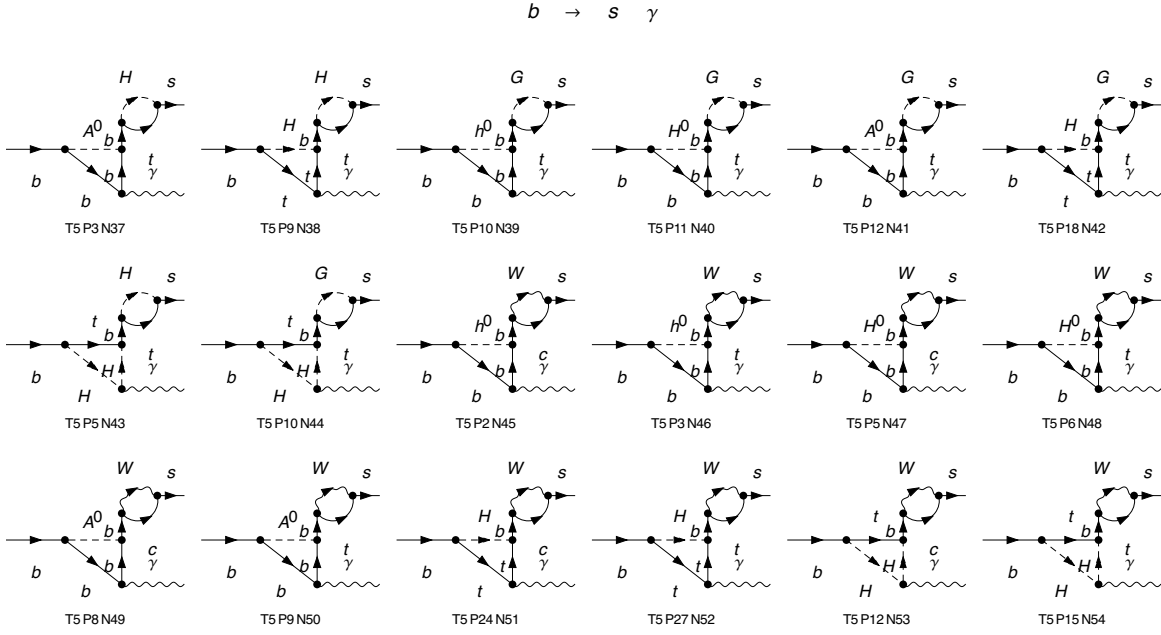


Figure A.5.: Third part of the diagrams contributing to the leading y_b^2 terms. Here contributions containing one external mixing self-energy are depicted.

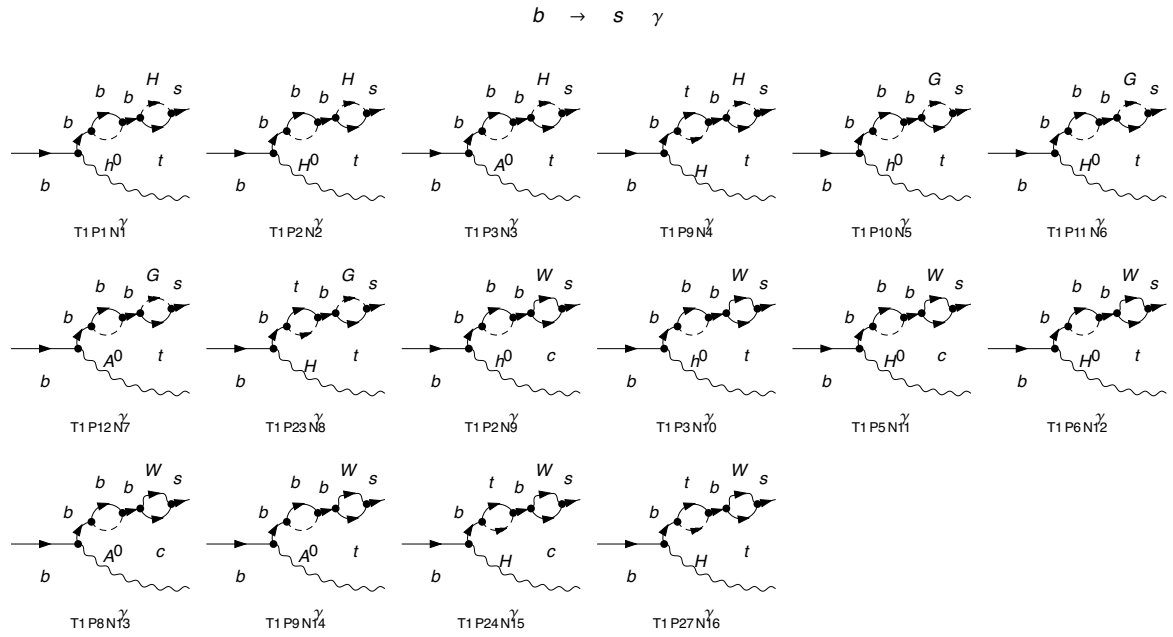


Figure A.6.: Fourth part of the diagrams contributing to the leading y_b^2 terms. Here all diagrams with two self-energy insertions are presented.

APPENDIX B

Feynman diagrams of the Higgs-coupling induced $\tan \beta$ enhanced terms in $b \rightarrow s\gamma$

In this appendix the relevant Feynman diagrams for the discussion of the contribution due to Higgs couplings in Section 3.3.4 are depicted. The diagrams are split into the triangle diagrams, the class with one external mixing self energy and the class with two external self energies. Non mixing external self energy contributions are considered by renormalisation of the fields. As explained in Section 2.2 the mixing self energies are considered as proper diagrams.

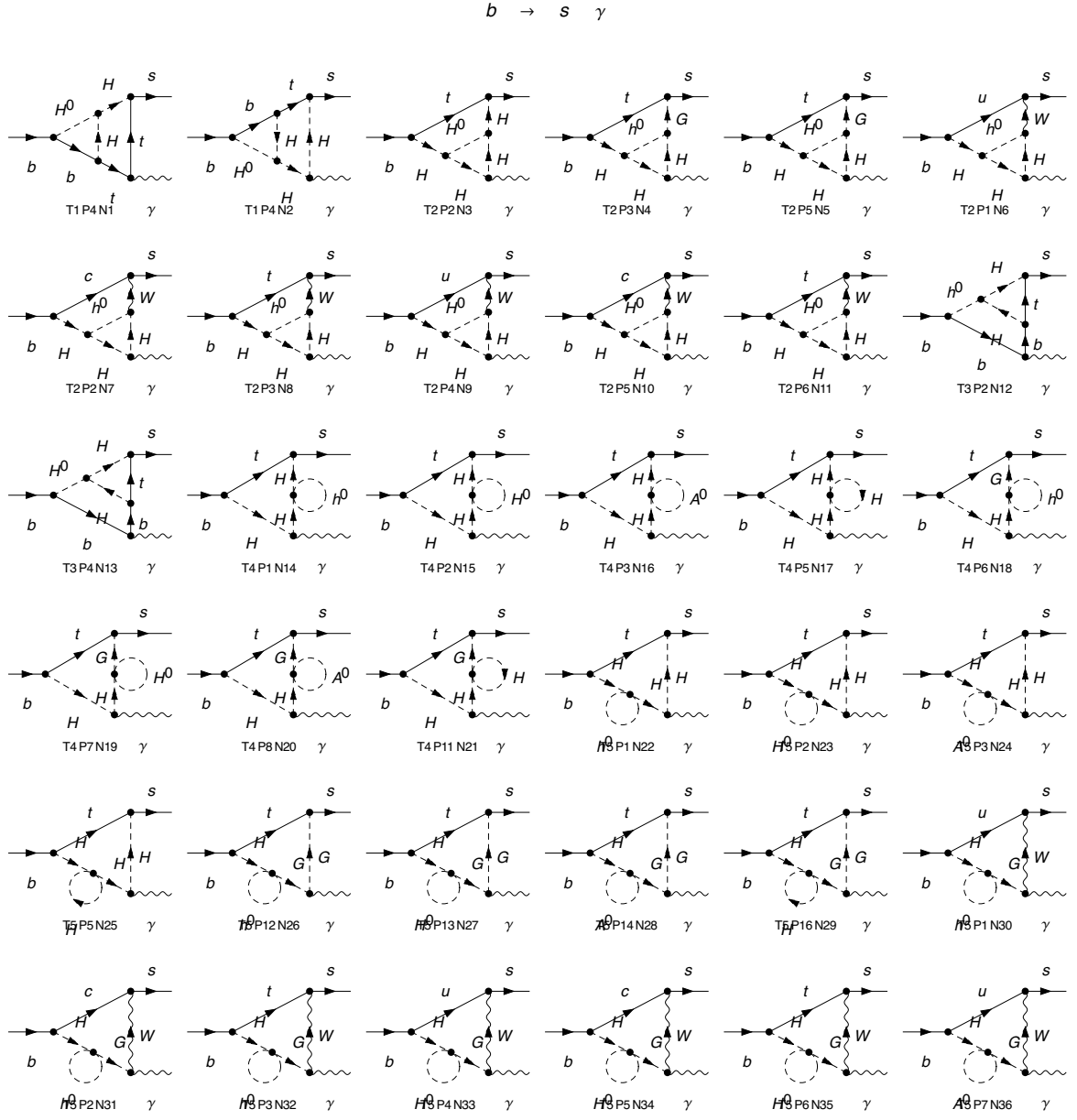


Figure B.1.: The diagrams depicted here constitute the contribution to the leading $\tan \beta$ term, where at least one of the $\tan \beta$ originates from a triple Higgs coupling.

B. Feynman diagrams of the Higgs-coupling induced $\tan \beta$ enhanced terms in $b \rightarrow s \gamma$

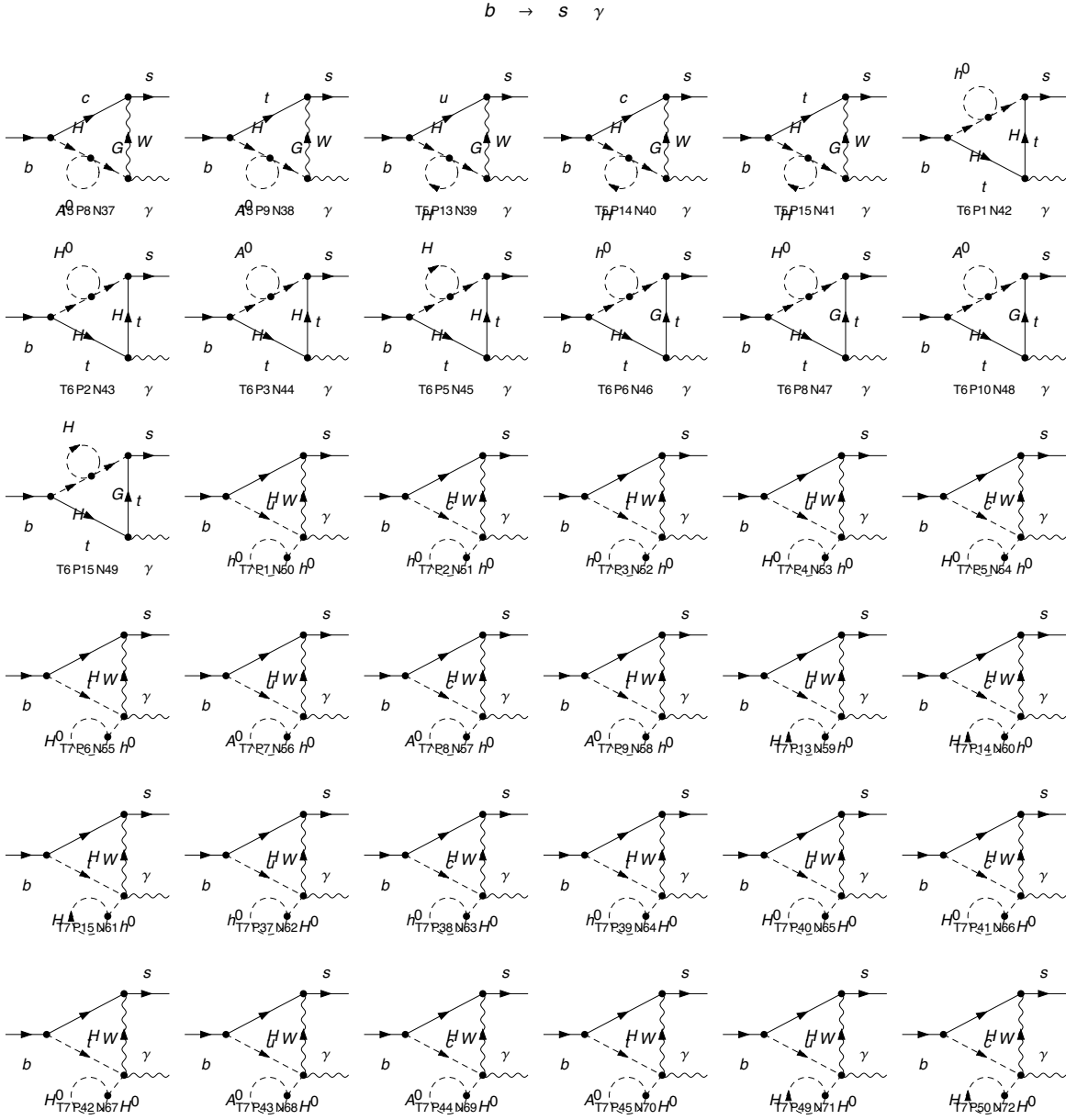


Figure B.2.: The diagrams depicted here constitute the contribution to the leading $\tan \beta$ term, where at least one of the $\tan \beta$ originates from a triple Higgs coupling.

$$b \rightarrow s \gamma$$

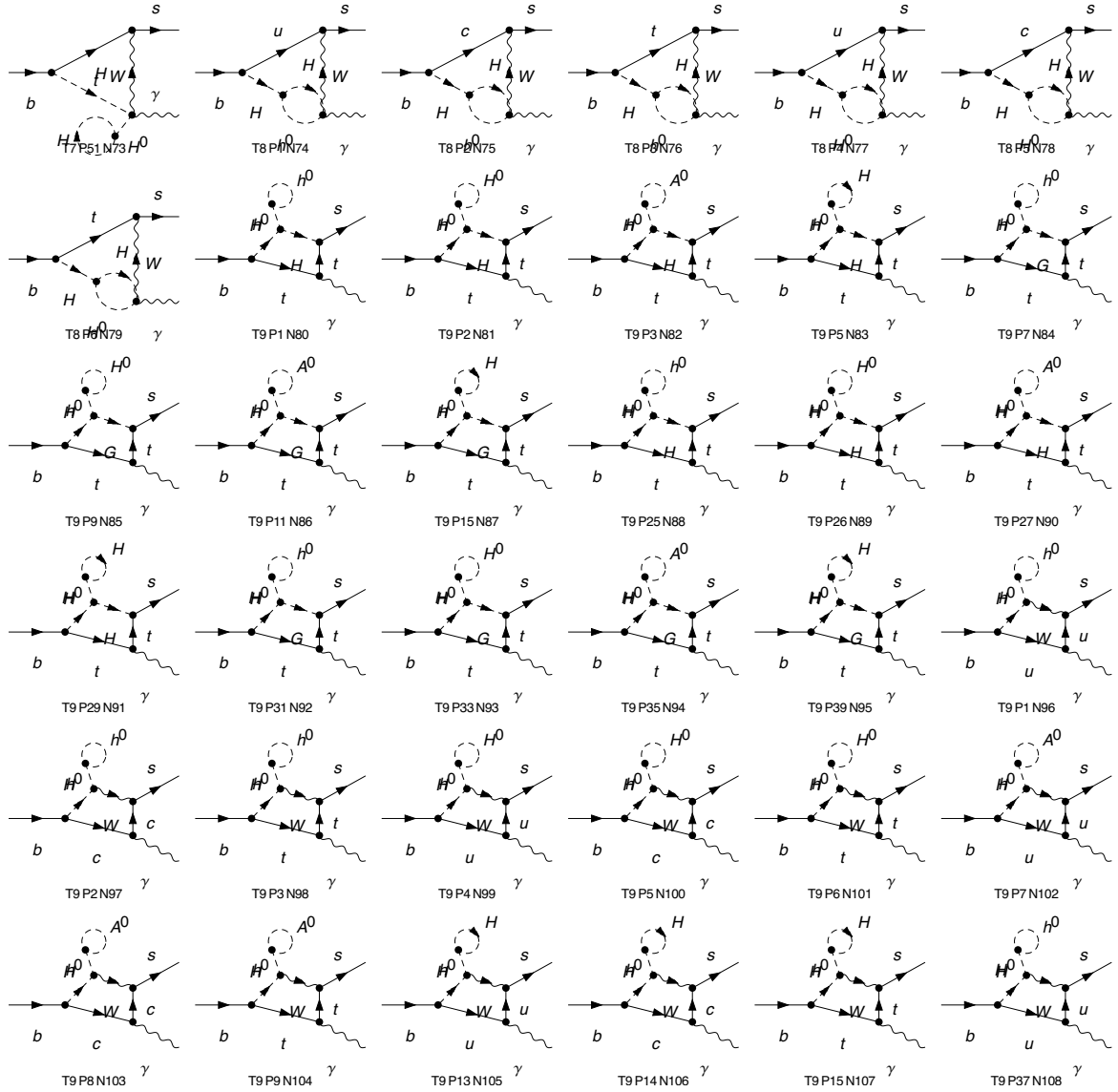


Figure B.3.: The diagrams depicted here constitute the contribution to the leading $\tan \beta$ term, where at least one of the $\tan \beta$ originates from a triple Higgs coupling.

B. Feynman diagrams of the Higgs-coupling induced $\tan\beta$ enhanced terms in $b \rightarrow s\gamma$

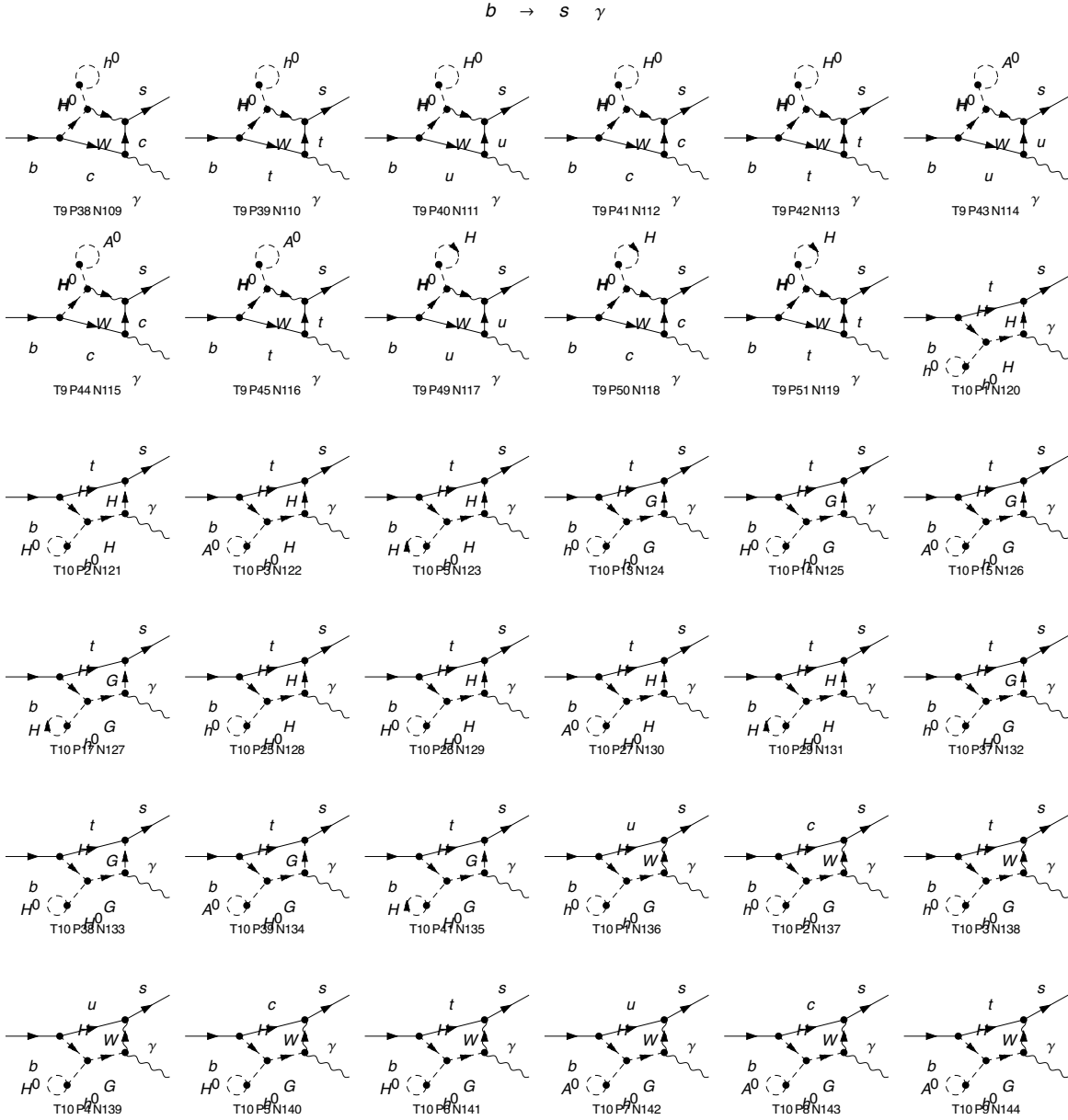


Figure B.4.: The diagrams depicted here constitute the contribution to the leading $\tan\beta$ term, where at least one of the $\tan\beta$ originates from a triple Higgs coupling.

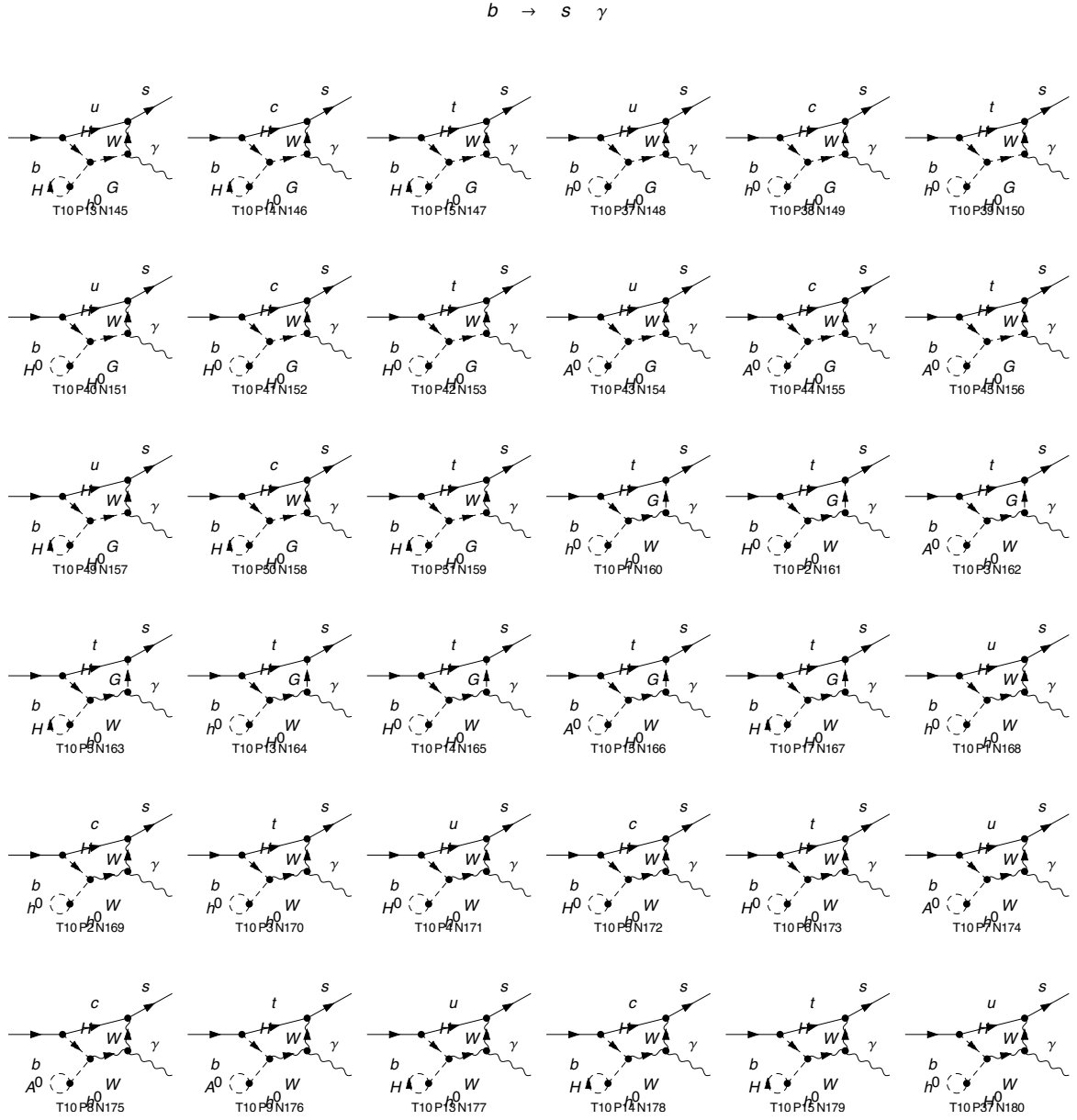


Figure B.5.: The diagrams depicted here constitute the contribution to the leading $\tan \beta$ term, where at least one of the $\tan \beta$ originates from a triple Higgs coupling.

B. Feynman diagrams of the Higgs-coupling induced $\tan \beta$ enhanced terms in $b \rightarrow s \gamma$

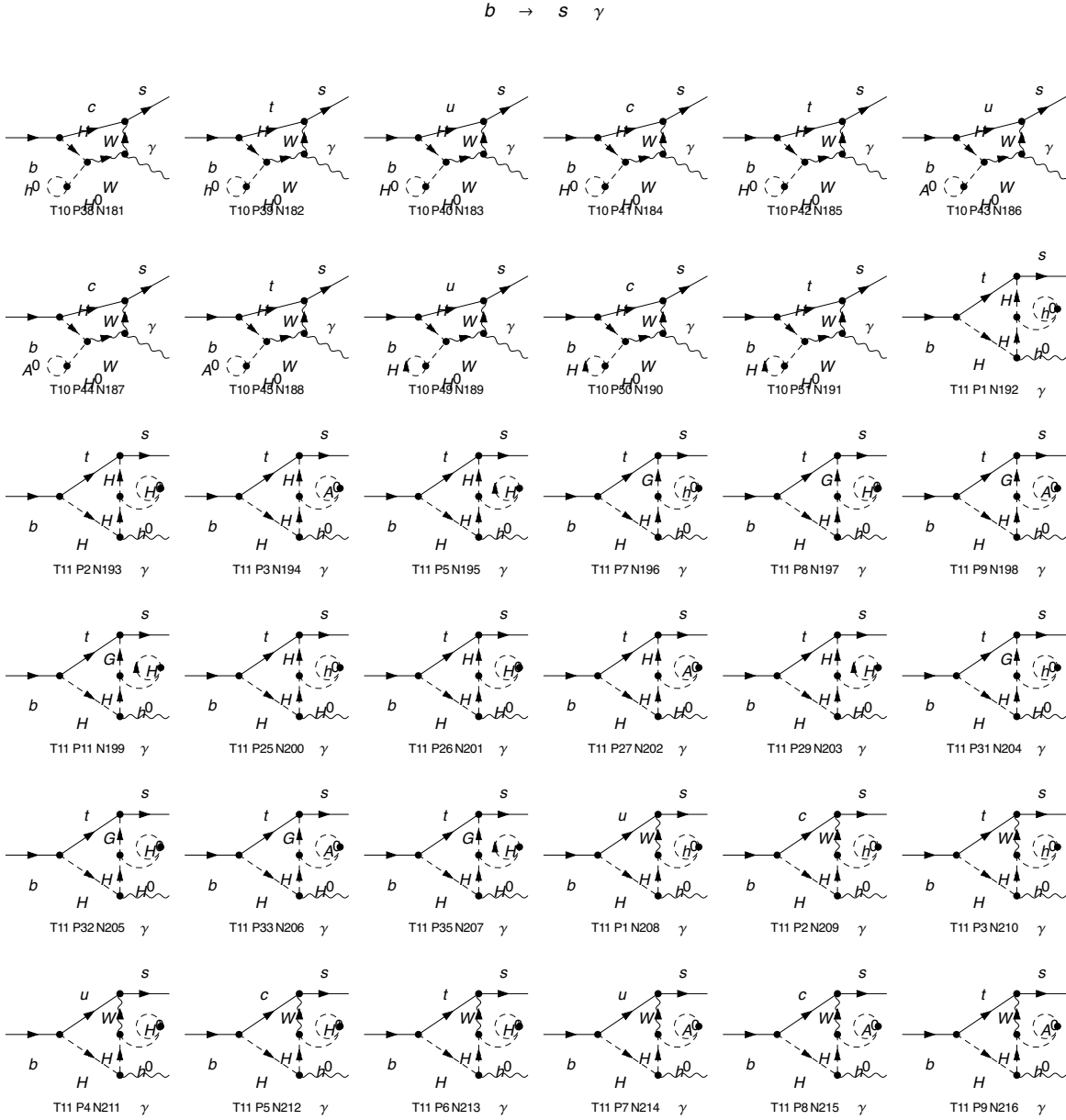


Figure B.6.: The diagrams depicted here constitute the contribution to the leading $\tan \beta$ term, where at least one of the $\tan \beta$ originates from a triple Higgs coupling.

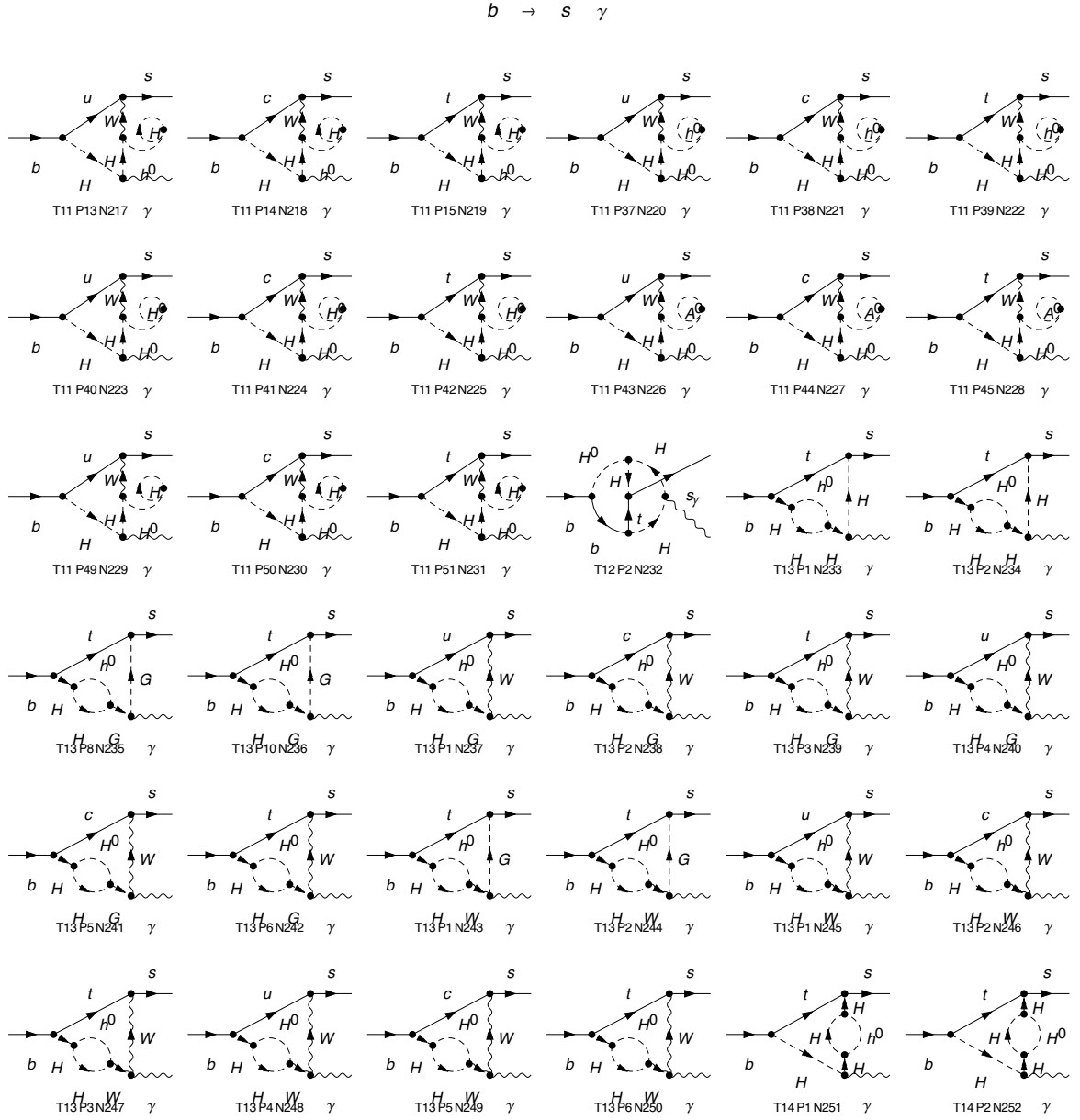


Figure B.7.: The diagrams depicted here constitute the contribution to the leading $\tan \beta$ term, where at least one of the $\tan \beta$ originates from a triple Higgs coupling.

B. Feynman diagrams of the Higgs-coupling induced $\tan \beta$ enhanced terms in $b \rightarrow s \gamma$

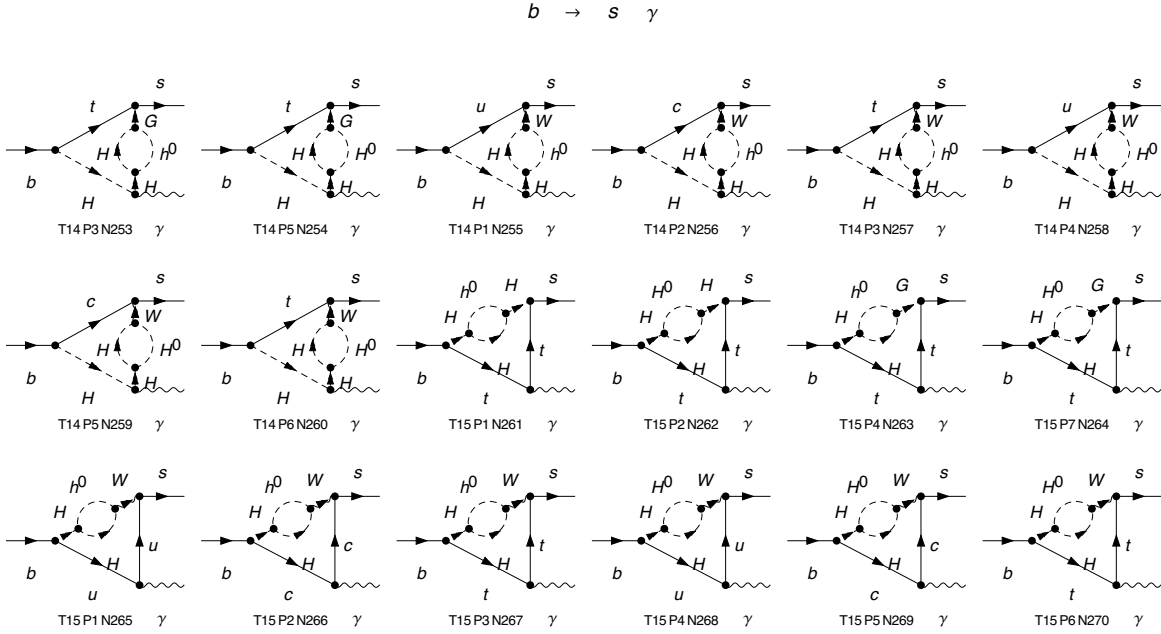


Figure B.8.: The diagrams depicted here constitute the contribution to the leading $\tan \beta$ term, where at least one of the $\tan \beta$ originates from a triple Higgs coupling.

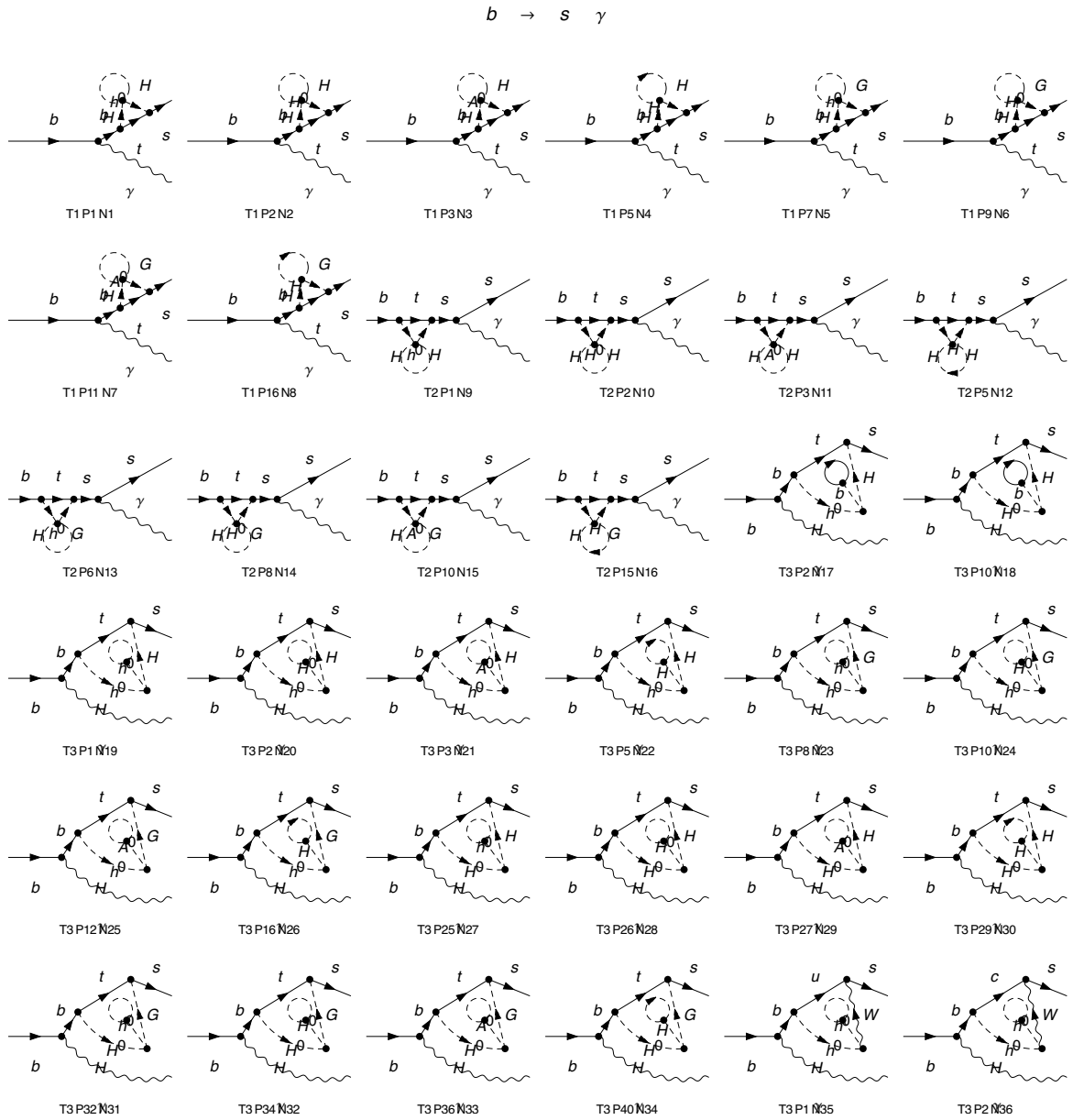


Figure B.9.: The diagrams depicted here constitute the contribution to the leading $\tan \beta$ term, where at least one of the $\tan \beta$ originates from a triple Higgs coupling.

B. Feynman diagrams of the Higgs-coupling induced $\tan \beta$ enhanced terms in $b \rightarrow s \gamma$

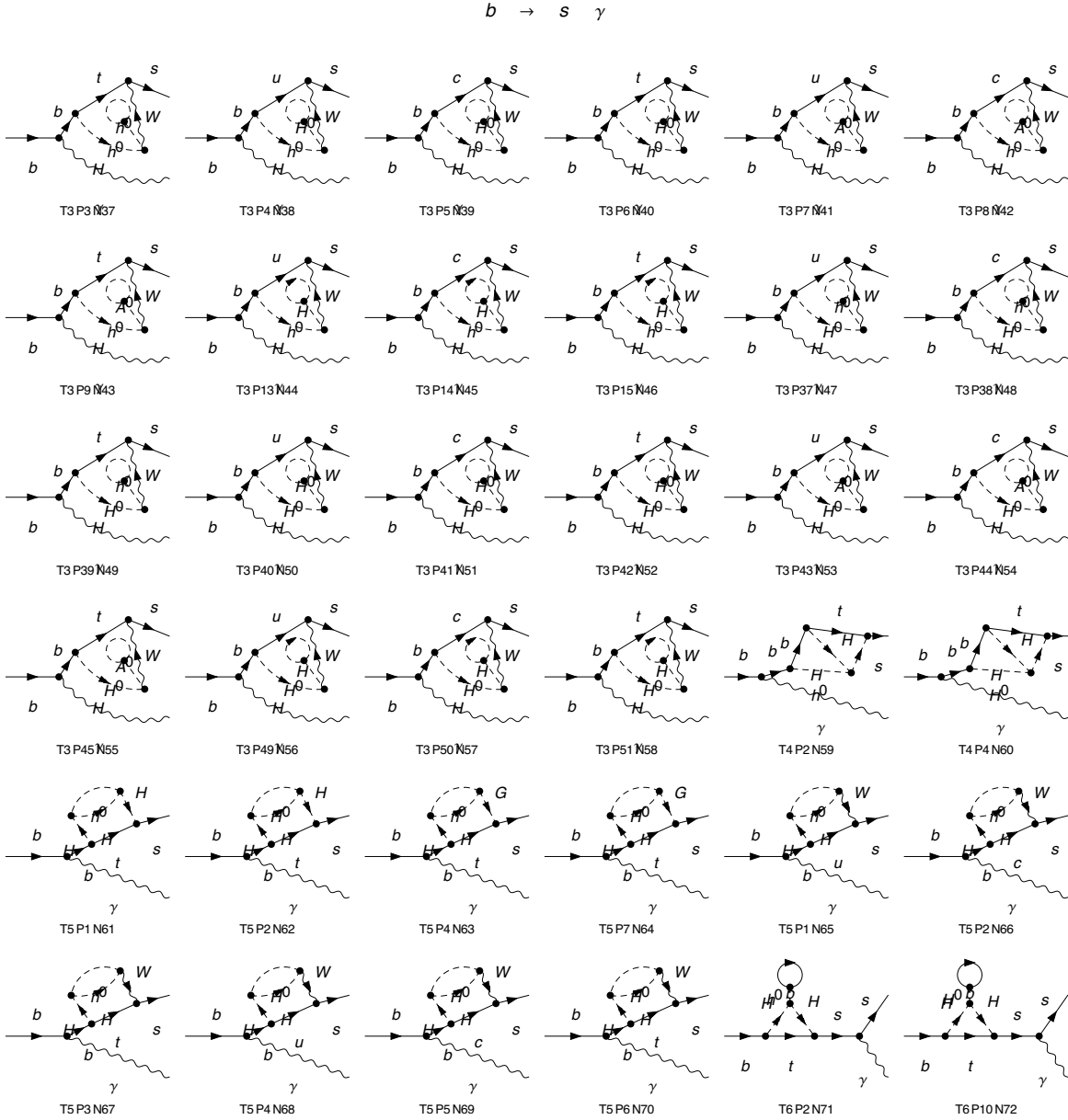


Figure B.10.: The diagrams depicted here constitute the contribution to the leading $\tan \beta$ term, where at least one of the $\tan \beta$ originates from a triple Higgs coupling.

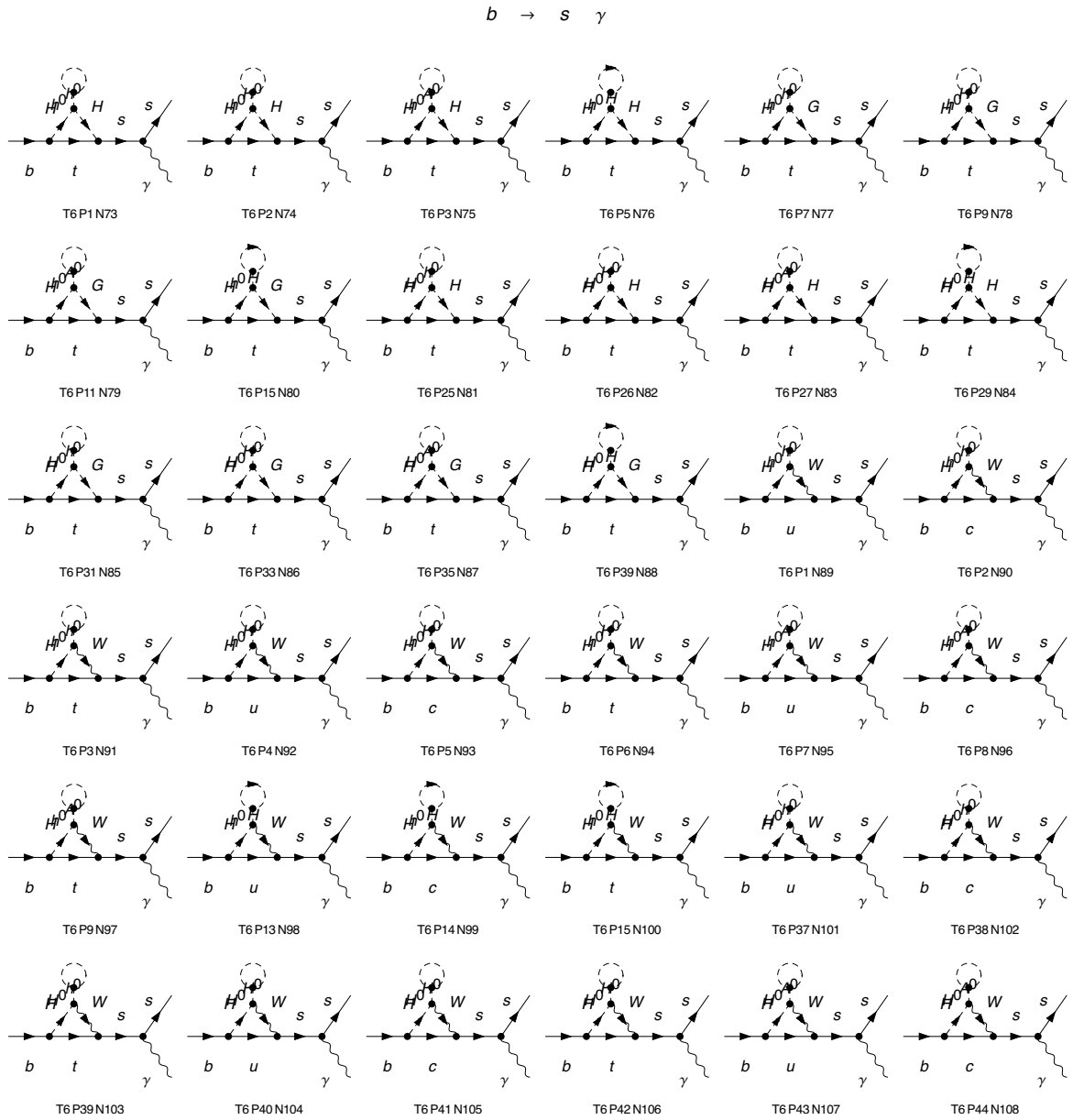


Figure B.11.: The diagrams depicted here constitute the contribution to the leading $\tan \beta$ term, where at least one of the $\tan \beta$ originates from a triple Higgs coupling.

B. Feynman diagrams of the Higgs-coupling induced $\tan \beta$ enhanced terms in $b \rightarrow s \gamma$

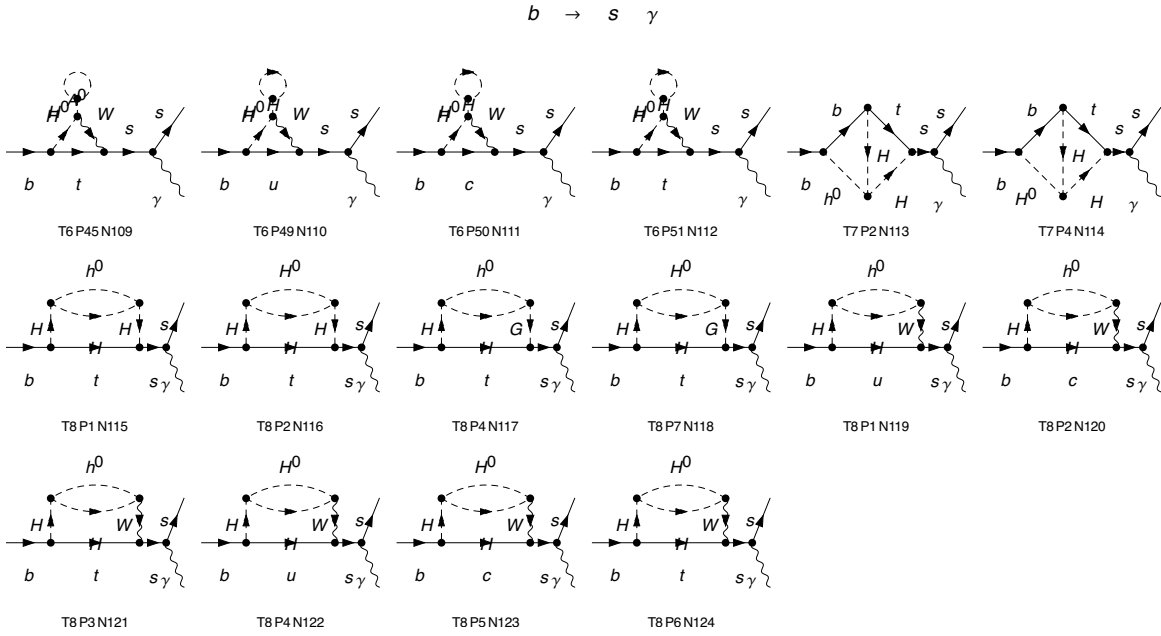


Figure B.12.: The diagrams depicted here constitute the contribution to the leading $\tan \beta$ term, where at least one of the $\tan \beta$ originates from a triple Higgs coupling.

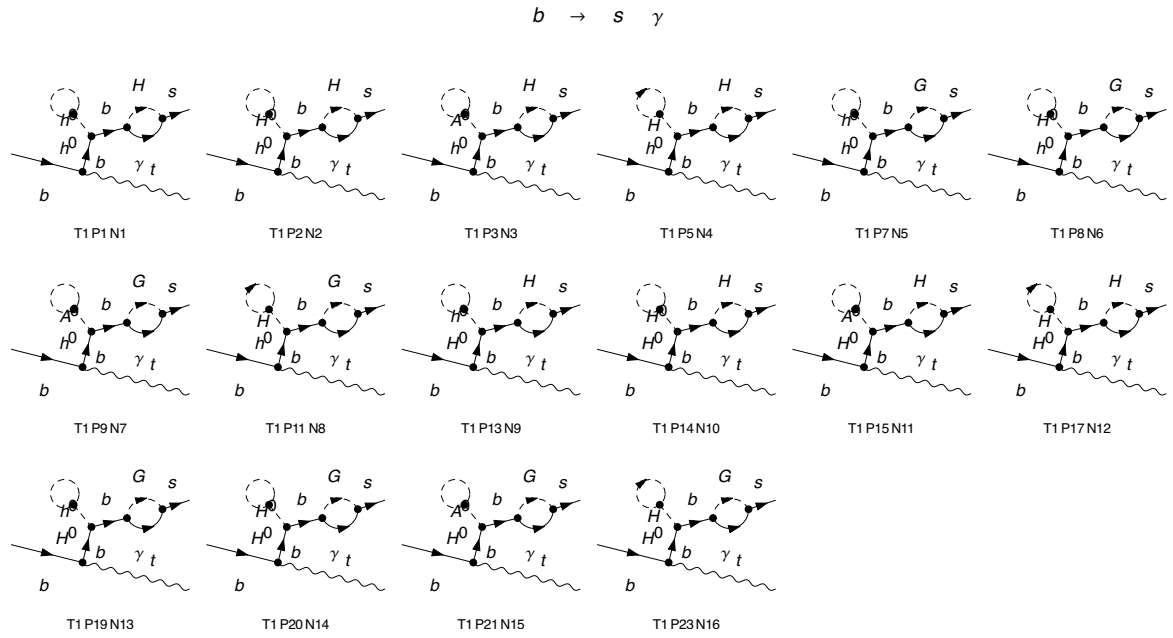


Figure B.13.: The diagrams depicted here constitute the contribution to the leading $\tan \beta$ term, where at least one of the $\tan \beta$ originates from a triple Higgs coupling.

Bibliography

- [1] A. Abdesselam et al. “Measurement of the inclusive $B \rightarrow X_{s+d}\gamma$ branching fraction, photon energy spectrum and HQE parameters”. In: *Proceedings, 38th International Conference on High Energy Physics (ICHEP 2016): Chicago, IL, USA, August 3-10, 2016*. 2016. arXiv: 1608.02344 [hep-ex].
- [2] Kazuo Abe et al. “A Measurement of the branching fraction for the inclusive $B \rightarrow X(s)\gamma$ decays with BELLE”. In: *Phys. Lett.* B511 (2001), pp. 151–158. arXiv: hep-ex/0103042 [hep-ex].
- [3] Tomohiro Abe et al. “Gauge invariant Barr-Zee type contributions to fermionic EDMs in the two-Higgs doublet models”. In: *JHEP* 01 (2014). [Erratum: JHEP04, 161(2016)], p. 106. arXiv: 1311.4704 [hep-ph].
- [4] A. G. Akeroyd et al. “Prospects for charged Higgs searches at the LHC”. In: *Eur. Phys. J.* C77.5 (2017), p. 276. arXiv: 1607.01320 [hep-ph].
- [5] Y. Amhis et al. “Averages of b -hadron, c -hadron, and τ -lepton properties as of summer 2016”. In: (2016). arXiv: 1612.07233 [hep-ex].
- [6] Bernard Aubert et al. “Measurement of the $B \rightarrow X_s\gamma$ branching fraction and photon energy spectrum using the recoil method”. In: *Phys. Rev.* D77 (2008), p. 051103. arXiv: 0711.4889 [hep-ex].
- [7] Julien Baglio et al. “Benchmarks for Higgs Pair Production and Heavy Higgs boson Searches in the Two-Higgs-Doublet Model of Type II”. In: *Phys. Rev.* D90.1 (2014), p. 015008. arXiv: 1403.1264 [hep-ph].
- [8] S. M. Barr, E. M. Freire, and A. Zee. “Mechanism for large neutrino magnetic moments”. In: *Phys. Rev. Lett.* 65 (21 Nov. 1990), pp. 2626–2629.

-
- [9] A. V. Bednyakov and A. F. Pikelner. “Four-loop strong coupling beta-function in the Standard Model”. In: *Phys. Lett.* B762 (2016), pp. 151–156. arXiv: 1508.02680 [hep-ph].
- [10] D. Binosi and L. Theussl. “JaxoDraw: A Graphical user interface for drawing Feynman diagrams”. In: *Comput. Phys. Commun.* 161 (2004), pp. 76–86. arXiv: hep-ph/0309015 [hep-ph].
- [11] Christoph Bobeth, Mikolaj Misiak, and Joerg Urban. “Matching conditions for $b \rightarrow s\gamma$ and $b \rightarrow sgluon$ in extensions of the standard model”. In: *Nucl. Phys.* B567 (2000), pp. 153–185. arXiv: hep-ph/9904413 [hep-ph].
- [12] Christoph Bobeth, Mikolaj Misiak, and Jorg Urban. “Photonic penguins at two loops and m_t dependence of $BR[B \rightarrow X_s l^+ l^-]$ ”. In: *Nucl. Phys.* B574 (2000), pp. 291–330. arXiv: hep-ph/9910220 [hep-ph].
- [13] Christoph Bobeth et al. “ $B_{s,d} \rightarrow l^+ l^-$ in the Standard Model with Reduced Theoretical Uncertainty”. In: *Phys. Rev. Lett.* 112 (2014), p. 101801. arXiv: 1311.0903 [hep-ph].
- [14] Manfred Böhm, Ansgar Denner, and Hans Joos. *Gauge Theories of the Strong and Electroweak Interaction*. 2001.
- [15] Francesca Borzumati and Christoph Greub. “2HDMs predictions for anti-B \rightarrow X(s) gamma in NLO QCD”. In: *Phys. Rev.* D58 (1998), p. 074004. arXiv: hep-ph/9802391 [hep-ph].
- [16] P. Breitenlohner and D. Maison. “Dimensional Renormalization and the Action Principle”. In: *Commun.Math.Phys.* 52 (1977), pp. 11–38.
- [17] Joachim Brod, Frank Fugel, and Bernd A. Kniehl. “Two-Loop Electroweak Corrections to the A0 gamma gamma and A0 g g Couplings of the CP-Odd Higgs Boson”. In: *Nucl. Phys.* B807 (2009), pp. 188–209. arXiv: 0807.1008 [hep-ph].
- [18] Joachim Brod and Martin Gorbahn. “Next-to-Next-to-Leading-Order Charm-Quark Contribution to the CP Violation Parameter ϵ_K and ΔM_K ”. In: *Phys. Rev. Lett.* 108 (12 Mar. 2012), p. 121801.
- [19] Andrzej J. Buras, Matthias Jamin, and Peter H. Weisz. “Leading and next-to-leading QCD corrections to ϵ -parameter and $B_0 - \bar{B}_0$ mixing in the presence of a heavy top quark”. In: *Nuclear Physics B* 347.3 (1990). ISSN: 0550-3213.

- [20] Andrzej J. Buras and Peter H. Weisz. “QCD Nonleading Corrections to Weak Decays in Dimensional Regularization and ’t Hooft-Veltman Schemes”. In: *Nucl. Phys.* B333 (1990), pp. 66–99.
- [21] S. Chen et al. “Branching fraction and photon energy spectrum for $b \rightarrow s\gamma$ ”. In: *Phys. Rev. Lett.* 87 (2001), p. 251807. arXiv: hep-ex/0108032 [hep-ex].
- [22] K. G. Chetyrkin. “A closed analytical formula for two loop massive tadpoles with arbitrary tensor numerators”. In: *3rd International Workshop on Software Engineering, Artificial Intelligence and Expert systems for High-energy and Nuclear Physics (AIHENP 93) Oberammergau, Germany, October 4-8, 1993*. 1993, pp. 559–563. arXiv: hep-ph/0212040 [hep-ph].
- [23] Konstantin G. Chetyrkin et al. “Massive Tadpoles: Techniques and Applications”. In: *Nucl. Part. Phys. Proc.* 261-262 (2015), pp. 19–30. arXiv: 1502.00509 [hep-ph].
- [24] Paolo Ciafaloni, Andrea Romanino, and Alessandro Strumia. “Two loop QCD corrections to charged Higgs mediated $b \rightarrow s \gamma$ decay”. In: *Nucl. Phys.* B524 (1998), pp. 361–376. arXiv: hep-ph/9710312 [hep-ph].
- [25] Marco Ciuchini et al. “Next-to-leading QCD corrections to $B \rightarrow X_s \gamma$: Standard model and two Higgs doublet model”. In: *Nucl. Phys.* B527 (1998), pp. 21–43. arXiv: hep-ph/9710335 [hep-ph].
- [26] John C. Collins. *Renormalization: An Introduction to Renormalization, the Renormalization Group and the Operator-Product Expansion*. Cambridge Monographs on Mathematical Physics. Cambridge University Press, 1984.
- [27] Andreas Crivellin, Julian Heeck, and Peter Stoffer. “A perturbed lepton-specific two-Higgs-doublet model facing experimental hints for physics beyond the Standard Model”. In: *Phys. Rev. Lett.* 116.8 (2016), p. 081801. arXiv: 1507.07567 [hep-ph].
- [28] Andreas Crivellin, Ahmet Kokulu, and Christoph Greub. “Flavor-phenomenology of two-Higgs-doublet models with generic Yukawa structure”. In: *Phys. Rev.* D87.9 (2013), p. 094031. arXiv: 1303.5877 [hep-ph].
- [29] Michał Czakon et al. “The $(Q_7, Q_{1,2})$ contribution to $\bar{B} \rightarrow X_s \gamma$ at $\mathcal{O}(\alpha_s^2)$ ”. In: *JHEP* 04 (2015), p. 168. arXiv: 1503.01791 [hep-ph].

-
- [30] Andrei I. Davydychev and J.B. Tausk. “Two loop selfenergy diagrams with different masses and the momentum expansion”. In: *Nucl.Phys.* B397 (1993), pp. 123–142.
- [31] Ansgar Denner. “Techniques for calculation of electroweak radiative corrections at the one loop level and results for W physics at LEP-200”. In: *Fortsch. Phys.* 41 (1993), pp. 307–420. arXiv: 0709.1075 [hep-ph].
- [32] Ansgar Denner and Thomas Sack. “Renormalization of the Quark Mixing Matrix”. In: *Nucl. Phys.* B347 (1990), pp. 203–216.
- [33] Ansgar Denner et al. “Gauge-independent \overline{MS} renormalization in the 2HDM”. In: *JHEP* 09 (2016), p. 115. arXiv: 1607.07352 [hep-ph].
- [34] A. Denner et al. “Feynman rules for fermion-number-violating interactions”. In: *Nuclear Physics B* 387.2 (1992), pp. 467–481. ISSN: 0550-3213.
- [35] Thomas Deppisch and Ulrich Nierste. “Large hierarchies in the MSSM Higgs sector - in preparation”. In: ().
- [36] F. Englert and R. Brout. “Broken Symmetry and the Mass of Gauge Vector Mesons”. In: *Phys. Rev. Lett.* 13 (1964), pp. 321–323.
- [37] Henning Flacher et al. “Revisiting the Global Electroweak Fit of the Standard Model and Beyond with Gfitter”. In: *Eur. Phys. J. C* 60 (2009). [Erratum: *Eur. Phys. J.* C71,1718(2011)], pp. 543–583. arXiv: 0811.0009 [hep-ph].
- [38] P. Gambino, P. A. Grassi, and F. Madricardo. “Fermion mixing renormalization and gauge invariance”. In: *Phys. Lett.* B454 (1999), pp. 98–104. arXiv: hep-ph/9811470 [hep-ph].
- [39] Paolo Gambino and Ulrich Haisch. “Complete electroweak matching for radiative B decays”. In: *JHEP* 10 (2001), p. 020. arXiv: hep-ph/0109058 [hep-ph].
- [40] S. L. Glashow. “Partial Symmetries of Weak Interactions”. In: *Nucl. Phys.* 22 (1961), pp. 579–588.
- [41] S. L. Glashow, J. Iliopoulos, and L. Maiani. “Weak Interactions with Lepton-Hadron Symmetry”. In: *Phys. Rev. D* 2 (7 Oct. 1970), pp. 1285–1292.
- [42] John F. Gunion and Howard E. Haber. “The CP conserving two Higgs doublet model: The Approach to the decoupling limit”. In: *Phys. Rev.* D67 (2003), p. 075019. arXiv: hep-ph/0207010 [hep-ph].

- [43] T. Hahn and M. Perez-Victoria. “Automatized one loop calculations in four-dimensions and D-dimensions”. In: *Comput.Phys.Commun.* 118 (1999), pp. 153–165. arXiv: hep-ph/9807565 [hep-ph].
- [44] Thomas Hahn. “Generating Feynman diagrams and amplitudes with FeynArts 3”. In: *Comput.Phys.Commun.* 140 (2001), pp. 418–431. arXiv: hep-ph/0012260 [hep-ph].
- [45] Thomas Hermann, Mikolaj Misiak, and Matthias Steinhauser. “ $\bar{B} \rightarrow X_s \gamma$ in the Two Higgs Doublet Model up to Next-to-Next-to-Leading Order in QCD”. In: *JHEP* 11 (2012), p. 036. arXiv: 1208.2788 [hep-ph].
- [46] Florian Herren and Matthias Steinhauser. “Version 3 of RunDec and CRunDec”. In: (2017). arXiv: 1703.03751 [hep-ph].
- [47] Peter W. Higgs. “Broken Symmetries and the Masses of Gauge Bosons”. In: *Phys. Rev. Lett.* 13 (1964), pp. 508–509.
- [48] G. 't Hooft and M. Veltman. “Regularization and renormalization of gauge fields”. In: *Nuclear Physics B* 44.1 (1972), pp. 189–213. ISSN: 0550-3213.
- [49] T. Huber and Daniel Maitre. “HypExp: A Mathematica package for expanding hypergeometric functions around integer-valued parameters”. In: *Comput. Phys. Commun.* 175 (2006), pp. 122–144. arXiv: hep-ph/0507094 [hep-ph].
- [50] Victor Ilisie. “New Barr-Zee contributions to $(\mathbf{g} - \mathbf{2})_\mu$ in two-Higgs-doublet models”. In: *JHEP* 04 (2015), p. 077. arXiv: 1502.04199 [hep-ph].
- [51] Matthias Jamin and Markus E. Lautenbacher. “TRACER version 1.1: A mathematica package for γ -algebra in arbitrary dimensions”. In: *Computer Physics Communications* 74.2 (1993), pp. 265–288. ISSN: 0010-4655.
- [52] F. Jegerlehner. “Facts of life with gamma(5)”. In: *Eur. Phys. J. C* 18 (2001), pp. 673–679. arXiv: hep-th/0005255 [hep-th].
- [53] Shinya Kanemura and Kei Yagyu. “Unitarity bound in the most general two Higgs doublet model”. In: *Physics Letters B* 751.Supplement C (2015), pp. 289–296. ISSN: 0370-2693.
- [54] Makoto Kobayashi and Toshihide Maskawa. “CP-Violation in the Renormalizable Theory of Weak Interaction”. In: *Progress of Theoretical Physics* 49.2 (1973), pp. 652–657.

-
- [55] J. G. Körner, D. Kreimer, and K. Schilcher. “A practicable γ_5 -scheme in dimensional regularization”. In: *Zeitschrift für Physik C Particles and Fields* 54.3 (Sept. 1992), pp. 503–512. ISSN: 1431-5858.
- [56] Marcel Krause et al. “Gauge-independent Renormalization of the 2-Higgs-Doublet Model”. In: *JHEP* 09 (2016), p. 143. arXiv: 1605.04853 [hep-ph].
- [57] J. Kuipers et al. “FORM version 4.0”. In: *Comput. Phys. Commun.* 184 (2013), pp. 1453–1467. arXiv: 1203.6543 [cs.SC].
- [58] S. A. Larin. “The Renormalization of the axial anomaly in dimensional regularization”. In: *Phys. Lett.* B303 (1993), pp. 113–118. arXiv: hep-ph/9302240 [hep-ph].
- [59] J. P. Lees et al. “Exclusive Measurements of $b \rightarrow s\gamma$ Transition Rate and Photon Energy Spectrum”. In: *Phys. Rev.* D86 (2012), p. 052012. arXiv: 1207.2520 [hep-ex].
- [60] J. P. Lees et al. “Measurement of $B(B \rightarrow X_s\gamma)$, the $B \rightarrow X_s\gamma$ photon energy spectrum, and the direct CP asymmetry in $B \rightarrow X_{s+d}\gamma$ decays”. In: *Phys. Rev.* D86 (2012), p. 112008. arXiv: 1207.5772 [hep-ex].
- [61] J. P. Lees et al. “Precision Measurement of the $B \rightarrow X_s\gamma$ Photon Energy Spectrum, Branching Fraction, and Direct CP Asymmetry $A_{CP}(B \rightarrow X_{s+d}\gamma)$ ”. In: *Phys. Rev. Lett.* 109 (2012), p. 191801. arXiv: 1207.2690 [hep-ex].
- [62] A. Limosani et al. “Measurement of Inclusive Radiative B-meson Decays with a Photon Energy Threshold of 1.7-GeV”. In: *Phys. Rev. Lett.* 103 (2009), p. 241801. arXiv: 0907.1384 [hep-ex].
- [63] Heather E. Logan and Ulrich Nierste. “ $B_{s,d} \rightarrow \ell^+\ell^-$ in a two Higgs doublet model”. In: *Nucl. Phys.* B586 (2000), pp. 39–55. arXiv: hep-ph/0004139 [hep-ph].
- [64] R. Mertig, M. Böhm, and A. Denner. “Feyn Calc - Computer-algebraic calculation of Feynman amplitudes”. In: *Computer Physics Communications* 64.3 (1991), pp. 345–359. ISSN: 0010-4655.
- [65] M. Misiak et al. “Updated NNLO QCD predictions for the weak radiative B-meson decays”. In: *Phys. Rev. Lett.* 114.22 (2015), p. 221801. arXiv: 1503.01789 [hep-ph].

- [66] Mikolaj Misiak and Matthias Steinhauser. “Three loop matching of the dipole operators for $b \rightarrow s\gamma$ and $b \rightarrow sg$ ”. In: *Nucl. Phys.* B683 (2004), pp. 277–305. arXiv: hep-ph/0401041 [hep-ph].
- [67] Mikolaj Misiak and Matthias Steinhauser. “Weak radiative decays of the B meson and bounds on M_{H^\pm} in the Two-Higgs-Doublet Model”. In: *Eur. Phys. J. C* 77.3 (2017), p. 201. arXiv: 1702.04571 [hep-ph].
- [68] Ulrich Nierste. “Indirect CP violation in the neutral kaon system beyond leading logarithms and related topics”. In: (1995). arXiv: hep-ph/9510323 [hep-ph].
- [69] Ulrich Nierste. “private communication”. In: ().
- [70] G. Passarino and M. Veltman. “One-loop corrections for e e annihilation into in the Weinberg model”. In: *Nuclear Physics B* 160.1 (1979), pp. 151–207. ISSN: 0550-3213.
- [71] Hiren H. Patel. “Package-X: A Mathematica package for the analytic calculation of one-loop integrals”. In: *Comput. Phys. Commun.* 197 (2015), pp. 276–290. arXiv: 1503.01469 [hep-ph].
- [72] C. Patrignani et al. “Review of Particle Physics”. In: *Chin. Phys.* C40.10 (2016), p. 100001.
- [73] Abdus Salam. “Weak and Electromagnetic Interactions”. In: *Conf. Proc.* C680519 (1968), pp. 367–377.
- [74] Vladyslav Shtabovenko, Rolf Mertig, and Frederik Orellana. “New developments in FeynCalc 9.0”. In: *Computer Physics Communications* 207 (2016), pp. 432–444. ISSN: 0010-4655.
- [75] V. A. Smirnov. *Feynman integral calculus*. 2006.
- [76] Vladimir A. Smirnov. “Applied asymptotic expansions in momenta and masses”. In: *Springer Tracts Mod. Phys.* 177 (2002), pp. 1–262.
- [77] Vladimir A. Smirnov. “Asymptotic expansions in limits of large momenta and masses”. In: *Commun.Math.Phys.* 134 (1990), pp. 109–137.
- [78] Seidensticker T. “Drei-Schleifen-Korrekturen im Standardmodell unter Verwendung asymptotischer Entwicklung”. In: *Diploma thesis, TTP* (1998).
- [79] T. L. Trueman. “Spurious anomalies in dimensional renormalization”. In: *Zeitschrift für Physik C Particles and Fields* 69.3 (Dec. 1995), pp. 525–536. ISSN: 1431-5858.

- [80] Steven Weinberg. “A Model of Leptons”. In: *Phys. Rev. Lett.* 19 (1967), pp. 1264–1266.
- [81] C. Wiegand. “Automatisierte Berechnung von Feynman-Diagrammen auf Zweischleifenordnung”. In: *Diploma thesis, TTP* (2013).
- [82] Lincoln Wolfenstein. “Parametrization of the Kobayashi-Maskawa Matrix”. In: *Phys. Rev. Lett.* 51 (1983), p. 1945.
- [83] M. F. Zoller. “Top-Yukawa effects on the β -function of the strong coupling in the SM at four-loop level”. In: *JHEP* 02 (2016), p. 095. arXiv: 1508.03624 [hep-ph].

Acknowledgements

First of all I want to thank Uli Nierste for the supervision of my PhD thesis and all the interesting discussions. Secondly I want to thank Matthias Steinhauser for acting as the second examiner and his comments on this thesis. On this note I want to thank Alexander Goedicke, Marta Moscati and Thomas Deppisch for reading parts of the thesis and their many helpful comments and suggestions.

I want to especially thank my fellow SysAdmins. Firstly the old generation Thomas Herman, David Kunz and Jens Hoff, from whom I learned a lot when starting out. Secondly and chiefly my long term colleague Alexander Goedicke, who was always happy to help and great to work with due to his calm and focused manner of working. Thirdly Martin Gabelmann who implemented a lot of the modernisation that made our lives easier. Next the colleagues from the ITP Pascal Nagel and Robin Roth, who were always happy to discuss and solve problems. Lastly our new generation David Wellmann and Konstantin Asteriadis, for taking over in the last few months.

I am grateful for a lot of interesting discussions with many members of the TTP. Chiefly among them is the beta tester of Medusa and agent of chaos Thomas Deppisch as well as the members of the TTP coffee break Wolfgang Hollik and Max Zoller, who often contributed to interesting physics discussions in an informal and very enjoyable format. I want to thank especially Martin Spinrath and Philipp Frings for their effort of creating a positive atmosphere at the institute, the interesting discussions and their support at crucial times of my PhD. I am also very grateful to my office mates Anastasiya Bierweiler, Simon Kast and Marta Moscati for the on and off topic discussions and the good (working) atmosphere.

I also want to thank Martina Schorn, Isabelle Junge and Barbara Lepold for the administrative support.

Furthermore I want to thank Marco Bonetti, Lorenzo (the magnificent) Tancredi,

Chris Wever, Konstantin Asteriadis, Marta Moscati and Kirill Kudashkin for the shared adventures that helped boost my morale.

Finally I want to thank my family for their invaluable and continuous support.